Formation et propriétés de materiaux Hydroxydes Doubles Lamellaires bi-intercalés

Yongjun Feng

UNIVERSITE BLAISE PASCAL

(U.F.R. de Recherche Scientifique et Technique)

ECOLE DOCTORALE DES SCIENCES FONDAMENTALES

THESE

Présentée pour obtenir le grade de

DOCTEUR D'UNIVERSITE

(Spécialité : Chimie, Sciences des Matériaux)

Par

Yongjun FENG

Formation and Properties of Second-stage Layered Double Hydroxide Materials.

Soutenue publiquement le 7 Decembre 2006, devant la commission d'examen :

Président :	Prof. D. O'Hare	Oxford University, Angleterre
Rapport eur:	Dr. P. RABU	Université Louis Pasteur, Strasbourg
	Prof. D. G. EVANS	Beijing University of Chemical Technology, Chine
Examinateurs :	Prof. P. MALFREYT	Université Blaise Pascal, Clermont-Ferrand
	Dr. B. LANSON	Université Joseph Fourier, Grenoble
	Dr. F. LEROUX	Université Blaise Pascal, Clermont-Ferrand
	Dr. C. TAVIOT-GUEHO	Université Blaise Pascal, Clermont-Ferrand

ACKNOWLEDGMENTS

My sincere thanks are given to my advisor Dr. Christine TAVIOT-GUEHO for her guidance, support, time, encouragement and comments from the beginning to the end of my thesis work.

I would like to express my special appreciation to Prof. D. O'Hare for his fruitful collaboration allowing me to obtain the Energy-dispersive X-ray Diffraction data, to Prof. D. G. Evans and Dr. P. Rabu for their helpful comments and constructive reports. I would also like to thank the other members of my graduate committee: Prof. P. Malfreyt, Dr. B. Lanson and especially Dr. F. Leroux for his productive discussions and his helpful advice during my studies. Additionally, I am greatly indebted to Dr. G. R. Williams for his kind help and his patient discussions on the data analysis of Energy-dispersive X-ray Diffraction.

Thanks are also extended to all the members in Inorganic Materials Laboratory (LMI) in Blaise Pascal University for their kindness and help: Prof. C. Forano, Prof. A. de Roy, Prof. M. de Roy, Dr. V. Prevot. I really appreciate the help from my friends，especially Erwan Geraud and Jairo Tronto with whom I have spent a nice time.

I owes special thanks to all the people who have dedicated part of their time to help me with the instrumentation needed to complete my thesis: J. Cellier (PXRD), Dr. D. Talor (EDXRD in Daresbury Laboratory, UK) and Mr. A. Neild (EDXRD in Daresbury Laboratory, UK).

I also thank Professor X. Duan at Beijing University of Chemical Technology in China for his advice and encouragement.

A very, very special thanks goes to my dear wife Xiaoyan for all the support,

time and patience she has given me to accomplish my thesis. I would also like to especially thank my family for all the support and time they have endured me throughout my studies.

This thesis has been made possible in part to due to the financial support from the region Council of Auvergne in France.

Yongjun FENG

AUBIERE, FRANCE

December 10, 2006

Contents

Introduction

The anion exchange properties of Layered Double Hydroxides (LDH) described by the general formula $[M^{2+}_{1-x}M^{3+}_{x}(OH)_2]A^{m-}_{x/m}\ nH_2O$ allow for the preparation of a wide range of host-guest assemblies. Of particular interest are the organic-inorganic hybrids LDH owing to their large fields of potential applications as catalyst, adsorbent for pollutants, nanofiller in polymer, vector for biological molecules...[1-8] Up to until a few years ago, most of the articles concerned with organic/inorganic anion exchanged LDH generally described the fully exchanged phases and only a few studies were reported on the anion-exchanged forms obtained at partial exchange rates probably because phase segregation was generally admitted for the exchange process in LDH system.

In recent years, the technological and experimental advances in energy dispersive X-ray diffraction using synchrotron X-ray sources have provided new possibilities for studying solid-state reactions. In particular, O'Hare *et al.* have shown the interest of this technique in the intercalation chemistry of layered materials.[9-12] In this way, these authors have demonstrated the ability of $LiAl_2(OH)_6Cl\ 2H_2O$ to form second-stage intermediates during the exchange reaction with a series of dicarboxylate anions.[12]

Such LDH heterostructures with alternate interlayer spaces occupied by two different anions offer new perspectives for LDH intercalation chemistry, particularly in

1 D. G. Evans and R. C. T. Slade, *Struct. Bond*., **2006**, *119*, 1.
2 B. Ballarin, M. Gazzano, R. Seeber,; D. Tonelli and A. Vaccari, *J. Elect. Chem.*, **1998**, *445*, 27.
3 L. Van der Ven, M. L. M. Van Gemert, L. F. Batenburg, L. F. Keern, L. H. Gielgens, T. P. M. Koster and H. R. Fischer, *Appl. Clay. Sci*., **2000**, *17*, 25.
4 Y. J. Feng, D. Q Li., Y. Wang, D. G. Evans and X. Duan, *Polym. Degrad. and Stabil.*, **2006**, *91*, 789.
5 J. Inacio, C. Taviot-Guého, C. Forano and J. P. Besse, *Appl. Clay Sci.*, **2001**, *18*, 255.
6 F. Leroux, *J. Nanosci. Nanotech.*, **2006**, *6(2)*, 303.
7 F. Leroux and C. Taviot-Gueho, *J. Mater. Chem.*, **2005**, *15 (35-36)*, 3628.
8 J. H. Choy, S. Y. Kwak, Y. J. Jeong, J. Portier and J. S. Park, *Angew. Chem. Int. Ed.*, **2000**, *39*, 4042.
9 G. R. Williams and D. O'Hare, *Chem. Mater.*, **2005**, *17*, 2632
10 G. R. Williams, thesis, **2005**, Oxford University
11 G. R. Williams, A. J. Norquist and D. O'Hare, *Chem. Mater*., **2004**, *16*, 975.
12 G. R. Williams and D. O'Hare, *Chem. Mater.*, **2005**, *17*, 2632.

the direction of multifunctional materials. Yet, at the time the present thesis work started, staging had been observed only in a few cases, mainly in $LiAl_2$ LDH system which constitutes a rare example of ordered LDH structure, and the reasons it took place were not clearly established. The objective of the present work was thus to further investigate staging phenomena in LDH system. By means of EDXRD technique, we investigated the anion-exchange process with different inorganic (Cl^-, F^-, CO_3^{2-}, SO_4^{2-} and $Fe(CN)_6^{3-}$) and organic anions (tartrate, succinate, adipate and styrene-4-sulfonate anions) for two LDH compositions : Zn_2Al and Zn_2Cr.

The first chapter is intended to provide a state of the art review of LDH materials, to describe their synthesis and characterization with emphasis on the structural aspects of LDH intercalation chemistry and to point out the potential applications.

An initial series of time-resolved in situ EDXRD experiments discussed in Chapter two was performed to determine the conditions of formation of LDH second-stage compounds. In the case of $[Zn_2Cr(OH)_6]Cl\ nH_2O$ and $[Zn_2Al(OH)_6]Cl\ nH_2O$, the exchange reactions of Cl^- anions by succinate and tartrate anions confirm the trends highlighted in a previous work,[13] in particular the existence of different exchange pathways depending on the nature of the intercalated anions. The aim of this first study was also to determine the different factors influencing the observation/formation of LDH second-stage materials including experimental parameters such as the addition rate of the guest anion solution, the temperature and also more fundamental parameters like the nature of the anion-exchange reaction itself involving either inorganic anions or both inorganic and organic anions.

13 J. Pisson, C. Taviot-Gueho, Y. Israeli, F. Leroux, P. Munsch, J. P. Itie, V. Briois, N. Morel-Desrosiers and J. P. Besse, *J. Phys. Chem. B*, **2003**, *107*, 9243.

In Chapter 3, we looked at the anion-exchange properties of LDH second-stage compounds. The two second-stage materials $[Zn_2Cr(OH)_6](succinate)_{0.25}Cl_{0.5}$ nH_2O LDH (Zn_2Cr-Succ/Cl) and $[Zn_2Cr(OH)_6](tartrate)_{0.25}Cl_{0.5}$ nH_2O LDH (Zn_2Cr-Tart/Cl) were isolated and then separately treated with organic adipate anions and inorganic fluoride anions. The reactions, followed in situ by EDXRD, showed highly selective anion-exchange properties with new second-stage intermediates forming.

The last chapter is devoted to the enlargement of this study towards multifunctional materials. Indeed, the exchange reactions with "functional" anions such as styrene-4-sulfonate anions and iron hexacyanoferrate anions were investigated and EDXRD data are briefly described.

Chapter 1 An Introduction to Layered Double Hydroxides and Staging in Lamellar Materials

I. Generalities on Layered Double Hydroxides

1.1 **Structural Considerations**

Layered double hydroxides (LDH), also called anionic clays, are host-guest layered materials[1-3]. Yet, contrary to cationic clays, LDH materials are quite rare in nature. Most of LDH are synthetic phases and their structure resembles the naturally occurring mineral Hydrotalcite $[Mg_6Al_2(OH)_{16}]CO_3{\cdot}4H_2O$, first discovered in 1842 and first prepared as a synthetic material in 1942 by Feitknecht[4, 5]. However, the detailed structural features of LDH were not understood until the late 1960's by Allmann[6], Taylor[7] and their co-workers.

LDH materials are mostly described by the general formula $[M^{2+}_{1-x}M^{3+}_{x}(OH)_2]A^{m-}_{x/m}{\cdot}nH_2O$, abbreviated hereafter as $M^{2+}_{R}M^{3+}$-A, where M^{2+} and M^{3+} are divalent and trivalent cations, respectively, A is an anion of valence *m* and $R = 1-x/x$ is the M^{2+}/M^{3+} molar ratio ($x = M^{3+}/(M^{3+}+M^{2+})$). The structure of LDH hydroxide layers is derived from that of brucite, $Mg(OH)_2$, which consists of $M(OH)_6$ octahedral units sharing four edges and three vertices and thus forming infinite layers with neutral charge. In LDH, a partial replacement of divalent cations by trivalent cations occurs resulting in a net positive charge, compensated by A^{m-} negative anions present in the interlayer space and surrounded by water molecules.

The main features of Hydrotalcite-like LDH are a large chemical variation and a random distribution of cations within the hydroxide layers. All divalent positive metal ions from Mg^{2+} to Zn^{2+} with an ionic radius in the range 0.65 - 0.80 Å and all transition metal trivalent ions (except Ti^{3+}) with an ionic radius in the range 0.62 – 0.69 Å (with the main exception of Al^{3+}: 0.50 Å) can enter into the composition of LDH hydroxide layers. Divalent and trivalent cations of close radius values enable a joint replacement and a larger chemical variation, and therefore a highly tunable layer charge density.

LDH materials consisting of more than two different cations in the sheets have been reported such as $(Cu_{0.4}Zn_{0.6})_6M_2(OH)_{16}CO_3{\cdot}4H_2O$ (M = Al, Cr and Ga) [8], Ni-Al-M-CO_3 (M=Cr or Fe) [9], $Cu_xNi_yMg_{2-x-y}$Al-CO_3 [10] and $[Fe^{II}_{1-x-y}Mg_yFe^{III}_x(OH)_2]$-$(OH)_x{\cdot}nH_2O$. [11] Note that the larger mean cation radius leads to the higher flattened degree of the octahedral environment of metal cations along the stacking direction compared with the regular polyhedron and then results to the lower layer thickness and the larger distance between metal cations. For example, by the comparison of Zn_3Al and Zn_2Cr based LDHs, the mean metal radius increases from 0.68 Å to 0.72 Å while the hydroxide layer thickness decreases from 2.071 Å to 2.020 Å and the mean cation distance from 3.083 Å to 3.120 Å.[12]

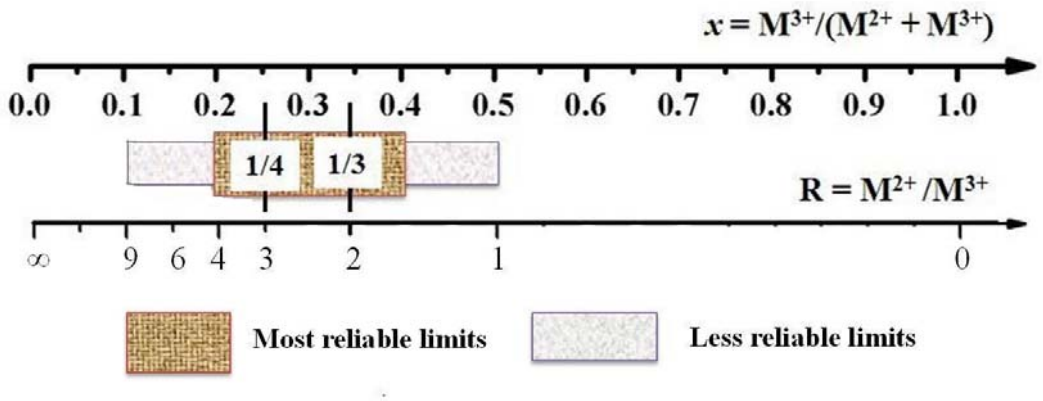

Figure 1-1: Comparison of trivalent metal ratio *x* scale and divalent versus trivalent *R* scale, and corresponding limits for LDH compositions. (see ref. 12)

In LDH systems ($M^{2+}_RM^{3+}$-A), the *R* value (M^{2+}/M^{3+} molar ratio) can be tuned in a relatively wide range without main structural change as shown in **Figure 1-1**.[12] The upper limit of *R* value could be needed to avoid a collapse of the interlayer domains due to a too long distance between these interlayer anions. The lower limit of *R* value generally results from the unavoidable electrostatic repulsion between neighboring trivalent metal cations (if $R < 2$) within the main layers and also the repulsion between the charge-balancing anions in the interlayer region. In order to obtain pure phases of LDH and avoid the formation of single hydroxides i.e. $M^{II}(OH)_2$ and $M^{III}(OH)_3$, the *R* values must be constrained in a certain range from 2 to 4, which corresponds to the *x*

value varying from 0.33 to 0.20. Yet, a wider range of *R* values has been reported: for $Mg_RGa\text{-}CO_3$, $1.8 \leq R \leq 12.9$ ($0.072 \leq x \leq 0.357$)[13]as well as for $[Fe^{II}_2Fe^{III}_2(OH)_8]\text{-}CO_3$, $R = 1$ ($x = 0.5$)[14]. While in other cases, a unique *R* value can only be stabilized, for example, $R = 2$ for Cu_2Cr[15], Zn_2Cr[16] and Ca_2Al [17]LDH and $R = 1/2$ in $LiAl_2$ LDH[18].

A great number of anions including inorganic anions and organic anions as presented below could occupy the interlayer region of LDH. The amount of the anions in the interlayer spacing is directly related to the charge density of the hydroxide layers which can be controlled by the M^{2+}/M^{3+} ratio whereas their arrangement depends on the interlayer packing related to the layer charge density as well as the anion size and the presence of water molecules; additional parameters such as the preparation route and the synthesis temperature may also influence the interlayer arrangement, especially in the case of organic intercalated molecule. The positive charge density (d_{charge}) of the hydroxide layers can be calculated as follows[19]:

$$d_{charge} = 1/S_{unit\ charge} = (e \cdot x)/(a^2 \cdot \sin 60°) \qquad \textbf{Equation 1-1}$$

where $S_{unit\ charge}$ is the area per unit charge, *e* is the charge of an electron, *x* is the mole fraction of the trivalent cation in the brucite-like layer, $M^{3+}/(M^{2+}+M^{3+})$ and *a* is the cell parameter of hexagonal unit cell.

i) inorganic anions: halide ions (F^-, Cl^-, Br^- and I^-); small oxo anions (CO_3^{2-}, NO_3^-, ClO_4^-, SO_4^{2-}, $S_2O_3^{2-}$ and CrO_4^{2-}, etc.); inorganic coordination compounds ($NiCl_4^{2-}$, $CoCl_4^{2-}$, $Fe(CN)_6^{3-}$ and $Fe(CN)_6^{4-}$, etc.); silicate anion ($SiO(OH)_3^-$).

ii) polyoxometalates: $[Mo_7O_{24}]^{6-}$, $[V_{10}O_{28}]^{6-}$, $[H_2W_{12}O_{40}]^{6-}$, $[PV_3W_9O_{40}]^{6-}$, $[SiV_3W_9O_{40}]^{7-}$, $[BVW_{11}O_{40}]^{7-}$ and $[SiW_{11}O_{39}]^{8-}$, etc.

iii) organic anions: (*di*)carboxylates (adipate, oxalate, succinate, benzoate, phthalate, terephthalate, p-methylbenzoate and p-hydroxybenzoate, etc.); anionic surfactants (alkyl sulfonates, alkyl sulfates, etc.); metallomacrocycles (Co(II) or Cu(II) phthalocyanine

tetrasulfonate, Mn(III)-meso-tetrakis-(2, 6-dichloro-3-sulfonato-phenyl)porphyrin, etc.); anionic polymer (polyacrylate, polyacrylonitrile, polyaniline, polyvinylsulfonate, polystyrenesulfonate and polyaspartate, etc.).

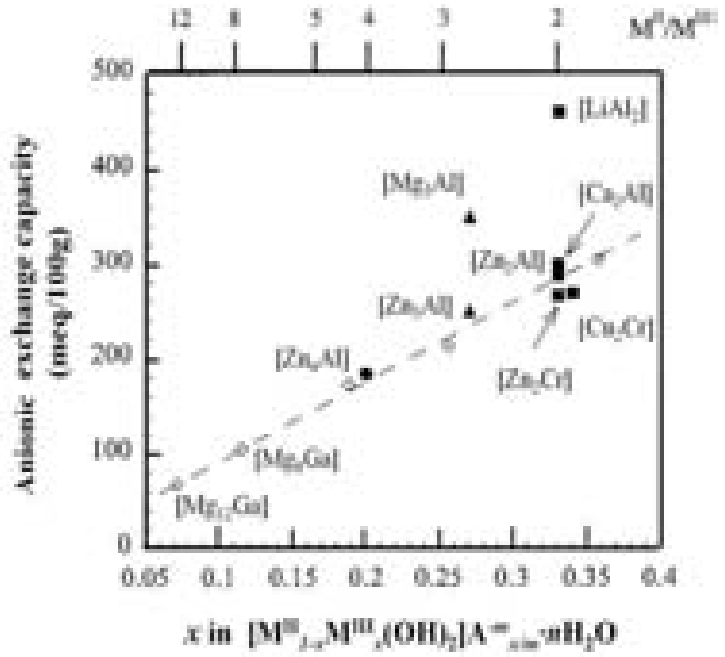

Figure 1-2: Variation of anionic exchange capacity (meq/100g) as a function of the amount of trivalent cation reported per formula weight (ref. 20).

The anionic exchange capacity (AEC, meq/100 g) of LDH is expressed in terms of millimoles of positive charge within the hydroxide layers per 100 gram of LDH based on the theoretical formula $[M^{II}_{1-x}M^{III}(OH)_2]A^{-m}_{x/m}\cdot nH_2O$ and depends on the amount of trivalent cations (x value in the general formula) present in the hydroxide layer. As reported for some LDH compositions in **Figure 1-2**[20], the values range from 200 to 450 meq/100g corresponding to the range of x value from *ca.* 0.33 to 0.20. For comparison, cationic clays present usually limited ionic exchange capacity close to 100 meq/100 g associated to average area per charge of 70 $Å^2$/charge. In the case of LDH materials, the average area per charge is much smaller with values from 25 to 40 $Å^2$/charge. This explains the differences observed in their intercalation and exfoliation chemistry.

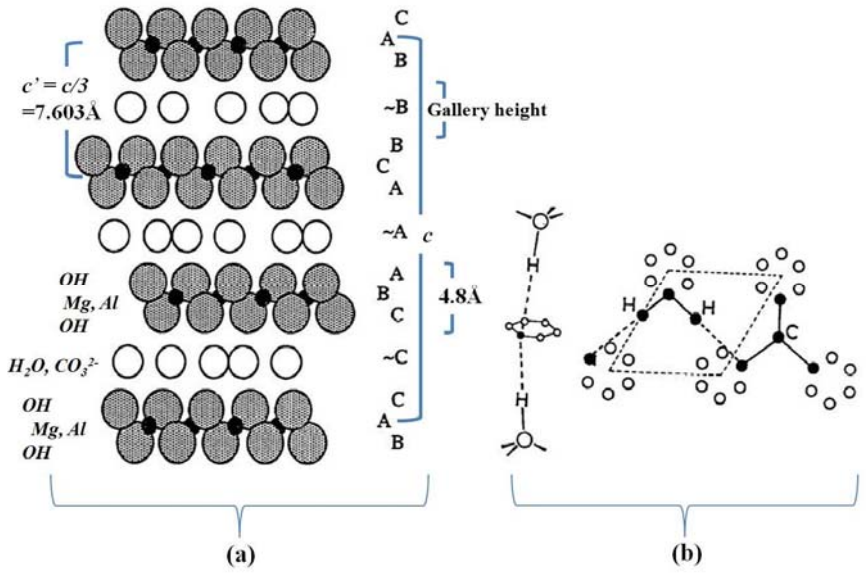

Figure 1-3**:** (a) Stacking sequence in Hydrotalcite ($[Mg_6Al_2(OH)_{16}]CO_3{\cdot}4H_2O$) with rhombohedral symmetry (ref. 21). (b) position of interstitial atoms between the hydroxide layers. Gallery height can be calculated by subtracting the layer thickness (~4.8 Å) from the basal spacing (*c'*). (ref. 22)

Synthetic LDH materials generally crystallize in the space group $R\bar{3}m$ adopting the same structure as the Hydrotalcite mineral $[Mg_6Al_2(OH)_{16}]CO_3{\cdot}4H_2O$ (**Figure 1-3**(a)). The hydroxide layers of Hydrotalcite are stacked with three layers per unit cell in rhombohedral symmetry. The parameters of the unit cell for Hydrotalcite are: a = 3.05 Å and c = 3c'= 22.81 Å (c' = 7.603 Å).[21] The distribution of the metal cations in the hydroxide layers is disordered. The carbonate anions and interstitial water molecules are likewise randomly located in the interlayer region. The oxygen atoms of the water molecules and of the carbonate anions are distributed approximately closely around the symmetry axes that pass through the hydroxyl groups of adjacent brucite-like layers (**Figure 1-3** (b)).[22] Preferential location of interlayer oxygen atoms could be found at about 0.56 Å radial distance from the three-fold axes.

Owing to their lamellar character and the disordered cationic distribution within the hydroxide layers, synthetic LDH materials are generally microcrystalline powders and structural studies are performed by Rietveld refinement of powder X-ray diffraction diagrams.

However, Ca_2Al and $LiAl_2$ LDH systems differentiate by an ordered distribution of cations in the hydroxide layers. Ca_2Al LDH refers to hydrocalumite-like LDH. The structure of Ca_2Al is based on corrugated brucite-like main layers with an ordered arrangement of Ca^{2+} and Al^{3+} ions, seven- and six- coordinated, respectively, in a fixed ratio of 2:1; the seventh apex of the Ca-polyhedron is a water molecule from the interlayer space (**Figure 1-4)**.[23] The general formula of this group is $[Ca_2M^{3+}(OH)_6]^+[A^{m-}_{1/m}\cdot nH_2O]^-$ with M^{3+} = Al^{3+}, Fe^{3+}, Cr^{3+}, Ga^{3+} and Sc^{3+}; the composition of the hydroxide layer of this structure type is thus limited.[24] It is widely assumed that the difference in size between Ca^{2+} and M^{3+} ions is responsible for their ordered arrangement in a fixed M^{2+}/M^{3+} ratio of 2:1. Besides, the size of Ca^{2+} and the pronounced anisotropy of coordination spheres around Ca^{2+} and M^{3+} are also suggested as the reason for the structural order in hydrocalumite-like compounds. [23] These lamellar calcium hydroxides salts have also been studied in details for their occurrence in the hydration process of cement compounds, known as Friedel's salts and AFm phase. [25, 26]

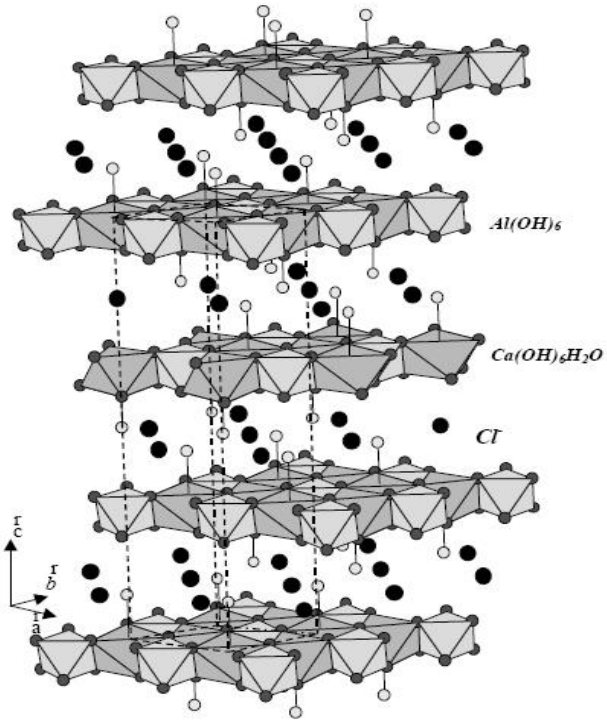

Figure 1-4: Crystal structure of $[Ca_2Al(OH)_6]Cl\cdot 2H_2O$ layered double hydroxides in *R*-3 group, the cell parameter *a* = 5.7487 (5) Å and *c* = 23.492 (1) Å. See ref. 23.

In the case of $LiAl_2$ LDH, two kinds of the hydroxide layer stacking forms have been found and depend on the polymorph of $Al(OH)_3$ i.e. the hexagonal form (*h*-$LiAl_2$) produced from the gibbsite and the rhombohedral form (*r*-$LiAl_2$) from the bayerite or nordstrandite. [27] Furthermore, the difference in layer stacking sequences is so important in the chemistry of the $LiAl_2$ LDH system. For instance, the structure of *h*-$[LiAl_2(OH)_6]Cl{\cdot}H_2O$ presented in **Figure 1-5**, Li^+ ions occupy the empty octahedral holes in the gibbsite-like $Al(OH)_3$ layers whereas the interlayer species such as Cl^- and H_2O are disordered over five sites located midway between the $Al(OH)_3$ layers. [28] The corresponding parameters of the unit cell are: $a = b = 5.10$ Å and $c = 14.30$ Å ($c = 2c'$) in the space group P63/mcm. The composition of this structure type is limited to $LiAl_2$ for the main layers but the interlayer chloride anions are possible to be exchanged by other inorganic and organic anion species.

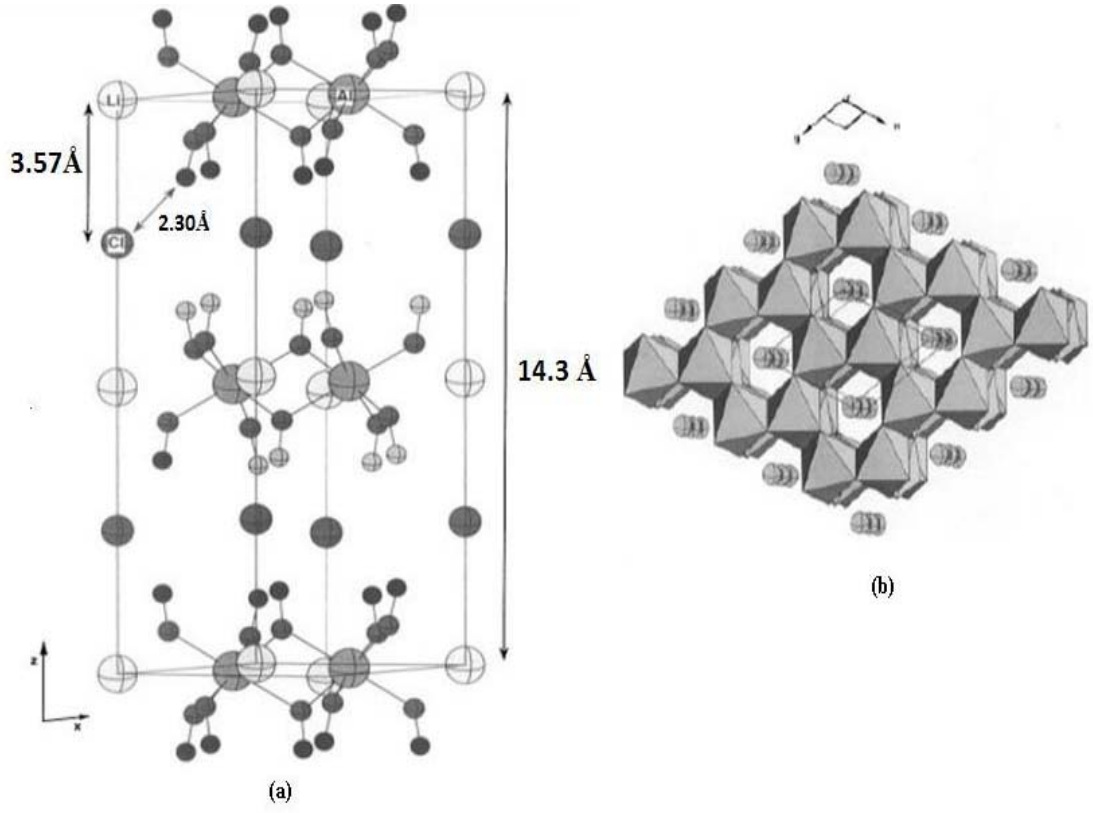

Figure 1-5: The structure of *h*-$[LiAl_2(OH)_6]Cl{\cdot}H_2O$: (a) view of the unit cell and (b) view down the (*001*) direction of the unit cell. See ref. 28.

1.2 **Synthesis Routes of LDH**

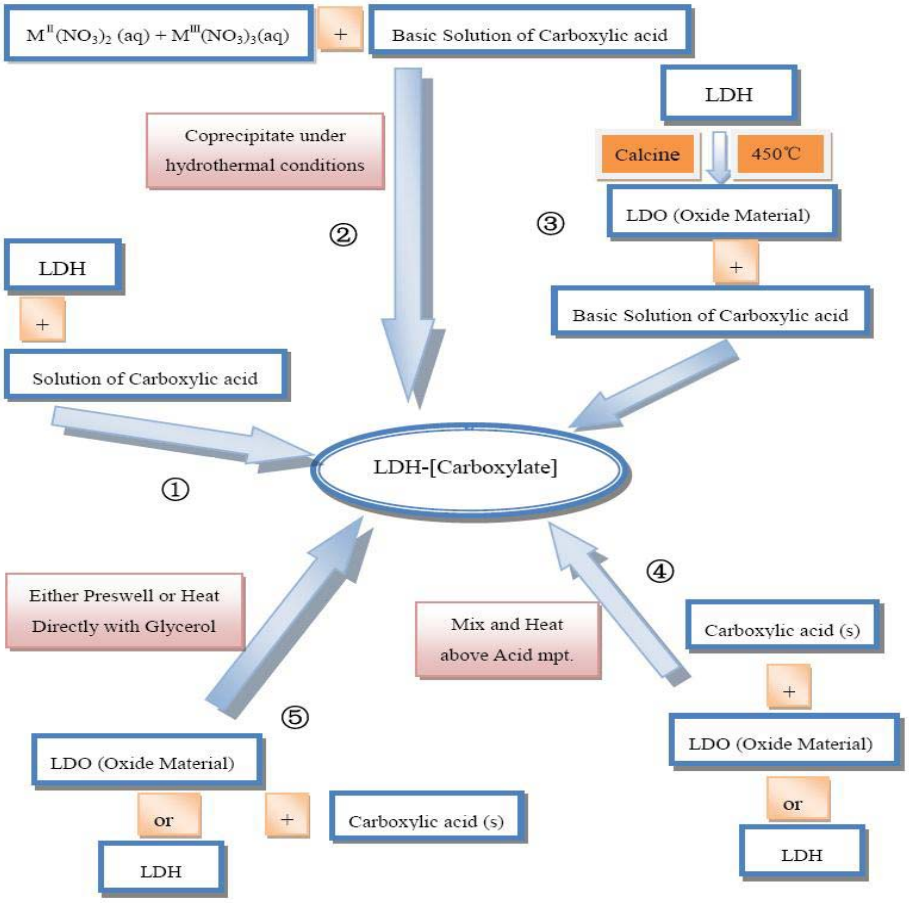

Figure 1-6: The five main experimental methods used for preparation of carboxylic acid intercalated LDH or LDO. See ref. 29.

LDH materials are usually prepared according to two methods which are coprecipitation and anion-exchange reactions. The choice between these two methods depends generally on the host composition and the properties of the guest anions. Other methods of LDH preparation are known summarized in **Figure 1-6** and several reviews on the synthesis methods of LDH have been published, [29-31] for example, S. Carlino describing intercalation mechanisms of a series of aliphatic and aromatic mono-and dicarboxylic acids into LDH and their calcined oxides (the so-called Layered Double Oxide, LDO).

1.2.1 Direct coprecipitation method

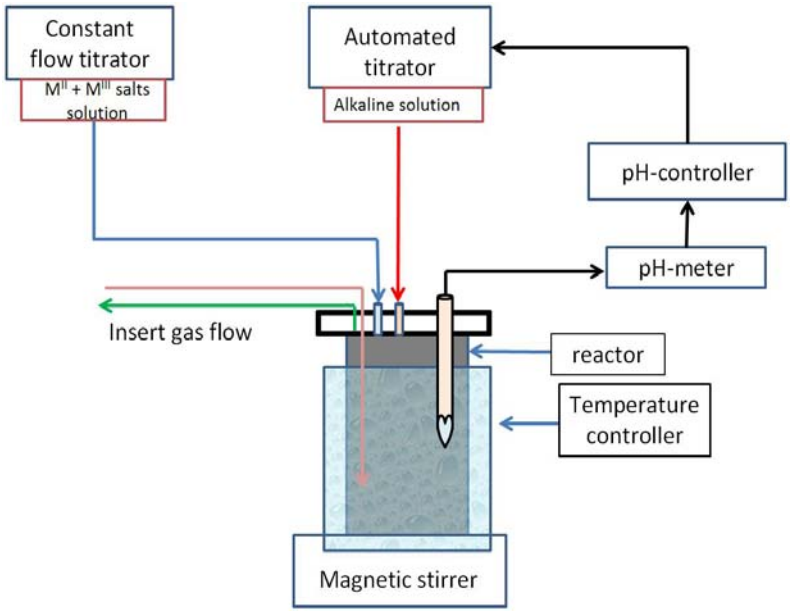

Figure 1-7**:** Experimental setup for the preparation of LDH materials by the coprecipitation method (see ref. 12).

This is the most common synthesis method of LDH materials (**Figure 1-7**).[32, 33] The general process of this method established by Miyata[34] is the simultaneous precipitation of the metal cations in the hydroxide form in the presence of a base solution (for example, NaOH) and the counter anions of the metal salts become the interlayer anions. The addition is often carried out at a constant pH value which depends on the metal cations nature and leads to the coprecipitation of the two metallic salts within the hydroxide layers. For the intercalation of other anions than the counter anions, the desired anions are initially introduced into the reacting flask in a large excess (an excess between 5 and 10 times over the M^{3+} content is commonly used). After complete addition of the metallic salts, the precipitate is aged in the mother solution for a few hours or several days and the LDH is then recovered by *ca.* four dispersion and centrifugation cycles in deionized and decarbonated water. So far, a lot of anion-intercalated LDH materials have been obtained by this method.

The mechanism of coprecipitation method relies upon the condensation of hexa-aqua complexes in solution in order to form the brucite-like layers with a distribution of both metallic cations and with solvated interlayer anions. [12] In order to obtain well crystallized LDH phases, some of the experimental parameters should be particularly controlled and optimized such as the pH, the temperature, the concentration of both metallic salts, the concentration of alkaline solution, the addition rate of reactants as well as the aging time and temperature of the precipitate.

1.2.2 Anion-exchange method

This method is based on the anion exchanged properties of LDH. The general process of this method can be described as following:

$$LDH \cdot A^{m-} + X^{n-} \rightleftarrows LDH \cdot (X^{n-})_{m/n} + A^{m-}$$

Based on the mass action law, working in excess of incoming anions (X^{n-}) will favor the exchange reaction of outcoming anions (A^{m-}) to generate the fully exchanged phase $LDH \cdot (X^{n-})_{m/n}$.

Anion exchange properties of LDH depend on LDH affinity towards outcoming and incoming anions. By comparing the equilibrium constant of exchange reactions between monovalent anions and divalent anions, Miyata proposed an order of anion selectivity: OH^- > F^- > Cl^- >Br^- > NO_3^- > I^- and CO_3^{2-} > $C_{10}H_4N_2O_8S^{2-}$ (Naphthol Yellow S) > SO_4^{2-}. These results suggest for example that NO_3^- anions are easily displaced by OH^- anions of higher affinity towards the metal hydroxide layers. This trend was later confirmed by microcalorimetric measurement. [35] Yamaoka *et al.* [36] also gave a comparative list for divalent oxoanions: HPO_4^{2-}, $HAsO_4^{2-}$ > CrO_4^{2-} > SO_4^{2-} >MoO_4^{2-}. Based on these observations, chloride and nitrate containing LDH are often used as precursors for anion-exchange reactions, and one should avoid carbonate or hydroxyl phase. The exchange process may be limited by the expansion of the interlayer space to accommodate large size anions. In this case, spaced LDH precursors intercalated with lauryl sulfate, p-

toluenesufonate, terephthalate, 2, 5-dihydroxy-1, 4- benzendisulfonate, 1, 5-naphthalenedisulfonate anions can be used as reported for the preparation of oxometalates anions-containing LDH as reported. [37, 38] An extended use of this guest displaced method have recently been reported by Valim *et al*.[39, 40], based on the formation and organic phase extraction of a salt dodecylsulfate anions LDH by a cationic surfactant (CTA) as illustrated in **Figure 1-8**.

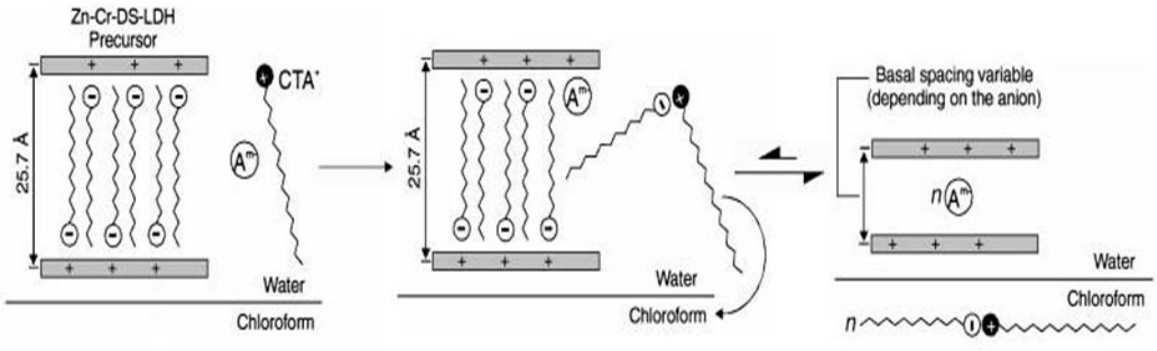

Figure 1-8**:** Scheme of anions exchange by the formation of a salt between an anionic and a cationic surfactant in LDH (DS = sodium dodecylsulfate, CTA^- = N-cetyl-N, N, N-trimethylammonium). See ref. 39.

The anion-exchange method is a straightforward way to prepare LDH containing a variety of organic or inorganic anions. Yet, it is subjected to the influence of some factors such as the pH value, the solvent and the temperature. For instance, the pH value plays an important role, since it determines the stability of the hydroxide layer and the properties of the incoming anions. Higher pH values (10.0-12.0) favor the intercalation of carbonate anions while lower pH values (4.5-6.0) benefits the liberation of initial anion as the conjugate acid and incorporation of a less basic anion from the reaction system.[41] Note that a pH value lower than 4.0 may result into the dissolution of LDH hydroxide layer. A suitable solvent may also favor the anion-exchange process. It was found that binary solvent mixtures of alcohol and toluene prevent dissolution of the Mg_2Al-CO_3 and preserve LDH layered crystal structure during the anion-exchange reaction of aliphatic α, ω-dicarboxylate anions.[42] Similarly, ethanol/water mixture as solvent can effectively reduce the dissolution of LDH host during the intercalation of heptamolybdate ($[Mo_7O_{24}]^{6-}$) [43] and decamolybdodicobaltate (III) anions

($[H_4Co_2Mo_{10}O_{38}]^{6-}$) [44] into Mg_RAl-LDH ($1.27 \leq R \leq 3.0$). Finally, O'Hare *et al.* also found that the mixed ethanol/water solvent may also improve the crystallinity and decrease the production of $Al(OH)_3$ as an undesired product during the exchange reaction involving all isomers of both pyridinecarboxylate and toluate in $[LiAl_2(OH)_6]Cl{\cdot}H_2O$.[45] In the other hand, to some extent, higher reaction temperatures favor the exchange reaction by lowering activation energy.

1.2.3 Other methods

The reconstruction of the LDH phase from calcined LDH derivatives (LDO) is reported as an alternative method for the preparation of hybrid LDH [46] and has also been largely used for the incorporation of bulky anions such as polyoxometalates anions.[47, 48] This method is more complicated compared with coprecipitation and anion-exchange methods. The calcination temperature and the composition of the hydroxide layers are the key factors influencing the reconstruction process.[49, 50] However, it is still difficult to avoid the existence of carbonate anions due to the high affinity towards the mixed oxide[51] and the production of some amorphous phases due to uncomplete reconstruction.

The hydrothermal method carried out in an autoclave under autogenous pressure is usually applied as a postsynthesis hydrothermal treatment to improve the crystallinity of LDH. [52] In a few occasions, this method was found effective for the intercalation of lower affinity anions.[53]

The salt-oxide method [54] is based on the slow addition of a solution of trivalent metal salt (acidic species i.e. $CrCl_3$, $AlCl_3$) on an aqueous suspension of the divalent metal oxide (basic species i.e. CuO, ZnO). The LDH phase is formed along the slow dissolution of divalent oxide and the reaction can be written as follows:

$$M^{II}O + M^{III}Cl_3 + (n-1)H_2O \rightarrow [M^{II}_{1-x}M^{III}_x(OH)_2Cl_x \cdot nH_2O + xM^{II}Cl_2.$$

For instance, Zn_2Cr-Cl, Zn_2Al-Cl and Cu_2Cr-Cl LDH compounds have been prepared *via* this method. [55]

1.3 **Structural Characterization of LDH**

The structural characterization of LDH often suffers from the poor crystallinity of the powders. Hence, together with powder X-ray diffraction (PXRD) technique, microscopy, X-ray Absorption Spectroscopy (XAS), Infrared (IR), Raman, Nuclear Magnetic Resonance (NMR) spectroscopies and Molecular Dynamic (MD) simulations are often used as complementary techniques to get a better view of LDH structure (**Figure 1-9**).

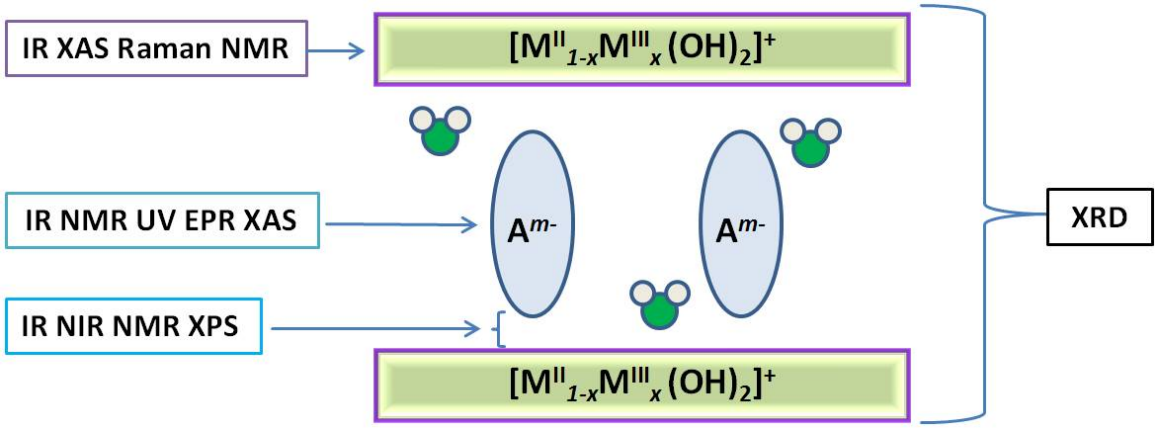

Figure 1-9**:** Possible structural information provided by different characterization technique.[56]

1.3.1 Powder X-ray Diffraction (PXRD)

Only a few minerals can be obtained in the form of single crystals and most of synthetic LDH are randomly oriented powders. Consequently, powder X-ray diffraction (PXRD) remains the main analytical technique for the structural characterization of LDH.

1.3.1.1 **Basic structural information from PXRD patterns**

As presented in **Figure 1-10**,[57] the typical features of PXRD patterns of all LDH are the presence of sharp and intense lines at low 2θ angle values corresponding to the basal *00l* reflections, and less intense lines at higher angular values corresponding to *01l*, *10l* and *11l* reflections. As said before, the patterns are generally indexed on the basis of an hexagonal unit cell in the space group $R\bar{3}m$ and then the unit cell parameters can be gained: $a = b = 2d_{110}$ and $c = 3\ d_{003}$.

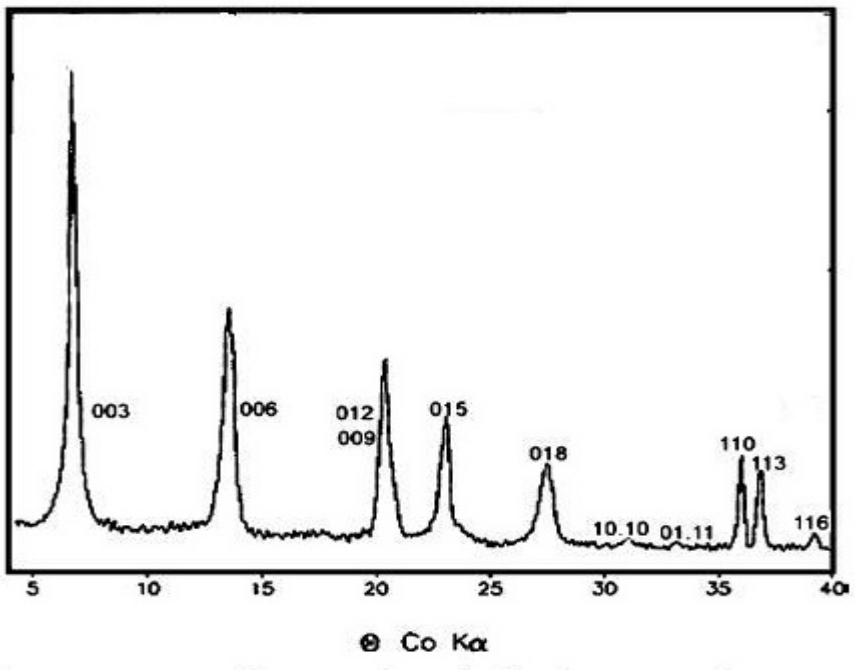

Figure 1-10**:** Powder X-ray diffraction patterns of a synthetic Hydrotalcite $[Mg_6Al_2(OH)_{16}](CO_3)\cdot 4H_2O$ (see ref. 57).

The *003* reflection corresponds to the interlayer distance d_{003} i.e. *d*-spacing and is equal to the gallery height plus the host hydroxide layer thickness of approximately 4.8 Å. Actually this value corresponds to the interlayer distance in brucite $Mg(OH)_2$ thus including the hydroxide layer thickness and the hydrogen bond distance between successive hydroxide layers. On the other hand, the structural study by neutron diffraction of $Zn_2Al\text{-}CO_3$ led to an hydroxide layer thickness of 3.9 Å including hydrogen atoms of OH groups.[58] Generally, the LDH hydroxide layer thickness is

relatively constant, little changes are observed as a function of cation composition. On the contrary, the gallery height depends on the size and orientation of the anion, [59-61] as well as on the layer charge density i.e. *x* value determining the interlayer packing (**Figure 1-11** (a))[62-64] and for some anions, on the degree of hydration[65-67].

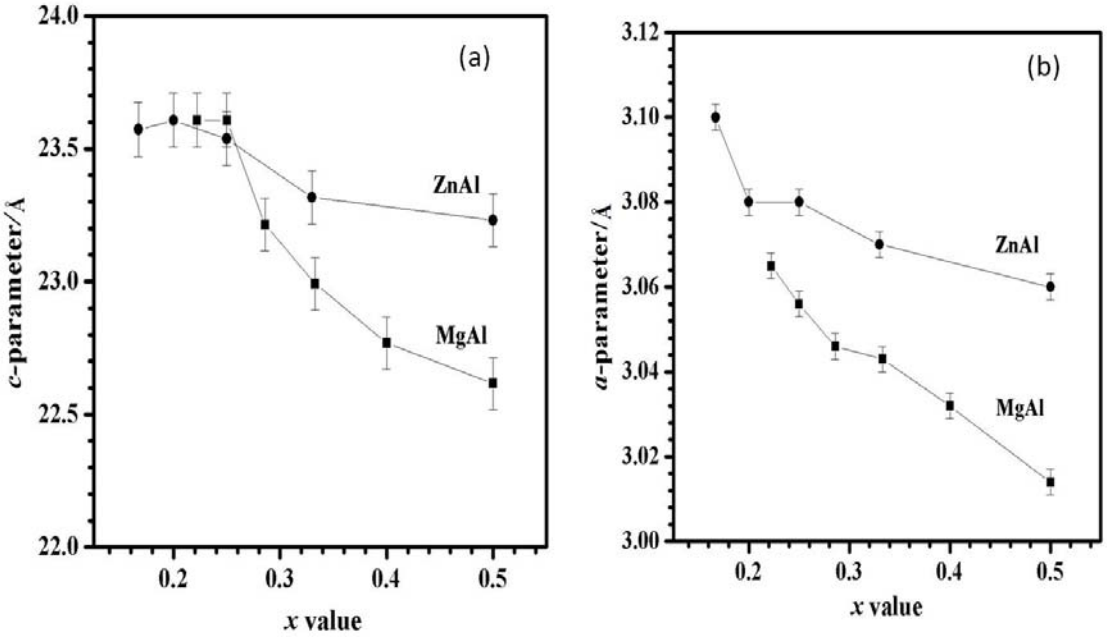

Figure 1-11**:** Variation of the hexagonal unit cell parameters of ZnAl-CO_3 and MgAl-CO_3 LDH with *x* value (M^{3+}/ (M^{2+}+M^{3+})). (ref. 3)

The *110* reflection can be used to estimate the *a* parameter of the unit cell, which corresponds to the distance between adjacent metallic cations within the hydroxide layers. It depends on the metal ionic radius ($r(M^{2+})$ and $r(M^{3+})$) and the *x* value (**Figure 1-11** (b)) according to the following equation[68]:

$$a = \sqrt{2}[(1-x) * r(M^{2+}) + x * r(M^{3+})] \qquad \textbf{Equation } 1\text{-}2$$

In these conditions, from the position of d_{110}, the *x* value can be determined.

1.3.1.2 **Rietveld Refinement**

The presence of broad and asymmetric diffraction lines due to simultaneous effect of small particle size (coherently diffracting domains) and lattice strains in the crystallite (structural defects, stacking faults) often hinder the structural analysis of LDH from the PXRD patterns. Because of these difficulties in calculating and interpreting the X-ray data, some imprecise results on the chemical features and the non-stoichiometric nature of LDH can be obtained.

A few structural studies based on the Rietveld refinement of PXRD patterns have been reported so far, for LDH intercalated with inorganic anions such as Cl^- [69] and CO_3^{2-} [70]. The crystal chemistry of LDH has been studied in details by Belloto *et al.* According to these authors, the disordered distribution of metal cations in LDH hydroxide layers originates from the compression of the layer. The absence of long range order comes from the already close OH-OH approach which prevents the layer distortions brought about the ordering process. In these conditions, long range ordering in LDH can happen only with cations of similar ionic radius as observed for Mg_2Ga-CO_3. [70]

1.3.1.3 **DIFFaX simulations**

DIFFaX (Diffracted Intensities From Faulted Xtals) method intends to interpret the patterns resulting from randomized stacking sequences.[71] In the case of LDH compounds, DIFFaX simulations of LDH have shown that the structural disorder contributes to the excessive and non-uniform broadening of diffraction lines and different types of disorder lead to the broadening of different sequences of reflection peaks.[72-74] For example, stacking faults broaden the *h0l*/*0kl* reflections, interstratification selectively broadens the *00l* reflections and turbostratic disorder broadens the *0kl* reflections. The occurrence of faults can be quantified by a “fault probability” (FP) between the rhombohedral and the hexagonal stacking. For instance, in the case of Mg_5Ga-CO_3, a FP value of 0.6 was

reported corresponding to a random layer sequence of 60° rhombohedral stacking and 40° hexagonal stacking (**Figure 1-12**). [70]

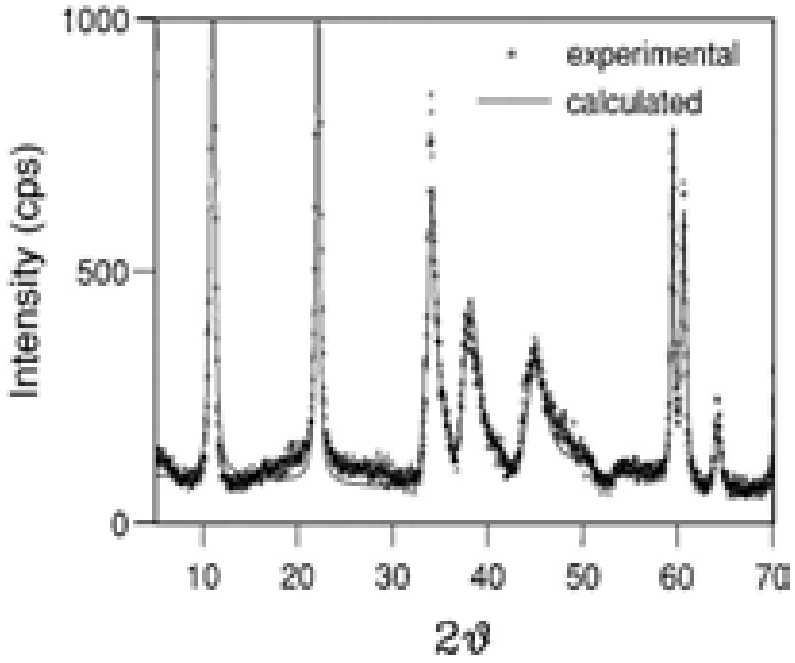

Figure 1-12**:** Comparison of X-ray powder diffraction patterns of measured $Mg_5Ga\text{-}CO_3$ LDH and a DIFFAX simulated pattern with randomized 60 ° rhombohedral stacking and 40 ° hexagonal stacking(Ref. 70).

1.3.1.4 **The electron density distribution**

In the case of hybrid LDH materials, the relative large number of *00l* reflections observed related to the large size of the intercalated anions, may allow to probe the structure of the interlayer space projected along the *c*-axis *via* Fourier transform analysis. [75-79]

Indeed, the one-dimensional electron density maps along the *c*-axis can be obtained from the following equation for centrosymmetric structures:

$$\rho(z) = \sum_{l=0}^{\infty} F_{00l} \cos(\frac{2\pi lz}{c}) \qquad \textbf{Equation } 1\text{-}3$$

and $F_{00l} = exp\{l\varphi(00l)\}\left|\sqrt{I(00l)}\right|$, where *l*, F_{00l}, *c*, φ, and I are the peak numbers (*00l*) of the diffraction order, the structure factors of the *00l* reflections, the layer distance in *c* direction, the phase and peak areas, respectively. The F_{00l} factors were derived from the intensities of a series corresponding *00l* reflection peaks corrected for Lorentz-polarization effects. The sign of the structure factor is obtained from the scattering contributions of the layers, assuming that the contribution of the intercalated anions is relatively small.

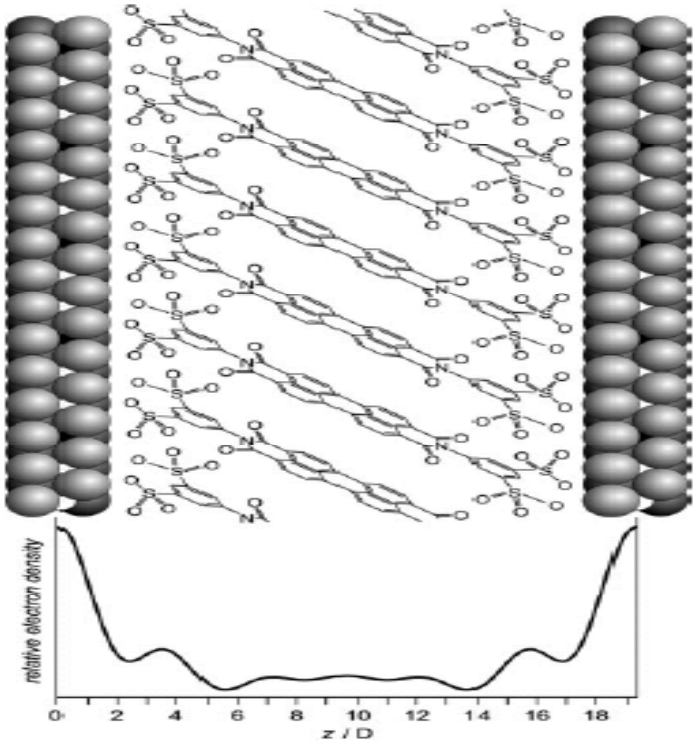

Figure 1-13**:** Model of the structure of Mg_2Al-PBITS and Zn_2Al-PBITS LDH together with the one-dimensional electron density projection along *c* axis. See ref. 80.

Successful applications of one-dimensional electron density distribution are reported on the structural studies of hybrid LDH materials[80-85]. For example, the structural model (**Figure 1-13**) of Mg_2Al-PBITS and Zn_2Al-PBITS LDH (PBITS = *N*, *N'*-di(phenyl-3, 5-disulfonic acid)perylene-3, 4, 9, 10-tetracarboxydiimide) was underpinned by the calculation of the one-dimensional electron density distribution along *c*-axis based on six and five *00l* reflections, respectively. [80] The highest electron density at *ca.* *z* = 3.5 Å and

15.5 Å results from the sulfate groups containing the most electron-rich atoms and the lowest electron density at *ca*. *z* = 5.5 Å and 13.5 Å is assigned to the N-C single bond. The broad region of medium electron density in the middle gallery is caused by the aromatic systems.

The one-dimensional electron density maps of Ca_2Al-VBS [83] and Zn_2Al-VBS [84] (**Figure 1-14**) have also been reported, calculated from the powder X-ray diffraction data. The calculations clearly indicate that VBS molecules in Ca_2Al-VBS and Zn_2Al-VBS are vertically orientated towards the hydroxide layers and the formation of intertwinned single layers of VBS makes the vinyl groups more suitable for a subsequent in situ thermal polymerization reaction.

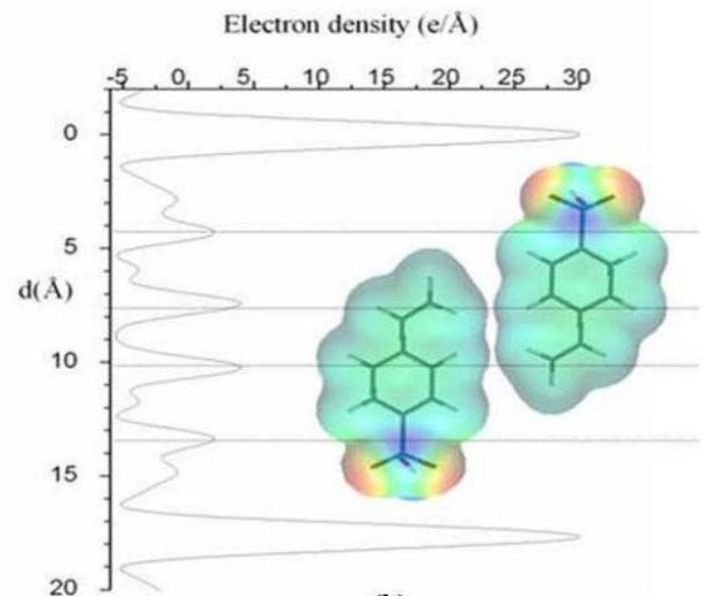

Figure 1-14: Model of the structure of Zn_2Al-VBS with the one–dimensional electron density map along the *c* axis. (ref. 84)

1.3.2 Microscopy

1.3.2.1 **Scanning electron microscopy (SEM) and transmission electron micro-scopy (TEM)**

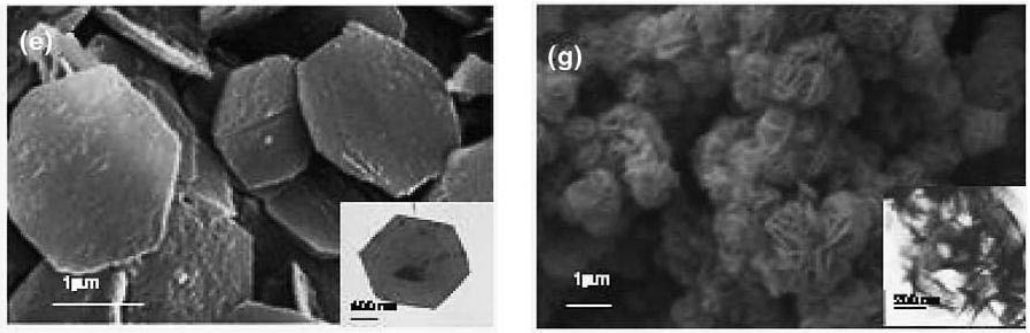

(a) (b)

Figure 1-15: SEM images of LDH obtained under different conditions: (a) Mg_2Al-Cl under urea thermal decomposition; (b) Ni_2Al-Cl under urea thermal decomposition. Inset images are the corresponding TEM. See ref. 88.

SEM and TEM provide general pictures of textural and crystal morphologies of LDH intercalates. LDH usually shows an hexagonal platelet morphology (**Figure 1-15** (a))[86, 87] and a sand rose aggregation of the hexagonal platelets (**Figure 1-15** (b)) [88]. Recently, Hu and O'Hare[89] have obtained Mg_2Al LDH with novel morphologies shown in **Figure 1-16**. system. A reverse micelle/ microemulsion system made of NaDDS (sodium dodecyl sulfate) and an organic solvent like isooctane utilized as nanoreactors have been used to produce these novel LDH particle morphologies. The starting nanoplatelet morphology evolves towards a belt-like morphology upon to the addition of a triblock copolymer to the above mixture while a rod-like morphology was observed after heating for 24 hours. Sun *et al*. also employed TEM and HRTEM (High Resolution TEM) to characterize the $MgAl_2O_4$ spinel structure as nanoplatelets and nanorods obtained from Mg-Al LDH after an hydrothermal and calcination treatments [90].

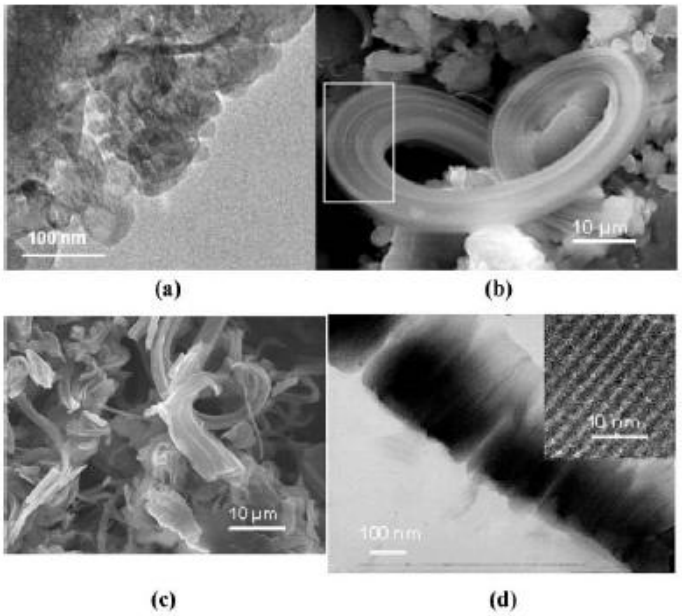

Figure 1-16**:** (a) TEM image showing Mg_2Al nanoplatelets; (b) SEM image showing a belt-like structure; (c) SEM and (d) TEM images of the rod-like structures. See ref. 89

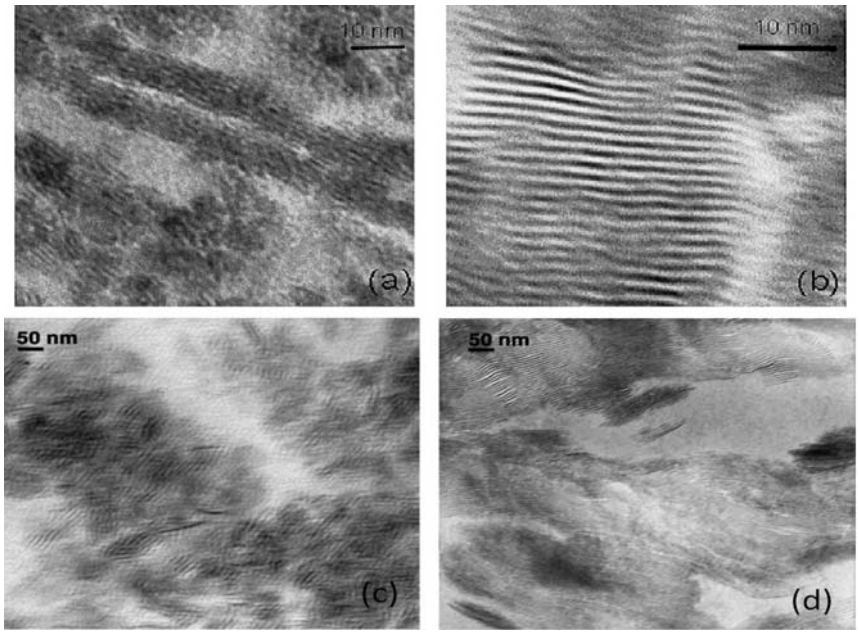

Figure 1-17**:** TEM images of (a) Zn_2Al-PyB, (b) Zn_2Cr-PyB, (c) Zn_2Cr-2-TPC and (d) Zn_2Al-2-TPC. PyB = 4-(1*H*-pyrrol-1-yl) benzoate anions and 2-TPC = 2-thiophenecarboxylate anions. See ref. 91 for (a) and (b) and ref. 92 for (c) and (d).

HRTEM can allow the observation of the interlayer distance as exemplified in **Figure 1-17** with the TEM observation of PyB (4-(1*H*-pyrrol-1-yl) benzoate anions) and 2-TPC (2-thiophenecarboxylate anions) intercalated into LDH. [91, 92] TEM is also extensively used to study the exfoliated structure of LDH[93] as well as the nanoscale dispersion of organic modified LDH in polymer [94].

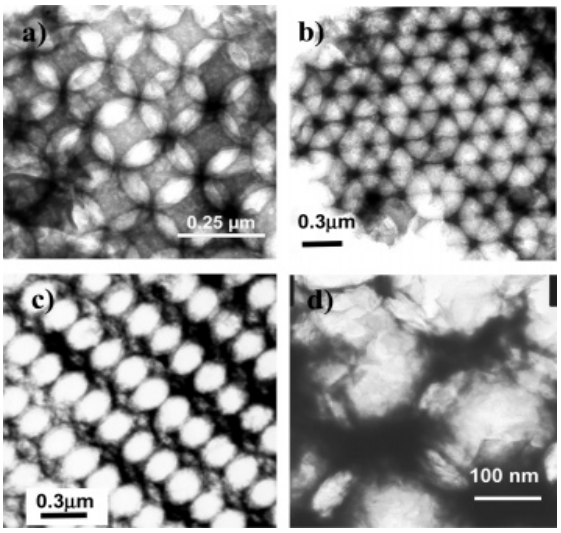

Figure 1-18: Tilting TEM graphs of macroporous Hydrotalcite sample showing the (a) [100], (b) [111], and (c) [211] directions indexed according to a fcc lattice and (d) TEM image showing the wall structure. See ref. 95.

On the other hand, Geraud *et al.* have synthesized three-dimensional ordered macroporous LDH using self-assembled colloidal crystal template and these authors have used tilting TEM images (**Figure 1-18**) to evidence the three-dimensional structure which may be related to planes of the original face-centered cubic (fcc) array of sphere [95].

1.3.2.2 **Fluorescence Microscopy**

Quite recently, the adsorption and desorption processes of a carboxylated perylene imide [N-(2, 6-diisopropylphenyl)-9-(4-carboxyphenyl) perylene-3, 4-dicarboximide, PMI-COOH] on an individual $[LiAl_2(OH)_6]OH$ LDH have been investigated by means

of in situ fluorescence microscopy.[96] The results clearly indicate that the exchange reaction of the carboxylate anions starts at the edge of LDH crystals and then is followed by diffusion inside the interlayer domain as shown in **Figure 1-19**.

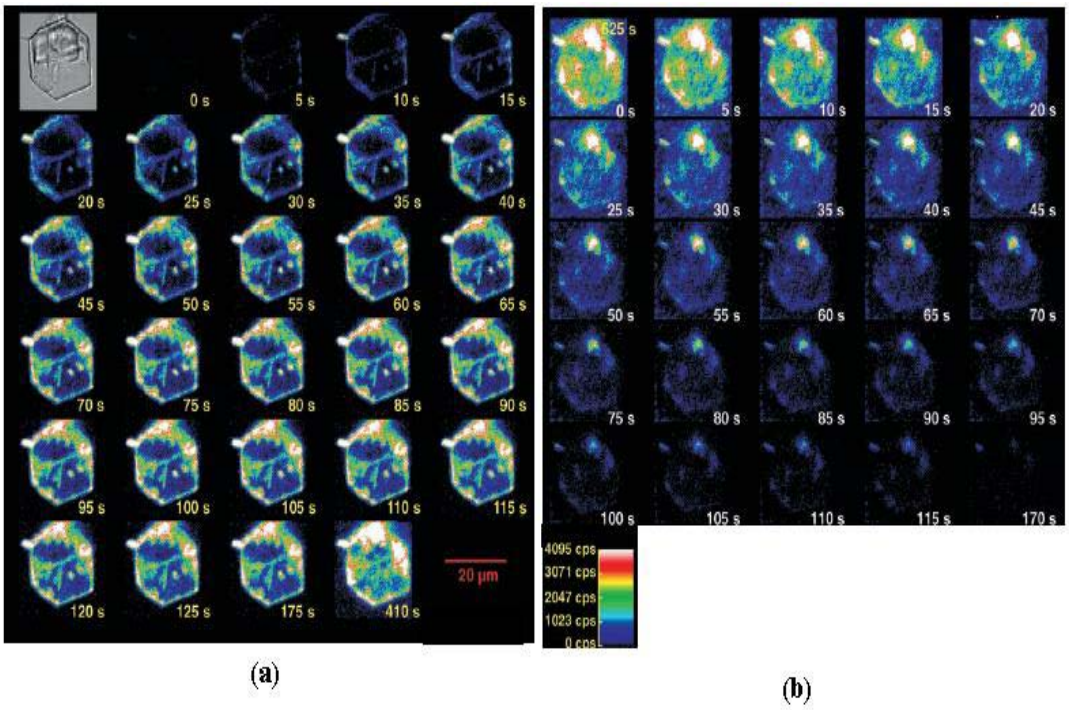

Figure 1-19**:** Time-dependent sorption of PMI-COOH on an individual LDH particle. (a) At time zero, 4 µL of a 0.13 mM PMI-COOH solution in MeOH are added to 996 µL of 50:50 MQ: MeOH above the LDH crystals, resulting in a 520 nM concentration. The fluorescence intensity is represented in false-color mode. (b) After 625 s, 100 µL of a saturated aqueous Na_2CO_3 solution are added to initiate PMI-COOH desorption, and the time is reset to 0 s. The transmission image is given in grey. See ref. 96.

1.3.2.3 **Atomic Force Microscopy (AFM)**

AFM has been used to evidence the adsorption of anions on the surface of LDH. For instance, a two-dimensional repeat unit with $a = 3.1 \pm 0.2$Å, $b = 3.1 \pm 0.2$Å and $\alpha = 58 \pm 3^o$ in **Figure 1-20** has been observed on the AFM image of the crystal surface of $[Mg_6Al_2(OH)_{16}](CO_3)_{0.5}Cl{\cdot}2H_2O$ LDH contacted with an aqueous solution of Na_2SO_4.[97] The use of AFM was also reported by O'Hare *et al.* for the characterization of single Mg_2Al- LDH layers coated in DDS (dodecyl sulfate) anions (**Figure 1-21**).[98]

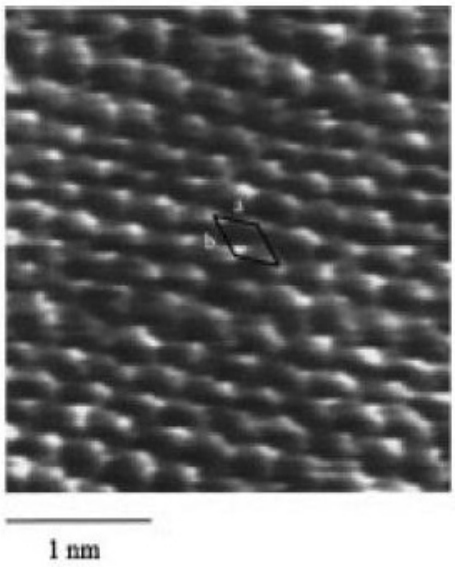

Figure 1-20: AFM image of a Hydrotalcite crystal $[Mg_6Al_2(OH)_{16}](CO_3)_{1/2}\cdot Cl\cdot 2H_2O$ in contact with an aqueous solution of 0.1 M Na_2SO_4 showing the unit lattice of a = 0.31 ± 0.02 nm, b = 0.31 ± 0.02 nm, and α = 58 ± 3°. See ref. 97.

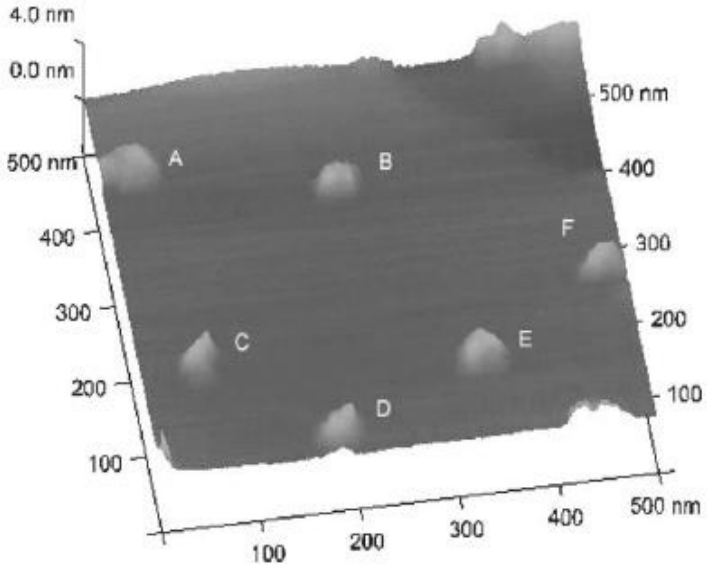

Figure 1-21: AFM image of the $[Mg_2Al(OH)_6](DDS)\cdot yH_2O$ monolayers. Individual particles are marked A-F. See ref. 98.

1.3.3 X-ray Absorption Spectroscopy (XAS)

XAS includes X-ray Absorption Near-Edge Spectroscopy (XANES) and Extended X-ray Absorption Fine-Structure (EXAFS) and supplies information concerning the local coordination and the chemical state of the absorber atom. As for NMR, this technique is very selective, since the absorption spectrum is directly related to the nature of the absorber atom.

The technique provides fine characterizations at a local scale: atomic coordination (i.e. type of neighboring atoms, bond length and coordination numbers) and chemical/oxidation state. The back scattering intensity for a given couple absorber/backscatter distance of *R* is as follows:

$$\aleph(\boldsymbol{k}) = \sum_{\boldsymbol{j}} \frac{\boldsymbol{N_j f_j(k) e^{-2k^2\sigma_j^2}}}{\boldsymbol{kR_j^2}} \mathbf{sin}[\boldsymbol{2kR_j + \delta_j(k)}] \qquad \textbf{Equation } 1\text{-}4$$

where $f(k)$ (the scattering amplitude) and $\delta(k)$ (the phase-shift) are photo-electron scattering properties of the neighboring atom, which depend on atomic number Z of the scattering atom. *R* (distance to neighboring atom), *N* (coordination number of neighboring atom) and σ^2 Debye-Waller factor can be determined by refinement.

In the case of LDH, XAS first was used to study the local order within the hydroxide layers as no long-range order (super-lattice) was thus evidenced for most compositions. Recently, this technique has been used to evaluate the distribution of Ni^{2+} and Ga^{3+} cations in the Ni-Ga LDH sheets for different ratios of Ni^{2+}/Ga^{3+} at the Ni and Ga *K*-edges (**Figure 1-22**), indicating that higher Ni/Ga ratio leads to a more ordered environment for Ga and less ordered for Ni.[99] Another study reports the use of XAS at the Co and Al *k*-edges for Co_RAl LDH (*R* from 2 to 5) indicated that *ca.* 30% Co^{2+} is oxidized to Co^{3+} and concomitantly some of Al^{3+} depart from the hydroxide layer for Co_5Al initial composition LDH.[100] The same authors studied the fine local structure of tetravalent cation in the systems: MgAlZr, MgAlSn and CoAlSn LDH by means of XAS at the Sn and Zr *k*-edges and proved that Zr^{4+} and Sn^{4+} cations are not

incorporated into LDH structure, but, in contrary to previous assumptions[101, 102] form amorphous oxides as nanodomains[103] and the phase segregation was observed directly by TEM [104].

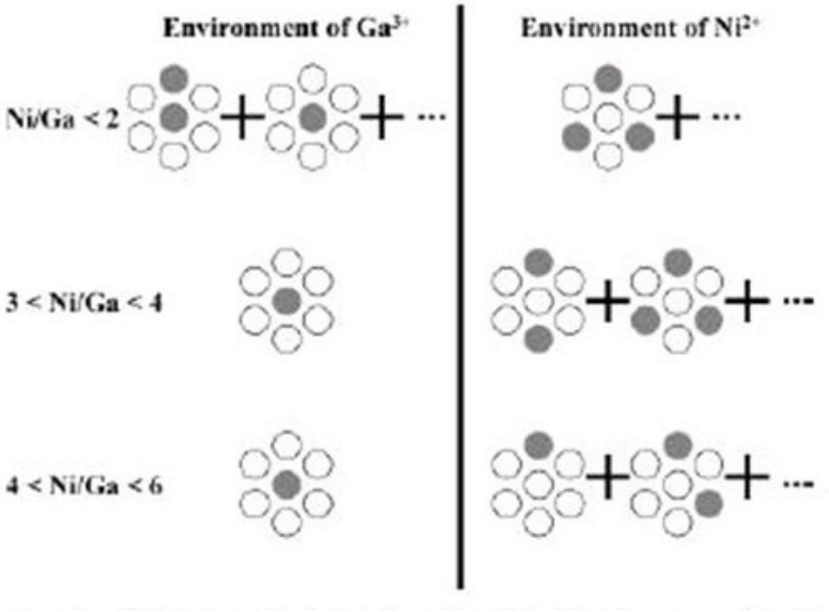

Figure 1-22: Schematic distribution of divalent and trivalent metals in LDH sheets for various Ni^{2+}/Ga^{3+} ratios. Grey circles: Ga^{3+} cations and open circles: Ni^{2+} cations. See ref. 99.

1.3.4 Infrared and Raman spectroscopy

Infrared (IR, usually referred to the mid-infrared in the range of 4000-300 cm^{-1}/wavenumber) and Raman spectroscopy have been mainly employed to study the structural accommodation of interlayer species and hydrogen bond network in LDH, particularly for oxo anions such as CO_3^{2-}, NO_3^{2-}, SO_4^{2-} and CrO_4^{2-} and organic carboxylate anions. [105-107] A relatively detailed assignment of the IR and Raman spectra of $(Mg, Zn)_3Al\text{-}CO_3$ LDH at 25 ℃ and in situ temperature during heat-treatment have been reported.[108-111] The Raman spectra show that water in LDH is hydrogen bonded to the interlayer anions and the hydroxyl surface thus bridging between the MOH surface to the carbonate anions.

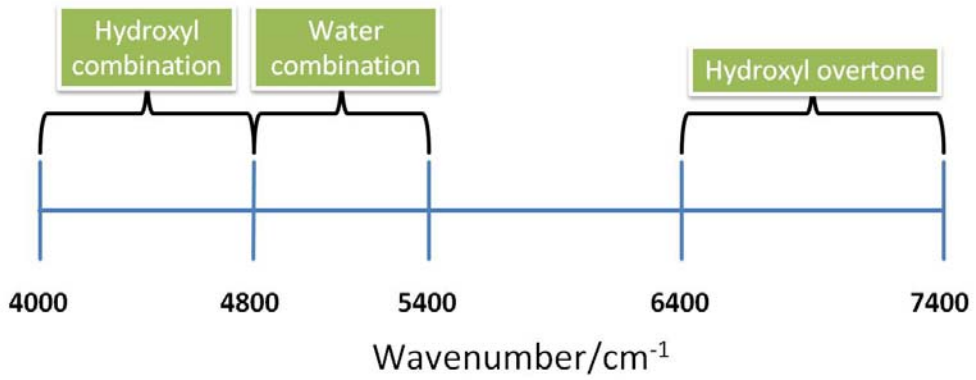

Figure 1-23: Three Near-IR spectral regions of interest for $M_3Al\text{-}CO_3$ (M = Mg, Zn or Ni) LDH. See ref. 113.

Compared to the mid-infrared, Near-IR (NIR, 12500-4000 cm^{-1}) has the higher sensitivity to the OH group environment and has been widely used to study other clay minerals i.e. kaolinite and montmorillonite.[112] On the contrary, there are only few reports of NIR for LDH characterization. Frost *et al.* consider three NIR spectral regions regarding $M^{II}_3Al\text{-}CO_3$ (M = Mg, Zn or Ni) as presented in **Figure 1-23** with a net distribution between the hydroxyl bands of the water and those from M-OH units.[113] These authors also indicate that NIR would be a potential tool to better understand the interactions between the hydroxyl surface and the interlayer anions.

1.3.5 Nuclear Magnetic Resonance (NMR)

Nuclear magnetic resonance (NMR) spectroscopy is an effective technique in studying the structural environments and dynamical behavior due to its unique ability to simultaneously probe element-specific local structure with high resolution and to investigate atomic and molecular motion. [114-116] NMR has been widely used to study inorganic LDH interlayered anions such as $^{13}CO_3^{2-}$ [117, 118], $^{1, 2}H_2O$ [119], $^{35}Cl^-$ [119, 120], $^{15}NO_3^-$ [120], $^{77}SeO_4^{2-}$ and $^{77}SeO_3^{2-}$ [121], $H_5B_3O_8^{2-}$ and $H_4B_4O_9^{2-}$ (^{11}B)[122] and organic anions such as carboxylate anions[123-127] and amino acids[128] as well as ^{27}Al and ^{24}Mg ions within the hydroxide layers [129]. On the other hand, for organic intercalates, NMR spectra enable a distinction to be made between dissociated and undissociated

carboxylate anions by means of the accurate calculation of the chemical shifts.[118] Furthermore, F. Leroux *et al.* have used ^{13}C NMR to study the in situ polymerization of the vinyl benzene sulfonate anions in the interlayer of Ca_2Al LDH, evidenced by the disappearance of the vinyl bond in 200 ℃.[130]

1.3.6 Molecular modeling and structure simulations

Understanding and predicting the properties of LDH require the exact knowledge of their structure. However, as already said in the previous sections, LDH compounds are polycrystalline materials. Because of structural disorder and small particle size, X-ray reflections tend to be broad and structural refinements from PXRD data have provided only limited resolutions. Consequently, interlayer arrangements are often postulated from the interlayer spacing determined from PXRD patterns, compared to the optimized minimum energy geometry of the free ion molecule. It is well known that interlayer arrangements depend strongly on the interlayer water content, the size of the intercalated guest and the charge density of the hydroxide layers influencing the packing of the interlayer region. Even the amount of interlayer water is difficult to determined since some water molecules are also on LDH particle surfaces and are indistinguishable from interlayer water in thermal analysis. Other techniques such as FT-IR, Raman, EXAF and NMR spectroscopes etc. have been widely used to characterize LDH (see previous sections) but these give limited information about arrangement of guests within the interlayer space. Therefore, for most LDH, the arrangement of interlayer anions and water molecules is not well understood and the structure of hydroxide layer is still under discussion. As a consequence, molecular modeling methods have been increasingly used in the past decade to simulate LDH structure and to better understand the interlamellar arrangement of intercalated organic molecules. [131-141]

The application of any computational molecular modeling techniques requires the use of interactomic potentials (force fields) that accurately account for the interactions

of all atoms in the modeled system. Yet, because of the structural disorder of most LDH, the force field parameterization is often not optimal and only qualitative or semi-qualitative structural information are obtained. On the other hand, the well ordered and well known structures of $LiAl_2(OH)_6Cl{\cdot}H_2O$[132] and $Ca_2Al(OH)_6Cl{\cdot}2H_2O$[133] were successfully reproduced by molecular modeling providing accurate set of potentials then used to simulate and better understand structures which have still not been resolved.

Two types of molecular dynamic (MD) simulations of LDH have been carried out so far. First of all energy minimization [132] and MD using generic force-field [131, 135, 136, 139, 140,] have been applied to study LDH crystal structures and to predict the orientation of interlayer anions. A good agreement between experimental and calculated interlayer distance is obtained in all cases, allowing the orientation of the guests to be determined related to the hydration state and the layer charge density.

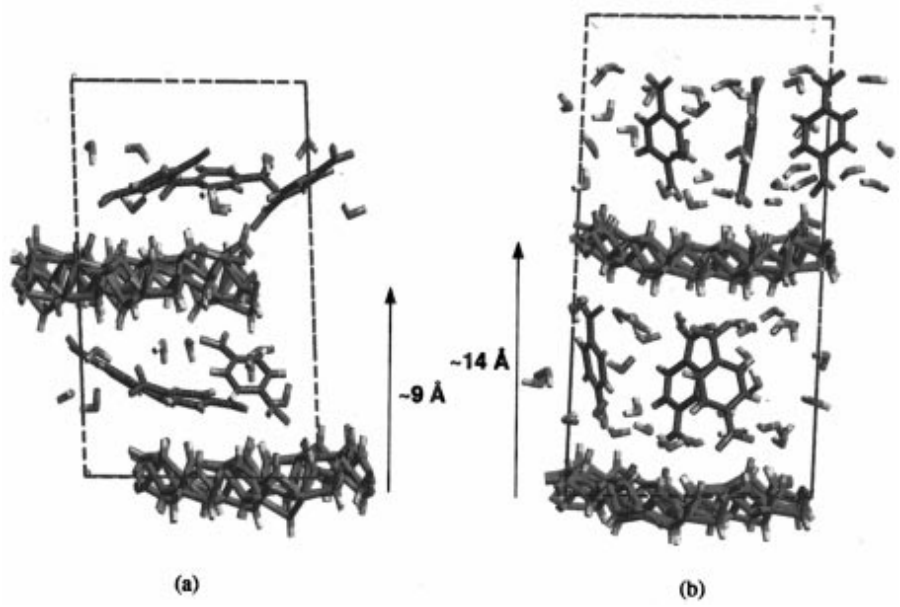

Figure 1-24: Snapshot of a simulation cell, following 40 ps of molecular dynamics at 300 K, containing MgAl(terephthalate) LDH *R*(3) with (a) 16 water molecules and (b) 64 water molecules. See ref. 131.

One of these studies has retained our attention since it concerns the phenomenon of interstratification in Mg_RAl-terephthalate LDH interpreted by the authors as an alternation of collapsed (dehydrated) and expanded (hydrated) interlayers. [135] MD simulations predict a gradual expansion of the interlayer accompanied by a change in the orientation of terephthalate anions from almost horizontal to vertical as the number of interlayer water molecules included in the simulation increased as presented in **Figure 1-24**. For high water content and layer charge, an interlayer separation of 14.0 Å is formed which corresponds to a vertical orientation of the terephthalate anions with respect to the hydroxide layers. For low water content and layer charge, an interlayer separation of 8.4 Å is obtained corresponding to a horizontal orientation of terephthalate. During cycles of dehydration-rehydration, PXRD indeed indicates the presence of the 14.0 Å and 8.4 Å units which coexist in varying proportions depending on the layer charge density and water content; in certain cases, a 22.4 Å interstratified phase is observed consisting of a regular alternation of 14.0 Å and 8.4 Å interlayers. Enthalpic calculations indicated that the symmetric distribution of the water molecules in adjacent interlayers is energetically more stable than either of the asymmetric distributions (**Table 1-1**). Assuming that interstratified phase observed experimentally consists of alternating hydrated and dehydrated interlayers, the authors concluded that this phase is enthalpically metastable. According to the authors, once the interstratified phase has formed, it is long-lived and separated from the equilibrium state by large energy barriers.

Table 1-1: Effect of water distribution on the calculated enthalpy, *H*, and coulombic interaction energy, *C*, of MgAl(terephthalate) *R*(2) LDH with 20 water molecules per simulation cell (ref. 131).

Water distribution per interlayer	***H*/kcal· mol^{-1}**	***C*/kcal· mol^{-1}**
10:10 (symmetric distribution)	-8590 ±20	-17 950 ±20
15:5 (asymmetric distribution)	-8540 ±20	-17 900 ±20
20:0(asymmetric distribution)	-8531 ±20	-17 870 ±20

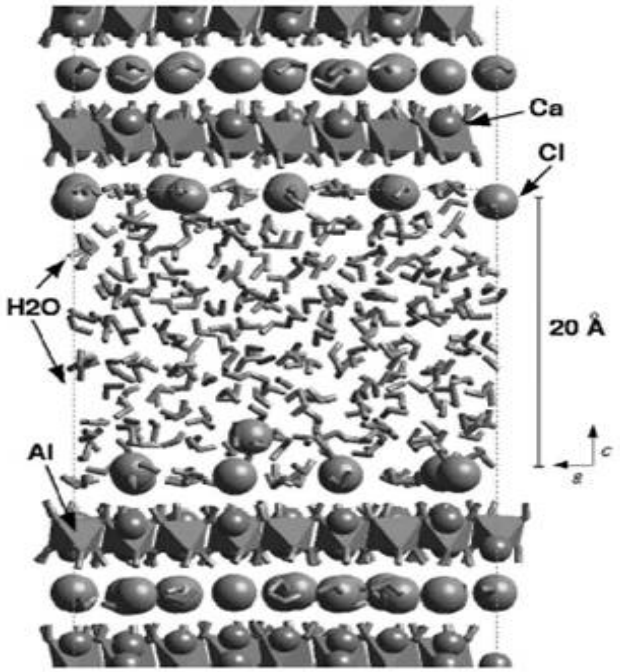

Figure 1-25: A snapshot of the simulation of hydrocalumite/water interface at 25 ℃. Octahedra portray Al layers. Small spheres are Ca; larger spheres are Cl. See ref. 133.

Other MD studies use the CLAYFF force field approach suitable for the simulation of hydrated and multicomponent mineral systems and their interface with aqueous solution. A main difference with other MD is that all atoms are considered complete movable allowing a more accurate representation of the dynamics of such phenomena as hydrogen bonding, adsorption and surface complexation. Using CLAYFF, Kalinichev *et al*. have studied the structure of hydrocalumite $Ca_2Al(OH)_6Cl{\cdot}2H_2O$ also known as Friedel's salt in cement chemistry and determined the dynamical behavior of Cl^- and H_2O molecules in the interlayer space and on the particle surface (**Figure 1-25**). [133] In contrast to the highly ordered arrangement of the interlayer water molecules deduced from the single crystal structure refinement, the simulations reveal significant dynamic disorder in water orientations. At all temperatures between -100 and +300 ℃, the water molecules undergo libration around an axis perpendicular to the layers. This result in breaking and reformation of hydrogen bonds with the neighboring Cl^- anions is in total agreement with ^{35}Cl NMR measurement. Besides, different coefficients of Cl^- anions and water molecules were calculated (**Table 1-2**). The diffusion coefficient of Cl^- anions as an outer-sphere

surface complex is at least 10 times that of interlayer Cl^- anions but is about an order of magnitude less than that of Cl^- in solution.

Table 1-2: Calculated diffusion coefficients of interlayer and surface species (cm^2/s). see ref. 133.

	Cl^-	**H_2O**
Interlayer	$<<10^{-7}$	$<<10^{-7}$
Surface (inner sphere)	8.1×10^{-7}	5.0×10^{-6}
Surface (outer sphere)	2.6×10^{-6}	1.3×10^{-5}
Bulk NaCl solution	1.1×10^{-5}	1.8×10^{-5}

1.4 **Applications of LDH**

Figure 1-26**:** Possible applications of LDH materials. See ref. 142.

On the basis of their structure and properties, a wide range of technologically important applications have been identified for LDH materials and summarized in **Figure 1-26**. [142] Recently, several reviews have been devoted to the applications of LDH as

catalyst or catalyst supports, sorbent for pollutant, vector for biological molecules, electrochemical sensors and filler in polymers.[143-145]

1.4.1 Catalysis

By far, the most important potential application of LDH is in the field of heterogeous basic catalysis due to their basic properties and the formation of homogeneous and stable dispersion of metal ion. Mixed metal oxides obtained by thermal decomposition of LDH can promote base-catalyzed reactions such as polymerization[146], condensation[147] and alkylation[148]. LDH can also be used as catalyst support for hydrogenation and stream reforming catalysts[149, 150]. On the other hand, the catalytic activity of uncalcined LDH has been scarcely studied owing to the low thermal stability of the layered structure and to the low specific surface area. Yet, they have been found to catalyze the halide-exchange reaction between alkyl halide. [151]

1.4.2 Sorbent for pollutant

The anion-exchange capacity of LDH higher than that of cationic clays makes them promising materials for the elimination of ecologically undesirable inorganic and organic anions. The removal of chromate[152, 153], nitrate, phosphate, arsenate or vanadate anions[154, 155] as well as humic substances[156, 157]and radioactive elements[158, 159] from contaminated water or waste streams by LDH have been demonstrated. Also numerous papers have reported the use of LDH or their calcined derivatives as organic contaminate adsorbents such as the adsorption of phenolic compounds[160, 161] and pesticides[162-165].

1.4.3 Vector/drug release

Hydrotalcite $Mg_6Al_2(OH)_{16}CO_3 \cdot 4H_2O$ is known to be an effective antacids,[166] but other bio-applications were recently reported. Many common nonsteroidal anti-inflammatory drugs[167-171] such as Diclofenac, Ibuprofen, Gemfibrozil and Naproxen have been incorporated in the interlayer space of LDH compounds via anion-exchange reaction as well as bio-related polymers and large bio-macromolecules such as polyaspartate[172], alginate[173] and DNA[174]. Apart from a chemical curiosity, the drug intercalated LDH hybrids as a controlled drug-release system could control the point of release and pharmokinetic profile by tuning the desired composition in the host layers. Besides, the host layers improve the long-term stability and storage since these drug molecules are isolated from the environment by the hydroxide layers. Another application largely described by Choy *et al.* in the literature is the use of LDH as DNA delivery system. Indeed, these authors have shown that LDH can protect DNA from degradation and the charge neutralization enhances the transfer of DNA-LDH hybrid into mammalian cells through endocytosic.[175]

1.4.4 Filler in polymer

LDH can enhance the mechanical properties, gas permeability and be of interest in polymer electrolyte. The incorporation of polymer between LDH galleries proceeds via different pathways such as coprecipitation, exchange[176], in situ polymerization[177]. The latter method presents the advantage to tune the tactility and the molecular weight of the generated polymer by varying the layer charge density and the particle size of the host structure, respectively. [20, 178, 179] A large variety of LDH/polymer systems can thus be obtained, thermally more stable than the pristine inorganic compound leading to potential applications in fire-retardant composites.[180] LDH/polymer nanocomposites can also be served as LDH inorganic fillers dispersed into a polymer. [179] For example, nanoparticles of Zn_3Al-dodecyl sulfate dispersed in the linear low density polyethylene (LLDPE) were found to enhance the thermal and mechanical properties of pure LLDPE.[181]

1.4.5 Nanoreactor

LDH can also provide a confinement for the organic moiety suitable after a charring process to the formation of high surface area (2300 $m^2 \cdot g^{-1}$) carbonaceous materials, using the interleaved monomers and polymers between the hydroxide layers of LDH as carbonaceous source.[182] Furthermore, a variety of nanoparticles such as Co, Ni, Pt, PbS, *etc.* have been prepared using LDH materials (Li_2Al, Mg_RAl, $Ni_{0.7}Al$ and $Co_{0.7}Al$ *etc.*) as a nanoreactor intercalated with complex anions containing the desired metal: $[M(EDTA)]^{2-}$ (M = Co^{2+}, Ni^{2+}), $[Pt(OH)_6]^{2-}$ and $[Pb(S_2O_3)_2]^{2-}$.[183-185] With this method, it is possible to avoid the aggregation and the formation of well dispersed nanoparticle was indeed observed.

II. Staging Phenomenon

1.5 **Staging Structure**

The study of multifunctional hybrid materials combining organic and inorganic structures is an emerging research area offering numerous scientific and technological benefits. Lamellar hosts are considered as promising with respect to this multifunctional character due to the possible synergetic effect between the host and the guest in the interlayer region. The functions of stabilization and protection can be viewed as synergetic effects as reported for the incorporation of organic chromophores with optical functions such as color, fluorescence, or nonlinear optical properties in inorganic hosts like zeolite [186] and LDH [82].

Layered inorganic materials such as hydroxide based compounds $M_2(OH)_3A \cdot 2H_2O$ (M = Co and Cr, A = anions),[187-190] bimetallic oxalate compounds $[cation][M^{II}M^{III}(ox)_3]$ (M^{II} = Mn, Fe, Co and Cu; M^{III} = Cr and Fe),[191] Zirconium phosphate,[192] phosphonate [193, 194] have been used to prepare nanoscale organic-inorganic layered complexes in efforts to

develop new functional materials with co-operative phenomena between the organic and the inorganic layers.

Some studies on the effects of the intercalation into layered hosts of species of interest in the field of magnetism, non-linear optics sensing devices and molecular recognition, can be found in the recent reviews.[195 - 199] In this respect, the staging phenomenon as encountered in a few occasions in clay minerals with a stacking of two or more kinds of layers, is a promising way to increase the multifunctional character of layered materials. Staging phenomena originally refer to intercalation on graphite system and it is often viewed as a way to reduce the energy barrier to an intercalation reaction. The literature describing graphite intercalation reactions contains numerous examples of staging intermediates involving the intercalation of every *n*th layer corresponding to the *n*th stage compound. Such a staging phenomenon has also been observed but only on a few occasions for transition metal dichalcogenides. In clay minerals, this phenomenon is referred to interstratification and represents the stacking of different kinds of layers. Only a few cases of staging have been reported in clay minerals and the scarcity of this phenomenon in other lamellar hosts than graphite has been rationalized theoretically mainly in terms of stiffness of the host planes.

Theoretical models of staging typically divide the host lattices into three classes from single atom layers like graphite to rigid many atom thick layers as found in clays, transition metal dichalcogenides belonging to the intermediate class.[200] The staging phenomena were first studied on graphite materials and two classical models of staging for graphite system, proposed by Rüdorff [201, 202], and Daumas-Hérold [203, 204] are proposed (**Figure 1-27**(a) and (b), respectively).[205] The former is hardly considered as it cannot interpret transformations from odd to even stages without a deintercalation-intercalation process. Owing to the scarcity of staging phenomena in lamellar materials other than graphite, the lack of staging observation has often been explained due to the rigidity of host planes[206, 207]. Daumas-Hérold thus imagined staging resulting from guest species diffusion towards the crystal center and only possible for flexible layers like the single-carbon honeycomb sheets of graphite. The order of staging is defined as the number of

empty layers between successive filled layers i.e. the stage number *n* indicates the numbers of the host layers between which adjacent intercalated layers are sandwiched.

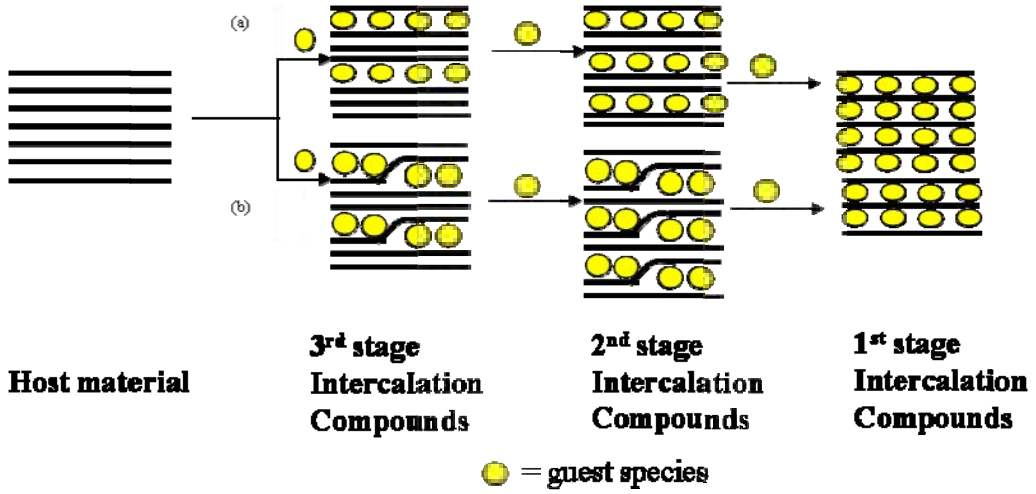

Figure 1-27: Schematic diagram showing the formation of the staged intercalation compounds for layer host material: (a) Rüdorff's model; (b) Daumas-Hérold's model. See ref. 205.

More recently, staging phenomena have been evidenced in LDH system. Kooli *et al.* have reported the occurrence of staging for Mg_2Al-terephtalate (at *ca.* 75 ℃) and Mg_2Al-benzoate (at *ca.* 100 ℃) upon heating.[208] Actually, in these cases, it is not a chemical staging but different interlayer arrangements of the same anions related to different hydration states. On the other hand, O'Hare *et al.* have observed the formation of second-stage intermediate during the intercalation of dicarboxylate anions in $LiAl_2(OH)_6Cl{\cdot}2H_2O$ by means of time-resolved in situ energy-dispersive X-ray diffraction. [209] Mixed hydroxide/azobenzene intercalates have also been obtained by direct coprecipitation in Mg_2Al system.[210]Finally, Taviot-Gueho *et al.* have detected the formation of second-stage intermediates during the anion-exchange reactions of succinate and tartrate anions with chloride anions in Zn_2Cr, Zn_2Al and Cu_2Cr systems.[211]

In the following sections are described the occurrence of staging phenomena in graphite, dichalcogenides, clay minerals and in more details in LDH.

1.6 **Staging Compounds**

1.6.1 Staging Graphite Intercalation Compounds

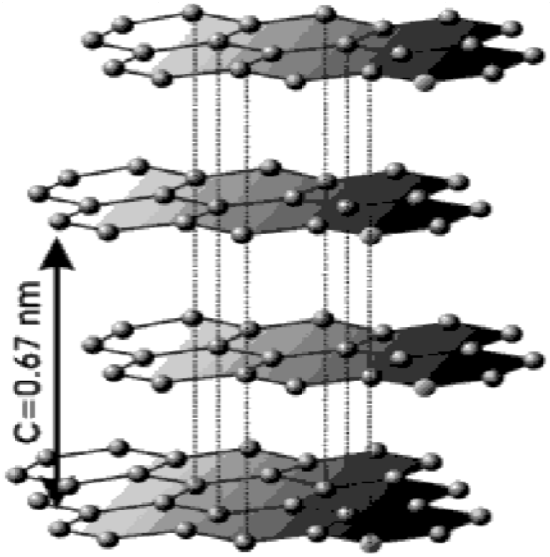

Figure 1-28**:** Structure of graphite, formed by *AB* stacking of graphene sheets. See ref. 212.

Graphite is an allotrope form of carbon consisting of graphene layers stacked by weak van der Waals forces along the *c*-axis in a staggered array with the basic interlayer space of 3.35Å (d_0, *c/2*) in **Figure 1-28**.[212] Since 1841, a great number of graphite intercalation compounds (GICs) have been obtained with a wide variety of guest species such as alkali metals, alkaline earth metals, rare earth elements, halogens, metal halides, metal oxides and acids for applications in many fields i.e. chemistry, physics, material science and electronic and electrical engineering. [212] The feasibility and the degree of intercalation are largely determined by the acidic properties of the intercalates and by the conditions of oxidation of the graphite matrix.[213] For example, strong inorganic acids i.e. HNO_3, H_2SO_4 and $HClO_4$ form highly saturated first-stage GIC while weak acid like CH_3COOH or H_3BO_3 are not intercalated into graphite at all.

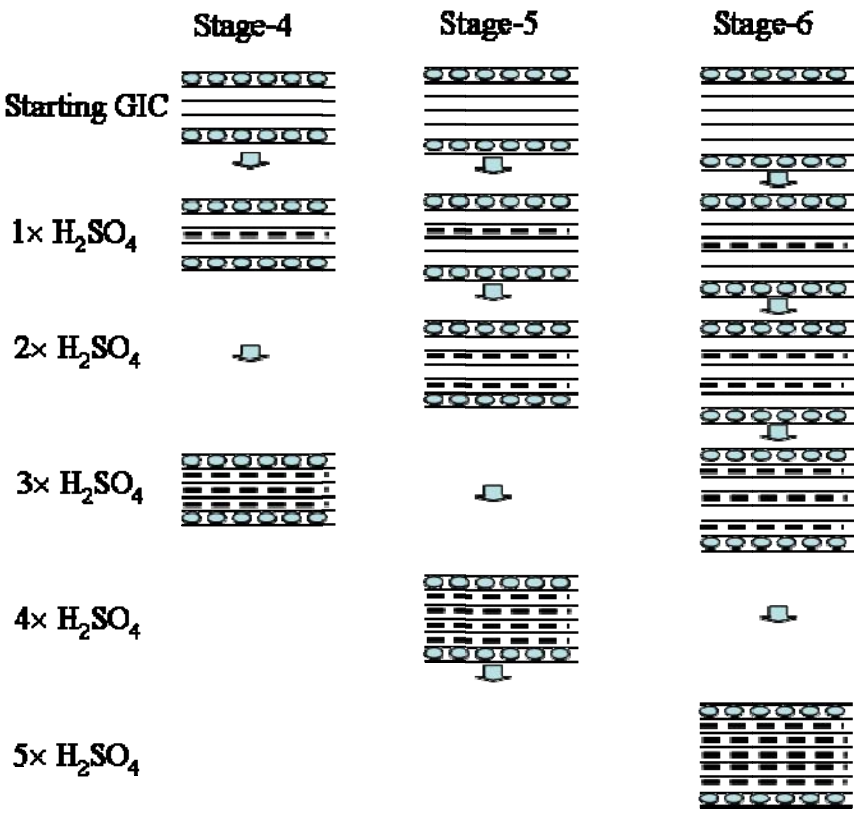

Figure 1-29: The schematic of the bi-intercalation process of H_2SO_4 into stage 4-6 $FeCl_3$-GICs. Circles represent $FeCl_3$ species and dot lines present H_2SO_4. See ref. 215.

The occurrence of staging structures in graphite is attributed to the flexible nature of the graphite sheets (single layer of carbon atom) according to the Daumas-Hérold's model of staging. Two kinds of staging structures are observed in graphite: one type corresponds to interlamellar spaces occupied by guest species and adjacent to empty spaces; in the other type, alternate interlayer spaces are occupied by two different guest species. The latter class refers to graphite bi-intercalation compounds (GBCs),[214] but also includes higher stage than second stage compounds such as third, fourth even sixth stage compounds. For example, Mizutani *et al*. studied the intercalation process of H_2SO_4 into n-1 vacant interlayers in stage n $FeCl_3$-GIC (n = 4, 5 and 6) according to the calculated intensities of the X-ray diffraction lines.[215] They found that the repulsion forces between $FeCl_3$ and H_2SO_4 layers and between two adjacent H_2SO_4 layers govern the intercalation process in term of the minimum repulsion (**Figure 1-29**), the latter force being stronger than the former. On the other hand, the electrostatic attraction

between negatively charged $MoCl_5$ and positively charged K^+ was responsible for the formation of staging compound during intercalation of K^+ into stage $MoCl_5$-GIC. [216]

Staging graphite compounds have been further investigated as microreactors for inorganic and organic reactions[217] in the interlayer spacing of graphite. It is worth mentioning that the stage number of the starting GICs determines the particle size of fine metallic particles obtained from the reduction of intercalated metal chloride.[218] For organic reactions, most of them were in relation with polymerization. In 1976, Beguin and Setton firstly thus reported the formation of biphenyl from benzene in the interlayer space of a staged graphite.[219]

1.6.2 Layered Dichalcogenides Staging Compounds

Layered dichalcogenides A_nMX_2 (A= alkali metal, M = transition metal, X = S and Se) materials can intercalate a wide range of guest cations and neutral species into the interlayer space between the negatively charged host layers.[220] Staging phenomena occur usually at low concentrations of intercalated guest cations and higher order staged compounds than 2, i.e. 3rd and 4th stage dichalcogenides intercalation compounds have been reported.[221-224] Factors such as the lattice energy, the electrostatic interaction of neighboring cation layers and the energy needed for the separation of the layers upon intercalation, have been considered for the explanation of the occurrence of high order staged compounds at low guest concentrations. Besides, the influence of kinetic factors is suggested as the mechanism of transition from stages with odd numbers to stages with even numbers i.e. from 3rd stage to 2nd stage. Models involving lattice strain mediated interactions and thermodynamic considerations have also been put forward to explain staging phenomena in this system.[225-227] However, these models mainly consider from the point of thermodynamic equilibrium. In fact, even at high temperature a second-stage compound may be formed as for $Cu_{2/3}(NbS_2)_2$.[228]

Moreover, higher stages are not observed if the guest species are of large size such as $(C_5H_5)_2Co^+$ and Ba^{2+} cryptate attributed to the strong mechanical energy needed for the

deformation of layers. The formation of 2nd and 3rd staging intermediates during the reaction process can effectively relax activation energies for the deformation of double or triple sheet packet units. Therefore, the flexibility properties of the sheet units in layered systems also play a significant role explaining the nonexistence of staging for "thick" layers like Ta_2S_2C and MoO_3.[229]

1.6.3 Fluorohectorite Clay Staging Compounds

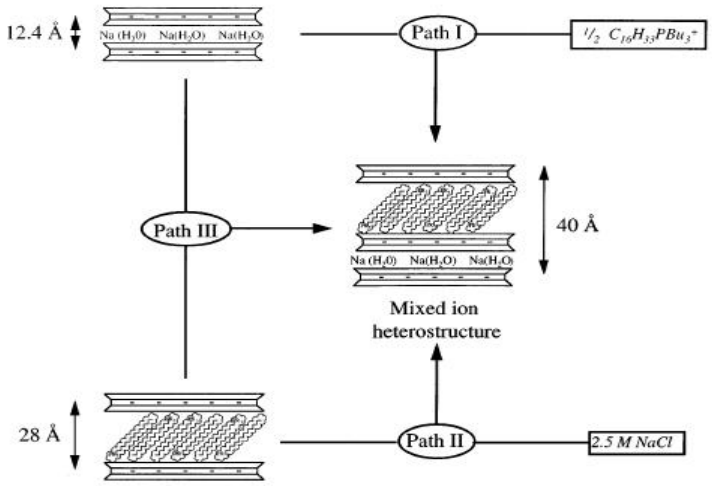

Figure 1-30: Three synthetic approaches to mixed ion heterostructures with regularly alternating galleries. Pathway I involves the addition of half a cation exchange equivalent of surfactant. Route II concerns the treatment of an organo clay with a concentrated NaCl solution while method III simply recombines the two homoionic end member clays. See ref. 230.

Fluorohectorite clays contain examples of 2nd stage heterostructures with distinguishable organic and inorganic galleries stacked in a regularly alternating fashion. W. L. Ijdo and T. J. Pinnavaia studied such fluorohectorite staging structures and established three pathways for explaining their formation (**Figure 1-30)**: pathway I involves the direct addition of surfactant cations of onium and sodium ions in a molar ratio of 0.5:1; pathway II is a reverse approach using a concentrated NaCl solution to treat with a homoionic organoclay; pathway III considers the reaction of equal molar quantities of the two end member homoionic clays in a water suspension.[230]

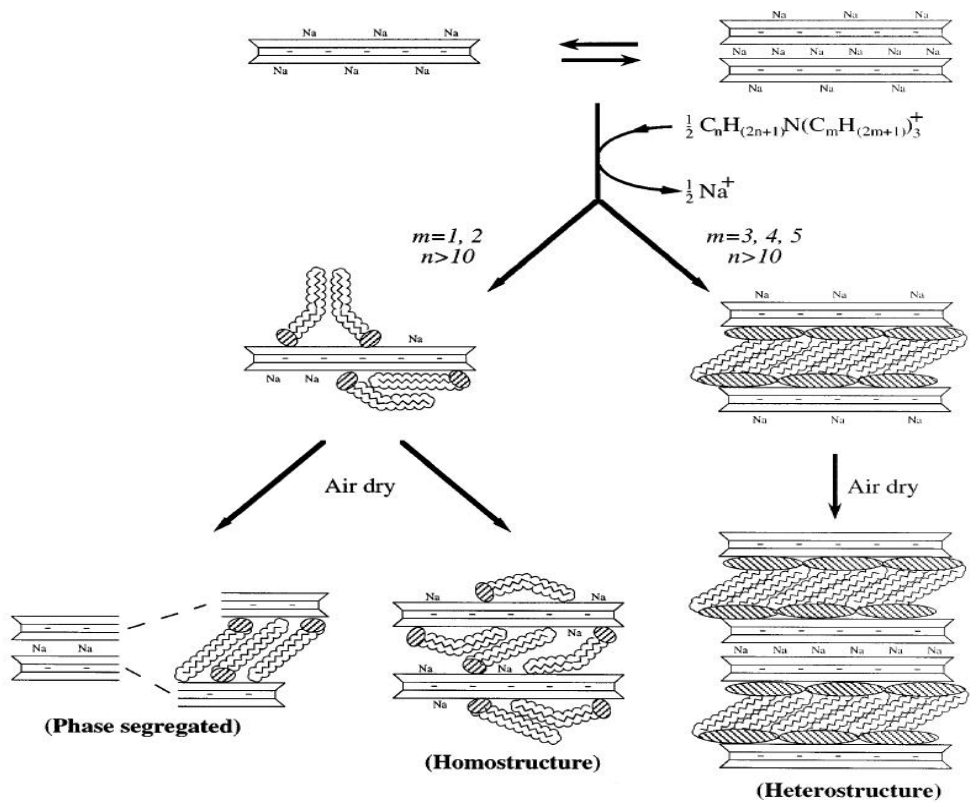

Figure 1-31: Summary of the reaction pathways observed during the intercalation reaction of $C_nH_{(2n+1)}N(C_mH_{(2m+1)})^{3+}$ cations (n ≥10; m = 1-5) into Na+-fluorohectorite leading to heterostructured, homostructured, and phase segregated mixed ion intercalates. See ref. 230.

In particular, the two authors focused on the effect of the onium ion ($C_nH_{(2n+1)}N(C_mH_{(2m+1)})_3^+$) geometry such as chain length and head group size on the formation of such staging materials as described in **Figure 1-31**: the alkyl chain of the onium ion n > 10 and the head group footprint m ≥ 3 favoring the formation of bipolar fluorohectorite staging materials. The formation of such heterostructure has been proposed as a result of the segregation of the hydrophobic organic cations and the hydrophilic inorganic cations on the internal and external surfaces of two-nanolayer tactoids during the ion exchange process.

Further, the same authors also studied fluorohectorite materials intercalated with [$C_{16}H_{33}EBu_3^+$] (E = N or P) onium ions (Q^+) and found that the size and charge of the initial metal ion located in the interlayer region do not play an important role because

this kind of heterostructure formation is not limited to Na^+ only but also available for other inorganic exchange cations such as Ca^{2+}, Ba^{2+}, Al^{3+} and Ce^{3+} ions. [231] When the fraction of onium ions is in the range from 0.33 to 0.50, there is no formation of 3rd stage phase as expected but a 2nd stage phase with alternate interlayers occupied by Na^+ ions and a mixture of onium ions and Na^+ ions as depicted in **Figure 1-32**.

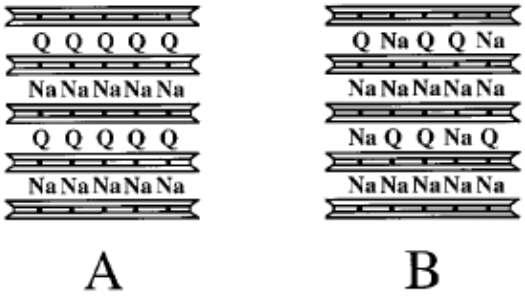

Figure 1-32**:** Schematic illustrations of gallery stacking patters in heterostructured mixed onium ion (Q+)-inorganic (Na+) ion fluorohectorites: (A) regularly alternating galleries of segregated onium and inorganic ions at f_Q = 0.50 (f_Q = $Q^+/(Q^+ + Na^+)$, mol/mol); (B) regularly alternating galleries of homoionic Na+ and alloylike mixed ion (Na+, Q+) galleries at onium ion compositions in the range $0.33 \leq f_Q \leq 0.50$. See ref. 231.

1.6.4 Staging Layered Double Hydroxides Compounds

The phenomenon of interstratification in anionic clays was first reported in 1987 by Drits *et al.* who described the structure of a mixed carbonate and sulfate LDH, a mineral phase consisting of alternating carbonate and sulfate interlayers. [232, 233]

In 1998, by means of in situ energy-dispersive X-ray diffraction (EDXRD) technique O'Hare *et al.* discovered that the intercalation of a variety of dicarboxylate anions (succinate, adipate, fumarate, maleate, L-maleate, phthalate and terephthalate) into $LiAl_2(OH)_6Cl{\cdot}2H_2O$ (hexagonal form, *h*-$LiAl_2$-Cl) proceeds via the formation of a second-stage intermediate with alternate interlayer spaces occupied by different anions, the initial anions i.e. Cl^- and the incoming organic anions. [209] Data for the intercalation of succinate anions into *h*-$LiAl_2$-Cl are shown in **Figure 1-33**. The intermediate decay

of the *001* Bragg reflection due to $LiAl_2$-Cl host (7.65 Å) following the addition of the succinate solution is accompanied by the growth of a reflection at 9.9 Å assigned to the *002* reflection of the second-stage intermediate $LiAl_2$-Succ/Cl (**Figure 1-33** (a)). This value multiplied by two gives the position of the 001 reflection of $LiAl_2$-Succ/Cl *i.e.* 19.8 Å which exactly corresponds to the sum of the interlayer distance of Cl^- anions (7.65 Å) and that of the fully exchanged phase $LiAl_2$-Succ (12.1 Å). Finally, the growth of the fully exchanged (or first stage) product $LiAl_2$-Succ is obtained but not until the intermediate has gone though its maximum and the starting phase $LiAl_2$-Cl has disappeared completely. From the variation of the intensity of the Bragg reflection (**Figure 1-33** (b)), it is possible to calculate the extent of reaction α, I_t / I_{max} (intensity at time t/maximum intensity), as a function of time *t*. The crossing of α(t) curves for $LiAl_2$-Cl and $LiAl_2$-Succ at α = 0 further indicates that the intercalation reaction is a two-step process involving the presence of an intermediate phase.

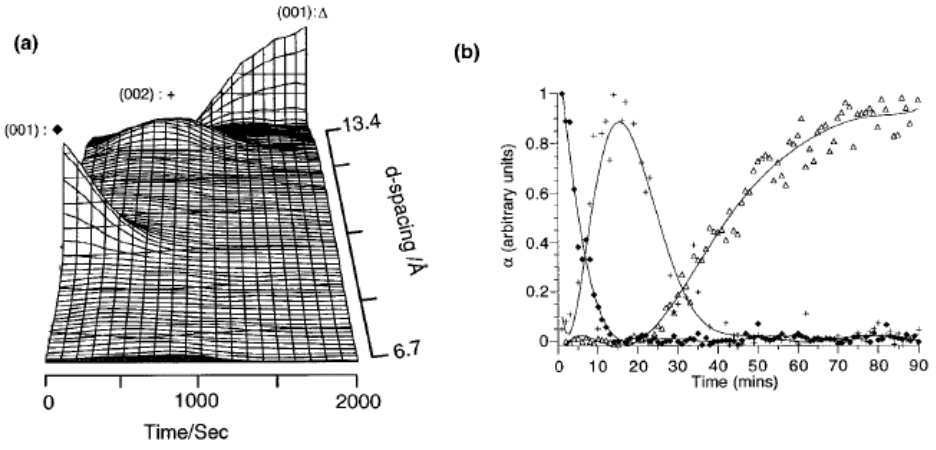

Figure 1-33: Time-resolved, in situ, energy-dispersive X-ray powder diffraction data showing the course of the ion-exchange reaction between $[Li_2Al(OH)_6]Cl{\cdot}H_2O$ and disodium succinate: (a) 3D stacked plot; (b) plot of integrated intensity of *001* reflection of the host (♦), *002* reflection of the second-stage intermediate (+) and *001* reflection of the final phase (Δ) as a function of time. See ref. 213.

Since this first study, these authors have performed several other studies to better understand the factors influencing staging during anion-exchange reactions in $LiAl_2$ LDH system.[234]For instance, they examined the intercalation of phosphonate anions into the hexagonal form *h*-$LiAl_2$-Cl and it was shown that methyl-, ethyl- and

benzylphosphonate all intercalate *via* a two-step mechanism whereas phenylphosphonate intercalates directly in a one-step process. [235, 236] On the other hand, one-step process was observed for the intercalation of all four phosphonate anions into the rhombohedral form of $LiAl_2$-Cl. The influence of the initial interlayer anions in $LiAl_2$-X (X = NO_3^- and Br^-) was also investigated and it was observed that staging intercalates are not formed with X = NO_3^- while X = Br^- second-stage intermediates are formed but only with certain organic anions like methylphosphonate, fumarate and succinate anions. Regarding the occurrence of staging phenomena in $LiAl_2$-LDH system, the conclusion is therefore that the nature of both the interlayer anions and the stacking sequence of layers (rhombohedral or hexagonal forms) influence the exchange reaction mechanism involving or not the presence of a second-stage intermediate.

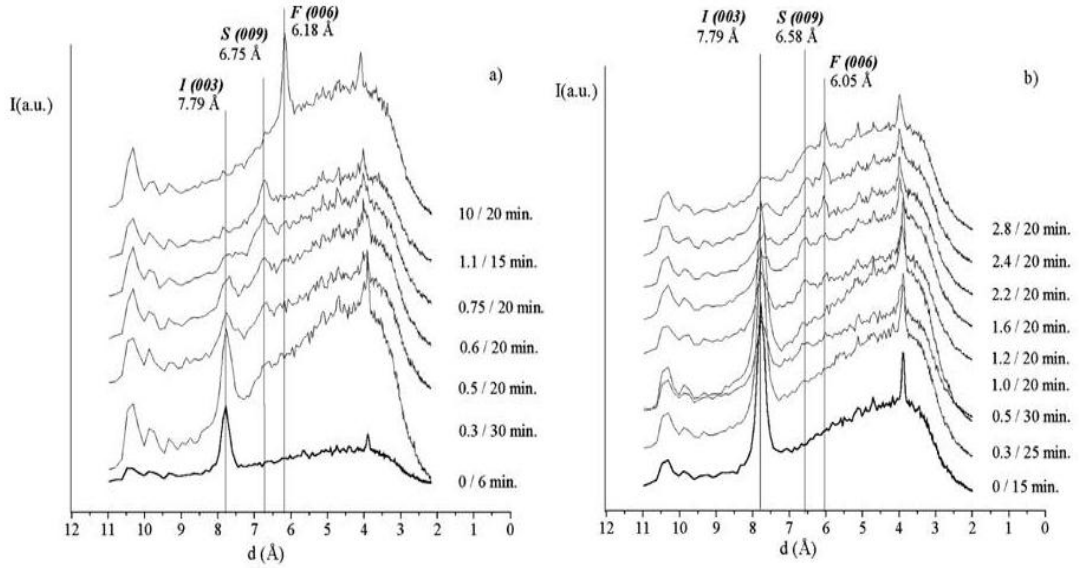

Figure 1-34: In situ energy-dispersive X-ray powder diffraction data showing the course of the anion-exchange reaction (a) between Zn_2Cr-Cl and tartrate anions (b) between Zn_2Cr-Cl and succinate anions. see ref. 211.

Though not clearly specified by O'Hare *et al.*, one might think at a first glance that staging in $LiAl_2$-LDH which is a rare example of LDH presenting an ordered structure, stems from this structural singularity. Yet in 2003, Taviot-Gueho *et al.*

showed that Zn_2Al-Cl, Zn_2Cr-Cl and Cu_2Cr-Cl (disordered LDH) also undergo staged intercalation reactions with succinate and tartrate anions. [211] Again by means of in situ EDXRD technique, the formation of second-stage intermediate was evidenced in all cases (**Figure 1-34**). However, depending on the nature of the organic anions, two exchange pathways were identified. For tartrate exchange, the mechanism resembles that reported by O'Hare *et al.* with $LiAl_2$-LDH [209] since the fully exchanged material is not observed until the intermediate has gone through its maximum and the chloride precursor has disappeared completely. For succinate exchange, the final product of intercalation and the second-stage intermediate simultaneously appear. Dried under vacuum, Zn_2Cr-Tart/Cl second-stage material undergoes a contraction of the interlamellar space associated with a reorientation of the tartrate anions in a flat position after the removal of interlayer water molecules. The contraction of the interlamellar distance observed *ca.* 2.9 Å is that expected for two different interlayer contents i.e. occupied by Cl^- and tartrate anions alternatively thus excluding the formation of interstratified phases associated with two different orientations of the same anion as reported for terephthalate anions in Mg_2Al-LDH (**Figure 1-35**) [208]. This example points out the eventual difficulty in attributing 2nd stage compounds arising from either "conformational" or "chemical" staging.

Regarding the occurrence of staging in LDH system, these authors suggested a segregation between organic and inorganic anions since staging has never been observed with mixed inorganic anion LDH. Therefore, second-stage intermediates would be a peculiarity of organic/inorganic systems resulting from a segregation between organic and inorganic anions.

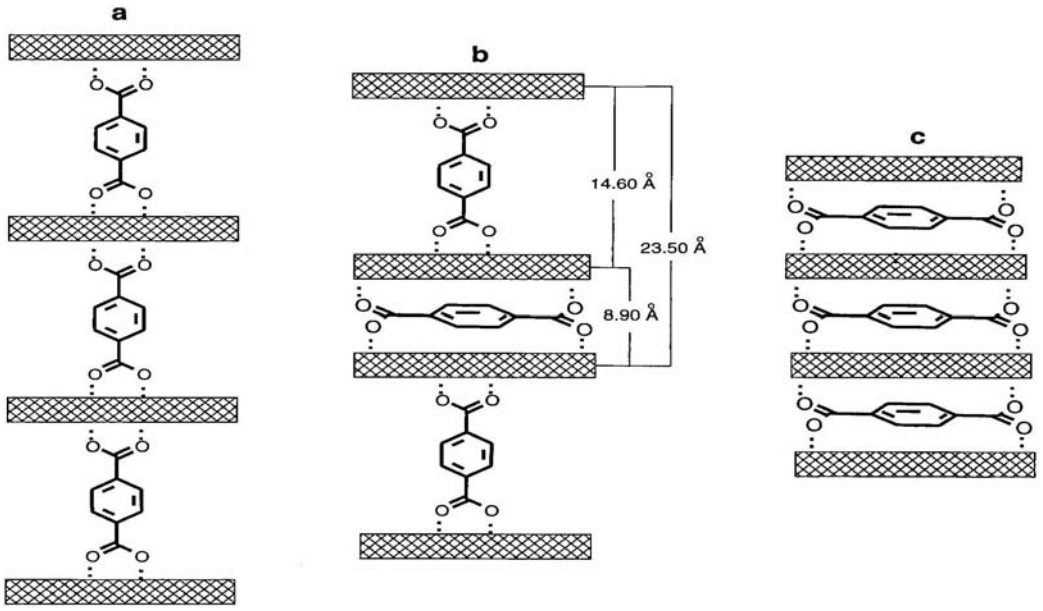

Figure 1-35**:** Proposed model for structural changes occurring during the heat treatment and loss of the interlayer water of Mg_2Al-Terephthalate at (a) 25 ℃, (b) 100 ℃ and (c) 200 ℃. See ref. 208.

Based on these studies, second-stage intercalates in LDH systems have only been seen to occur as intermediates during intercalation reactions. However, the literature contains one example of second-stage intercalate obtained by direct coprecipitation reported by Iyi *et al.* [210] These authors observed the formation of mixed hydroxide/azobenzene intercalate for Mg_2Al-LDH associated with the formation of bipolar two-nanolayer tactoids; the hydrophobic binding effect and the size of organic anions combined with the layer charge density of LDH hydroxide layers would exclude the inorganic anions from the interlayer space leading to the formation of bipolar two-layer nanoparticles; staging structures are then formed upon stacking of the so-called tactoids during the drying steps as depicted in **Figure 1-36**.

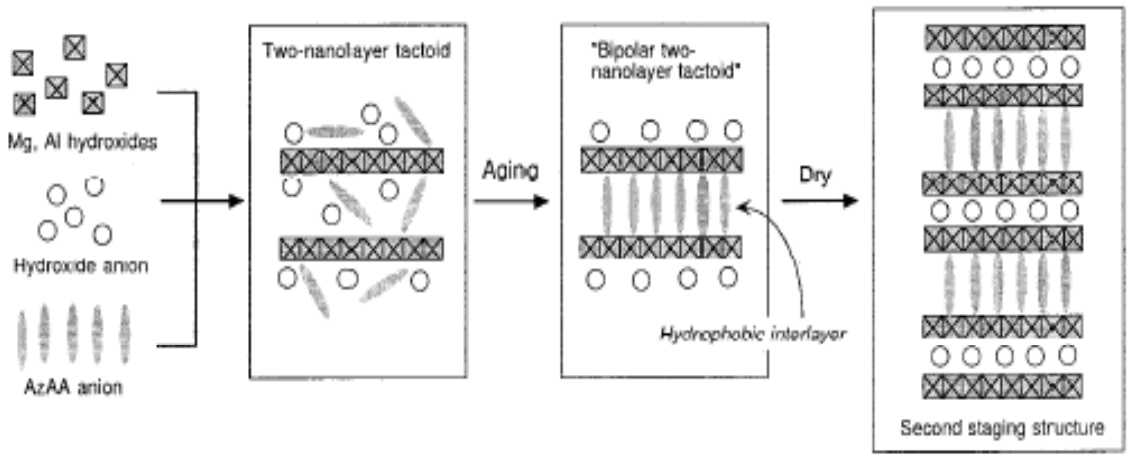

Figure 1-36**:** Scheme of the formation of second-staging via tactoids for the AzAA/Mg_2Al LDH complexes prepared by a coprecipitation. AzAA is (4-Phenylazo-phenyl)-acetic acid. See ref. 210.

The aim of this thesis is to further investigate the formation of LDH second-stage materials, and to enlarge the study to other compositions than $LiAl_2$ LDH already examined in detail by O'Hare's group in Oxford. We also aim to determine the factors influencing the formation of such heterostructures, investigate their anion-exchange properties and finally look at their applications in the field of multifunctional materials.

1.7 **In Situ Energy-dispersive X-ray Diffraction**

There is detailed introduction concerning in situ EDXRD in G. R. Williams' thesis[237]. Compared with angular-dispersive X-ray diffraction used as the standard characterization technique in solid state laboratories, in situ energy-dispersive X-ray diffraction using Synchrotron radiation has two main advantages: (*i*) a wide range of *d*-spacings can be observed simultaneously, then it is possible to detect all the phases involved in an intercalation reaction i.e. the host materials, any intermediates and the final product at the same time; (*ii*) the short time of data collection down to 1 s, thus smaller than the average reaction time for solid state intercalation reactions. Hence, it is possible to obtain both qualitative and quantitative information regarding to the reaction mechanisms and kinetics.

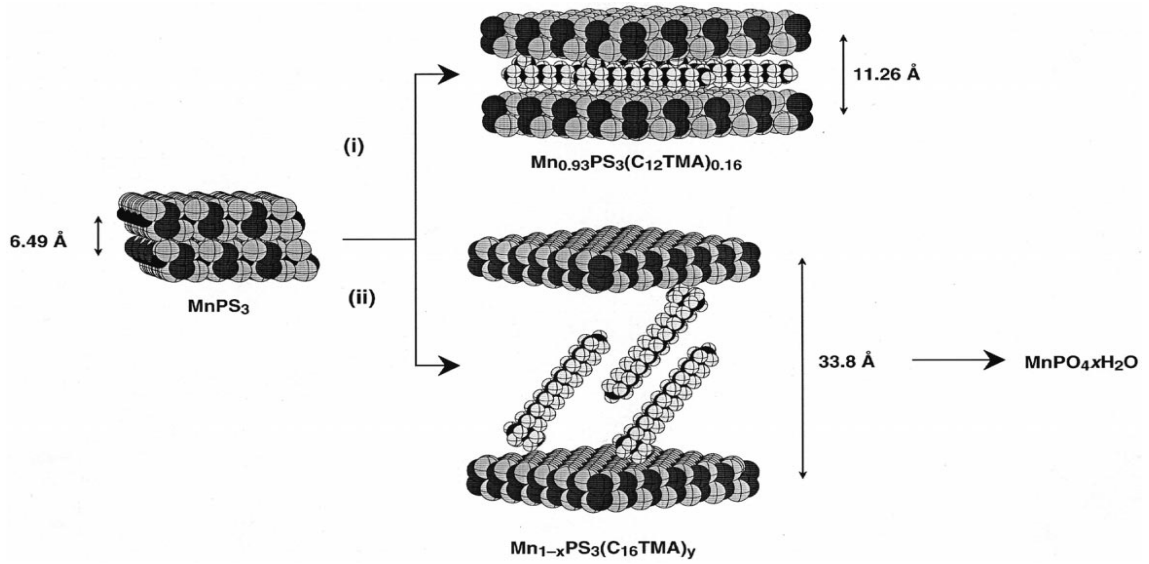

Figure 1-37: Synthesis of long chain ammonium intercalates of $MnPS_3$: (*i*) $MnPS_3$ (150 mg) + $C_{12}TMABr$ (1 mmol) in 5 cm^3 water at 120 ℃, (*ii*) $MnPS_3$ (150 mg) + $C_{16}TMABr$ (1 mmol) in 5 cm^3 water at 120 ℃. See ref. 238.

EDXRD has been used to perform in situ kinetic studies on the intercalation of a variety of guest species in host layered materials as reviewed by O'Hare *et al.*[238]. For example, the kinetic studies on the intercalation of cations (K^+, PyH^+ (Py = C_5H_5N), NMe_4^+) and the long chain ammonium ions i.e. dodecyltrimethylammonium ($C_{12}TMA$), hexadecyltrimethylammonium ($C_{16}TMA$) and octadecyltrimethylammonium ($C_{18}TMA$) into $MnPS_3$ lamellar host (in **Figure 1-37**) have been investigated, as well as the intercalation of cobaltocene, Co(η-C_5H_5)$_2$, into the layered dichalcogenides ZrS_2, 2H-SnS_2, 2H-$SnSe_2$, 2H-TaS_2, 2H-NbS_2, 1T-TaS_2 and TiS_2.[239] In this latter case, it was found that the rate of intercalation is independent on the initial Co(η-C_5H_5)$_2$ concentration over a wide concentration range. On the other hand, the rate of intercalation of the lithium salts (LiX; X = Cl, Br, NO_3 and OH) into Gibbsite (γ-$Al(OH)_3$) during the formation of $LiAl_2$-X LDH and $LiAl_2$-SO_4 LDH have been determined by EDXRD. Finally, the in situ EDXRD spectra recorded following the addition of an aqueous solution of hexadecyltrimethylammonium chloride ($C_{16}H_{33}N^+Me_3Cl^-$) to kanemite ($NaHSi_2O_5 \cdot 3H_2O$) at 70 ℃ showed that a layered phase formed at the initial step later transforms into a silicate-organic mesophase which is a precursor to the hexagonal mesoporous silicate (FSM-16) as described in **Figure 1-38**.

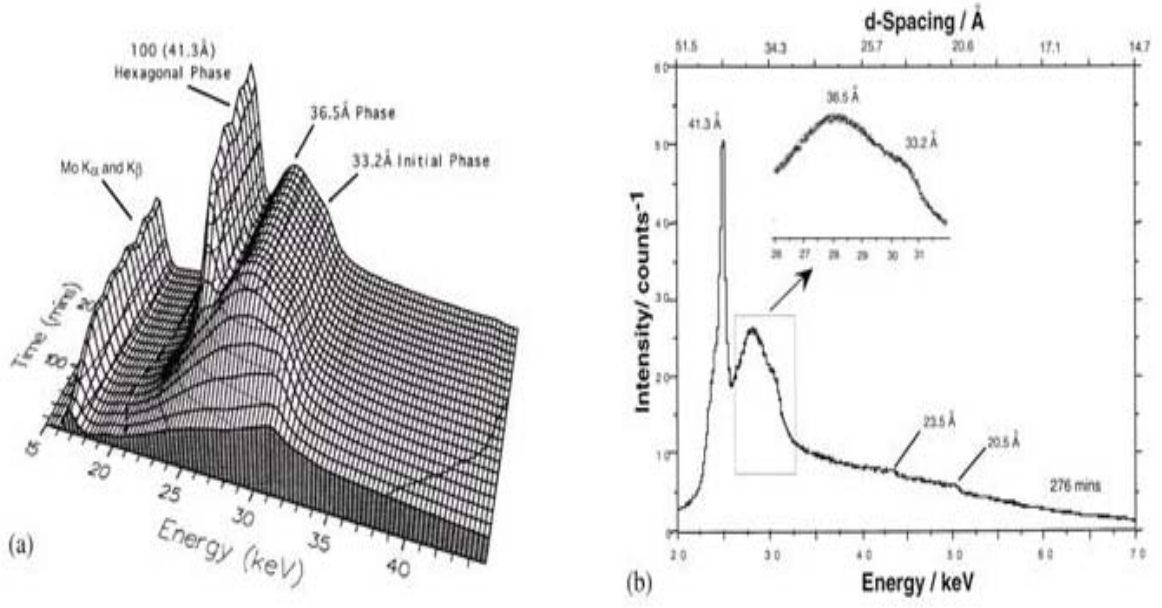

Figure 1-38: (a) Three-dimensional stacked plot showing the energy dispersive powder X-ray diffraction spectra recorded following addition of 0.1 M hexadecyltrimethylammonium chloride ($C_{16}TMA^+Cl^-$) to kanemite in water at 70 ℃. (b) The final in situ EDXRD spectrum taken after reaction completion, showing all observable diffraction features. See ref. 238.

EDXRD experiments described in the following were performed at Daresbury laboratory on station 16.4 using the experimental set-up developed by O'Hare *et al.* The usable extracted X-ray flux is continuous within the energy range of 5 to 120 keV and the energy storage ring is operated under extremely high vacuum (pressures below 10^{-10} Torr). The data collected using the energy-dispersive method can be converted to *d*-spacing via combination of Bragg's law with the Planck relation as follows:

$$E = hc/\lambda \qquad \textbf{Equation } 1\text{-}5$$

gives

$$2d\ \sin\theta = hc/E \qquad \textbf{Equation } 1\text{-}6$$

$c = 3 \times 10^8 m\ s^{-1}$, $h = 6.626 \times 10^{-34} J.s$ and $e = 1.602 \times 10^{-19} c$ then

$$d = 6.1992/E \cdot \sin\theta \qquad \textbf{Equation } 1\text{-}7$$

In **Equation 1-7**, E is the energy of a photon in keV, *d* is the corresponding *d*-spacing in Å, and θ is the fixed detector angle used in the EDXRD experiments.

1.7.1 Experimental Setup

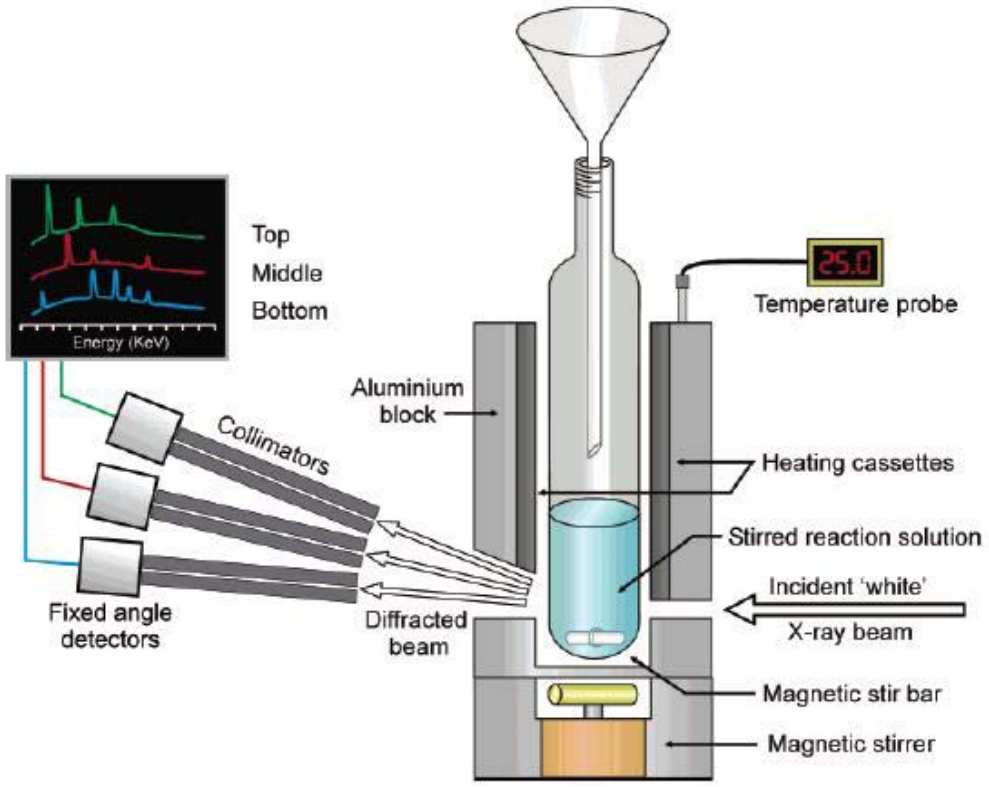

Figure 1-39**:** The experimental apparatus used to perform time-resolved in situ EDXRD experiments. See ref. 238.

The experimental setup at Station 16.4 for the study of intercalation reactions by EDXRD is presented in **Figure 1-39**. [240, 241] As can be seen, there are three detectors and each detector is separated by approximately 2º in 2θ in order to cover a different range of *d*-spacing. [235] There is overlap between the range covered by each detector in order to ensure that no reflections are missed.

The equipment has been successfully used by O'Hare *et al.* for studying a number of intercalation reactions such as the intercalation of carboxylate and phosphonate anions into $LiAl_2$-LDH and the intercalation of sulfates drugs and agrochemicals into a variety of materials i.e. Li_2Al-Cl [242, 243] and Ca_2Al-NO_3 [244].

1.7.2 Data and Kinetic Analysis

An automated Gaussian fitting routine is used to obtain the peak integrated areas of the Bragg reflections I_{hkl}.[245] These values are subsequently converted into the extent of reaction α at time *t* defined as:

$$\alpha(t) = I_{hkl}(t)/I_{hkl}(max) \qquad \textbf{Equation } 1\text{-}8$$

where $I_{hkl}(t)$ is the area of a given *hkl* peak at a certain time *t* and $I_{hkl}(max)$ is the maximum area of this peak.

Information on reaction mechanism can be deduced from the shape of $\alpha(t)$ plot[246]. For solid state reaction, the kinetic equation of Avrami and Erofe'ev is the most commonly employed and expressed as follows:

$$\alpha(t) = 1 - \exp[-(kt)^n] \qquad \textbf{Equation } 1\text{-}9$$

where k is the rate constant and n is the so-called Avrami exponent. The Sharp and Hancock expression corresponding to the Log-linearized form of the Avrami and Erofe'ev equation[247]:

$$\ln(-\ln(1-\alpha)) = n\ln k + n\ln t \qquad \textbf{Equation } 1\text{-}10$$

is used to calculate the values of k and n. If there is a linear relationship between $\ln(-\ln(1-\alpha))$ and $\ln t$, the value of n is the gradient of the line and the value of k can be obtained from the ordinate intercept. Avrami exponent can be used to describe the reaction mechanisms involved and possible values for intercalation into a layered host are summarized in **Table 1-3** [248]. Yet, the interpretation of these values can be difficult, and a given value does not unequivocally allow the determination of the reaction mechanism.

For a layered host, nucleation sites are the edges of the crystallite from which guest anions enter the interlayer space and the nuclei growth corresponds to the diffusion of guest molecules into the interlayer region in two dimensions (λ = 2). Consequently, nucleation rate (β) may be either phase boundary controlled (the rate is limited by the expansion of interlayer space to accommodate the guest) or diffusion controlled (the rate is controlled by the diffusion of guest anions in the interlayer region).

Table 1-3**:** Nuclei growth models possible for intercalation into a layered double host. See ref. 248.

Dimension of growth (λ)	**Nucleation rate (β)**	**Exponent value Phase boundary controlled (*n*)**	**Diffusion controlled (*m*)**
1	Deceleratory	1-2	0.5-1.5
2	Zero (instantaneous)	2	1
2	Deceleratory	2-3	1-2

**for phase boundary controlled process, $n= \beta + \lambda/2$; for diffusion controlled process, $n= \beta + \lambda$.*

On the other hand, there is the other possibility that the guest species enter the interlayer regions as soon as they reach the layer edges. The whole reaction proceeds purely diffusion controlled process and different models exist summarized in **Table 1-4** used to describe such diffusion processes in various dimensions[249].

Table 1-4: Possible equations describing diffusion controlled reactions. See ref. 248.

Growth	**Equation**
One-dimension diffusion	$\alpha^2 = kt$
Two-dimension diffusion	$(1-\alpha)\ln(1-\alpha) + \alpha = kt$
Three-dimension diffusion	$[1-(1-\alpha)^{\frac{1}{3}}]^2 = kt$

1.8 **References**

1 V. Rives (ed) *Layered Double Hydroxides: Present and Future*. **2001**, Nova Science Publishers, New York.

2 A. I. Khan, D. O'Hare, *J. Mater. Chem.*, 2**002**, *12*, 3191.

3 D. G. Evans and R. C. T. Slade, *Struct. Bond*., **2006**, *119*. 1.

4 F. Feitknecht, *Helv. Chim. Acta*., **1942**, *25*, 131.

5 F. Feitknecht, *Helv. Chim. Acta*., **1942**, *25*, 555.

6 R. Allamnn, *Acta. Cryst. B*, **1968**, *24*, 972.

7 H. F. W. Taylor, *Miner. Mag*., **1969**, *37*, 338.

8 J. G. Nunan, P. B. Himelfarb, R. G. Herman, K. Klier, C. E. Bogdan and G. W. Simmons, *Inorg. Chem.*, **1989**, *28*, 3868.

9 F. Kooli, K. Kosuge and A. Tsunashima, *J. Solid State Chem*., 1**995**, *118*, 285.

10 Y. J. Feng, D. Q. Li, C. X. Li, Z. H. Wang, D. G. Evans and X. Duan, *Acta Chimica Sinica*, **2003**, *61*, 78.

11 J. W. Boclair, P. S. Braterman, *Chem. Mater*., **1999**, *11*, 298.

12 A. De Roy, *Mol. Cryst. Liq. Cryst*., **1998**, *311*, 173.

13 E. Lopez-Salinas, M. Garcia-Sanchez, J. A. Montoya, D. R. Acosta, J. A. Abasolo and I. Schifter, *Langmuir*, **1997**, *13*, 4748.

14 L. Legrand, M. Abdelmoula, A. Géhin, A. Chausé and J. M. R. Génin, *Electrochim. Acta*, **2001**, *46(12)*, 1815.

15 C. Bigey, C. Depege, A. de Roy and J. P. Besse, *J. Phys. IV*, **1997**, *7*, 949.

16 K. J. Martin and T. J. Pinnavaia, *J. Am. Chem. Soc*., **1986**, *108*, 541.

17 R. Allmann, *N. Jb. Miner. Mh.*, **1977**, 136.

18 C. J. Serna, J. L. Rendon and J. E. Iglesias, *Clays Clay Miner.*, **1982**, *30 (3)*, 180.

19 J. H. Choy and Y. H. Son, *Bull. Korean Chem. Soc.*, **2004**, *25*, 122.

20 F. Leroux and J. P. Besse, *Chem. Mater*., **2001**, *13*, 3507.

21 R. Allmann, *Chimia*, **1970**, *24*, 99.

22 H. F. W. Taylor, *Miner. Mag.*, **1973**, *39*, 377.

23 I. Rousselot, C. Taviot-Gueho, F. Leroux, P. Leone, P. Palvadeau and J. P. Besse, *J. Solid State Chem*., **2002**, *167*, 137.

24 A. G. Kalinichev and R. J. Kirkpatrick, *Chem. Mater.*, **2002**, *14*, 3539.

25 V. Fernon, A. Vichot, P. Colombet, H. van Damme and F. Begin, *Mater. Sci. Forums*, **1994**, *152-153*, 307.

26 H. Kuzel and H. Baier, *Eur. J. Mineral*., **1996**, *8*, 129.

27 A. M. Fogg, A. J. Freij and G. M. Parkinson, *Chem. Mater.*, **2002**, *14*, 232.

28 A. V. Besserguenev, A. M. Fogg, R. J. Francis, S. J. Price and D. O'Hare, *Chem. Mater*., **1997**, *9*, 241.

29 S. Carlino, *Solid State Ionics*, **1997**, *98*, 73.

30 S. P. Newsman and W. Jones, *New J. Chem.*, **1998**, *22*, 105.

31 V. Rives and M. A. Ulibarri, *Coordi., Chem. Rev*., **1999**, *181*, 61.

32 W. Reichle, *Solid State Ionics*, **1986**, *22*, 135.

33 W. Reichle, *J. Catal.*, **1985**, *94*, 547.

34 S. Miyata, *Clays Clay Miner*., **1983**, *11*, 305.
35 Y. Israeli, C. Taviot-Guého, J. P. Besse, J. P. Morel and N. Morel-Desrosiers, *J. Chem. Soc. Dalton Trans.*, **2000**, *5*, 791.
36 T. Yamaoka, M. Abe and M. Tsuji, *Mater. Res. Bull.*, **1989**, *24*, 1183.
37 M. A. Drezdon, *U S patent*, **1987**, 4 774 212 .
38 M. A. Drezdon, *Inorg. Chem*., **1988**, *27(25)*, 4628.
39 E. L. Crepaldi, P. C. Pavan and J. B. Valim, *Chem. Commun*., **1999**, 155.
40 E. L. Crepaldi, P. C. Pavan and J. B. Valim, *J. Mater. Chem.*, **2000**, *10*, 1337.
41 A. De Roy, C. Forano and J. P. Besse, in *Layered Double Hydroxides: Present and Future*, edited by V. Rives (Nova Science Publishers, Inc., New York),**2001**, 1.
42 J. H. Lee, S. W. Rhee and D. Y. Jung, *Chem. Mater.*, **2004**, *16*, 3774.
43 T. Hibino and A. Tsunashima, *Chem. Mater.*, **1997**, *9*, 2082.
44 J. J. Bravo-Suarez, E. A. Paez-Mozo and S. T. Oyama, *Chem. Mater*., **2004**, *16*, 1214.
45 L.X. Lei, R. P. Vijayan and D. O'Hare, *J. Mater. Chem*., **2001**, *11(12)*, 3276.
46 T. Sato and A. Okuwaki, *Solid State Ionics*, **1991**, *45 (1-2)*, 43.
47 K. Chibwe and W. Jones, J. Chem. Soc., *Chem. Commun.*, **1989**, 926.
48 E. Narita, P. Kaviratna and T. J. Pinnavaia, *Chem. Lett.*, **1991**, 805.
49 T. Sato, H. Fujita, T. Endo, M. Shimada and A. Tsunashima, *React. Solids*, **1988**, *5*, 219.
50 F. Kooli, V. Rives and M. A. Ulibarri, *Mater. Sci. Forum*, **1994**, *152-153*, 375.
51 W. Kagunya, M. Chibwe and W. Jones, *Mol. Cryst. Liq. Cryst*., **1994**, *244*, 155.
52 M. R. Kang, H. M. Lim, S. C. Lee. S.H. Lee and K. J. Kim, *Adv. Technol. Mater. Mater. Process.*, **2004**, *6(2)*, 218.
53 M. Ogawa and S. Asai, *Chem. Mater.*, **2000**, *12*, 3253.
54 H. P. Boehm, J. Steinle and C. Vieweger, *Angew. Chem. Int. Ed. Engl*., **1977**, *16*, 265.
55 K. El Malki, A. De Roy and J. P. Besse, *Eur. J. Solid State Inorg. Chem*., **1989**, *t26*, 339.
56 V. Prevot, Thesis, Blaise Pascal University, **1999**.
57 T. S. Stanimirova, G. Kirov and E. Dinolova, *Mat. Sic. Lett.*, **2001**, *20*, 453.
58 H. Roussel, Thesis, Blaise Pascal University, **1999**.
59 S. P. Newman and W. Jones, *New J. Chem.*, **1998**, *22*, 105.
60 A. De Roy, J.P. Besse and P. Bondot, *Mat. Res. Bull.*, **1985**, *20*, 1091.
61 T. Sato, T. Wakabayashi and M. Shimada, *Ind. Eng. Chem., Prod. Res. Dev*., **1986**, *25*, 89.
62 G. Mascolo and O. Marino, *Miner. Mag.*, **1980**, *43*, 619.
63 G. Mascolo, O. Marino and A. Cantarelli, *Trans. J. Brif. Ceram*., **1980**, *79*, 6.
64 T. Sate, H. Fujita, T. Endo and M. Shimada, *React. of Solids*, **1988**, *5*, 219.
65 V. Prevot, C. Forano and J. P. Bess, *Inorg. Chem.*, **1998**, *37*, 4293.
66 G. J. Ross and H. Kodama, *Amer. Min.*, **1967**, *52*, 1037.
67 G. W. Brindley and S. Kikkawa, *Clays Clay Miner.*, **1980**, *28*, 87.
68 G. W. Brindley and S. Kikkawa, *Am. Miner.*, **1979**, *64*, 836.
69 A. Ennadi, A. Legrouri, A. De Roy and J. P. Besse, *J. Solid State Chem*., **2000**, *152*, 568.
70 M. Bellotto, B. Rebours, O. Clause, J. Lynch, D. Bazin and E. Elkaim, *J. Phys. Chem*., **1996**, *100*, 8527.
71 H. Dittrich and M. Wohlfahrt-Mehrens, *Int. J. Inorg. Mater.*, **2001**, *3*, 1137.
72 G. S. Thomas and P. V. Kamath, *J. Chem. Sci.*, **2006**, *118(1)*, 127.
73 A. V. Radha, C. Shivakumara and P. V. Kamath, *Clays Clay Miner.*, **2005**, *53(5)*, 520.

74 G. S. Thomas, M. Rajamathi and P. V. Kamath, *Clays Clay Miner.*, **2004**, *52(6)*, 693.
75 Y. J. Liu, J. L. Schindler, D. C. DeGroot, C. R. Kannewurf, W. Hirpo and W. G. Kanatzidis, *Chem. Mater.*, **1996**, *8*, 825.
76 X. Zhang and M. M. Lerne, *Chem. Mater*., **1999**, *11*, 1100.
77 X. Zeng and G. Ungar, *Polymer*, **1998**, *19*, 4523.
78 T. Adach, H. Takahashi, K. Ohki and I. Hatta, *Biophys. J*., **1995**, *68*, 1850.
79 T. Itho, N. Ohta, T. Schichi, T. Yui and K. Tagaki, *Langmuir*, **2003**, *19*, 9120.
80 J. Bauer, P. Behrens, M. Speckbacher and H. Langhals, *Adv. Funct. Mater.*, **2003**, *13(3)*, 241.
81 G. Renaudin, F. Kubel, J. P. Rivera and M. François, *Cem. Concr. Res.*, **1999**, *29*, 1937.
82 El M. Moujahid, F. Leroux and J. P. Besse, *J. Mater. Chem.*, **2002**, *12*, 3324.
83 F. Leroux and C. Taviot-Guého, *J. Mater. Chem.*, **2005**, *15*, 3628.
84 W. K. Kuks and Y. D. Huh, *J. Mater. Chem.*, **1997**, *7*, 1933.
85 T. Itoh, T. Shichi, T. Yui, H. Tahahashi, Y. Inui and K. Takagi, *J. Phys. Chem. B*, **2005**, *109*, 3199.
86 W. T. Reichle, *Solid State Ionics*, **1986**, *22*, 135.
87 J. M. Fernandez, C. Barriga, M. A. Ulibarri, F. M. Labajos and V. Rives, *J. Mater. Chem.*, **1994**, *4*, 1117.
88 S. Vial, V. Prevot and C. Forano, *J. Phys. Chem. Solids*, **2006**, *67*, 1048.
89 G. Hu and D. O'Hare, *J. Am. Chem. Soc*., **2005**, *127*, 17808.
90 G. B. Sun, L. N. Sun, H. Wen, Z. Q. Jia, K. L. Huang and C. W. Hu, *J. Phys. Chem. B*, **2006**, *110*, 13375.
91 J. Tronto, F. Leroux, E. L. Crepaldi, Z. Naal, S. I. Klein and J. B. Valim, *J. Phys. Chem. Solids*, **2006**, *67*, 968.
92 J. Tronto, K. C. Sanchez, E. L. Crepaldi, Z. Naal, S. I. Klein and J. B. Valim, *J. Phys. Chem. Solids*, **2004**, *65*, 493.
93 L. Z. Qiu, W. Chen and B. J. Qu, *Polymer*, **2006**, *47*. 922.
94 L. C. Du, B. J. Qu, Y. Z. Meng and Q. Zhu, *Compos. Sci. Tech.*, **2006**, *66*, 913.
95 E. Geraud, C. Prevot, J. Ghanbaja and F. Leroux, *Chem. Mater.*, **2006**, *18*, 238.
96 M. B. J. Roeffaers, B. F. Sels, D. Loos, C. Kohl, K. Mullen, P. A. Jacobs, J. Hofkens and D. E. De Vos, *Chem. Phys. Chem*., **2005**, *6*, 2295.
97 K. Yao, M. Taniguchi, M. Nakata, M. Takahashi and A. Yamagishi, *Langmuir*, **1998**, *14*, 2410.
98 G. Hu, N. Wang, D. O'Hare and J. Davis, *Chem. Commun.*, **2006**, 287.
99 G. Defontaine, L. J. Michot, I. Bihannic, J. Ghanbaja and V. Briois, *Langmuir*, **2004**, *20*, 11213.
100 F. Leroux, E. M. Moujahid, C. Taviot-Guého and J. P. Besse, *Solid State Sci.*, **2001**, *3*, 81.
101 S. Velu, V. Ramaswamy, A. Ramani, B. M. Chanda and S. Sivasanker, *Chem. Commun.*, **1997**, 2107.
102 S. Velu, K. Suzuki, M. Okazaki, T. Osaki, S. Tomura, and T. Ohashi, *Chem. Mater.*, **1999**, *11*, 2163.
103 M. Intissar, J. C. Jumas, J. P. Besse, and F. Leroux, *Chem. Mater.*, **2003**, *15*, 4625.
104 M. Intissar, F. Malherbe, V. Prevot and F. Leroux, *J. Colloid Interface Sci.*, **2006**, *299*, 747.
105 J. T. Kloprogge and R. L. Frost, *J. Solid State Chem*., **1999**, *146*, 506.
106 H. Zhang, K. Zou, S.-H. Guo and X. Duan, *J. Solid State Chem*., **2006**, *179 (6)*, 792.
107 J. Perez-Ramirez, G. Mul and J. A. Moulijn, *Vibra. Spec*., **2001**, *27*, 75.
108 T. J. Kloprogge, R. L. Frost., *Phys. Chem. Chem. Phys.*, **1999**, *1*, 1641.
109 T. J. Kloprogge and R. L. Frost, *Appl. Catal. A*, **1999**, *184*, 61.

110 T. E. Johnson, W. Martens, R. L. Frost, Z. Ding and J. T. Kloprogge, *J. Raman Spectrosc.*, **2002**, *33*, 604.
111 R. L. Frost, M. L. Weier and J. T. Kloprogge, *J. Raman Spectrosc.*, **2003**, *34*, 760.
112 S. Petit, A. Decarreau, F. Martin and R. Buchet, *Phys. Chem. Miner.*, **2004**, *31*, 585.
113 R. L. Frost, Z. Ding and J. T. Kloprogge, *Canad. J. Analy. Sci. Spectrosc.*, **2000**, *45 (4)*, 96.
114 Y. Kim, R. J. Kirkpatrick and R. T. Cygan, *Geochem. Cosmochim. Acta*, **1996**, *60*, 4059.
115 R. J. Kirkpatrick, Y. Ping, X. Q. Hou and Y. Kim, *Am. Mingeral.*, **1999**, *84*, 1186.
116 X. Q. Hou, R. J. Kirkpatrick, Y. Ping, D. Moore and Y. Kim, *Am. Mineral.*, **2000**, *85*, 173.
117 A. Van der Pol, B. L. Mojet, E. Van de Ven and E. de Boer, *J. Phys. Chem.*, **1994**, *98*, 4050.
118 S. Carlino and M. J. Hudson, *J. Mater. Chem.*, **1994**, *4*, 99.
119 G. Marcelin, N. J. Stockhausen, J. F. M. Post and A. Schutz, *J. Phys. Chem.*, **1989**, *93*, 4646.
120 J. Dupuis, J. P. Battut, Z. Fawal and H. Hajjimohamad, *Solid State Inoincs*, **1990**, *42*, 251.
121 X. Q. Hou and R. J. Kirkpatrick, *Chem. Mater.*, **2000**, *12*, 1890.
122 M. del Arco, S. Gutierrez, C. Martin, V. Rives and J. Rocha, *J. Solid State Chem.*, **2000**, *151*, 272.
123 R. S. Maxwell, R. K. Kukkadapu, J. E. Amonette and H. Cho, *J. Phys. Chem. B*, **1999**, *103*, 5197.
124 S. Carlino and M. J. Hudson, *J. Mater. Chem.*, **1995**, *5*, 1433.
125 H. Nakayama, S. Hirami and M. Tsuhaka, *Chem. Lett.*, **200**4, *33 (6)*, 712.
126 S. Gago, M. Pillinger, T. M. Santos and I. S. Goncalves, *Ceramics*, **2004**, *48 (4)*, 155.
127 L. Mohanambe and S. Vasudevan, *J. Chem. Sci.*, **2006**, *118 (1)*, 105.
128 H. Nakayama, N. Wada and M. Tsuhako, *Inter. J. Pharm.*, **2004**, *269 (2)*, 469.
129 K. J. D. Mackenzie, R. H. Meinhold, B. L. Sherriff and Z. Xu, *J. Mater. Chem.*, **1993**, 1263.
130 L. Vieille, C. Taviot-Gueho, J. P. Besse and F. Leroux, *Chem. Mater.*, **2003**, *15*, 4369.
131 S. P. Newsman, S. J. Williams, P. V. Coveney and W. Jones, *J. Phys. Chem. B*, **1998**, *102*, 6710.
132 A. M. Fogg, A. L. Rohl, G. M. Parkinson and D. O'Hare, *Chem. Mate*r., **1999**, *11*, 1194.
133 A. G. Kalinichey, R. J. Kirkpatrick and R. T. Cygan, *Am. Mineral.*, **2000**, *85*, 1046.
134 J. W. Wang, A. G. Kalinichey, R. J. Kirkpatrick and X. Q. Hou, *Chem. Mater.*, **2001**, *13*, 145.
135 S. P. Newsman, T. D. Cristina and P. V. Coveney, *Langmuir*, **2002**, *18*, 2933.
136 H. C. Greenwell, W. Jones, S. P. Newsman and P. V. Coveney, *J. Mol. Struct.*, **2003**, *647*, 75.
137 R. T. Cygan, J. J. Liang and A. G. Kalinichev, *J. Phys. Chem. B*, **2004**, *108*, 1255.
138 G. M. Lombardo. G. C. Pappalardo, F. Punzo, F. Costantino, U. Constantino and M. Sisani, *Eur. J. Inorg. Chem.*, **2005**, 5026.
139 L. Mohanambe and S. Vasudevan, *Langmuir*, **2005**, *21*, 10735.
140 L. Mohanambe and S. Vasudevan, *J. Phys. Chem. B*, **2005**, *109*, 15651.
141 P. P. Kumar, A. G. Kalinichev and R. J. Kirkpatrick, *J. Phys. Chem. B*, **2006**, *110(9)*, 3841.
142 F. Li and X. Duan, *Struct. Bond.*, **2006**, *119*, 193.
143 F. Cavani, F. Trifiro and A. Vaccari, *Cataly. Today*, **1991**, *11*, 173.
144 D. G. Evans and X. Duan, *Chem. Commun.*, **2006**, 485.
145 G. R. Williams and D. O'Hare, *J. Mater. Chem.*, **2006**, *16*, 1.
146 T. Nakatsuka, H. Kawasaki, S. Yamashita and S. Kohjiya, *Bull. Chem. Soc. Japan*, **1979**, *52*, 2449.
147 W. T. Reichle, *J. Catal.*, **1980**, *63*, 295.
148 B. M. Choudary, M. L. Kantam, V. Neeraja, K. K. Rao, F. Figuras and L. Delmotte, *Green Chem.*, **2001**, *3*, 257.
149 F. Basile, G. Fornasari, E. Poluzzi and A. Vaccari, *Appl. Clay Sci.*, **1998**, *13*, 329.

150 J. Barrault, A. Derouault, G. Courtois. J. M. Maissant, J. C. Dupin, C. Guimon, H. Martinez and E. Dumitriu, *Appl. Catal. A*, **2004**, *262*, 43.
151 B. F. Sels, D. E. De Vos and P. A. Jacobs, *Cataly. Rev*., **2001**, *43 (4)*, 443.
152 B. Houri, A. Legrouri, C. Forano and J. P. Besse, *Czech. Chem. Commun.*, **1998**, *63*, 732.
153 S. W. Rhee, M. J. Kang, H. Kim and C. H. Moo, *Environ. Technol.*, **1997**, *18*, 231.
154 L. M. Parker, N. B. Milestone and R. H. Newman, *Ind. Eng. Chem. Res.*, **1995**, *34*, 1196.
155 F. Kovanda, E. Kovacsova and D. Kolousek, *Collect. Czech. Chem. Commun.*, **1999**, *64*, 1517.
156 S. Amin and G. G. Jayson, *Water Res.*, **1996**, *30*, 299.
157 Y. Seida and Y. Nakano, *Water Res*., **2000**, *34(5)*, 1487.
158 G. Fetter, E. Ramos, M. T. Olguin, P. Bosch, T. Lopez and S. Bulbulian, *J. Radioanal. Nucl. Chem.*, **1997**, *222*, 63.
159 M. J. Kang, S. W. Rhee, H. Moon, V. Neck and Th. Fanghanel, *Radiochim. Acta*, **1996**, *75*, 169.
160 M. C. Hermosin, I. Pavlovic, M. A. Ulibarri and J. Cornejo, *J. Environ. Sci. Health, Part A*, **1993**, *28(9)*, 1875.
161 M. C. Hermosin and J. Cornejo, *J. Environ. Qual*., **1993**, *22(2)*, 325.
162 Y. Seida and Y. Nakano, *Water Res*., **2000**, *34(5)*, 1487.
163 R. Celis, W. C. Koskinen, A. M. Cecchi, G. A. Bresnahan, M. J. Carrisoza, M. A. Ulibarri, I. Pavlovic and M. C. Hermosin, *J. Enviorn. Sci. Health, Part B*, **1999**, *34*, 929.
164 M. V. Villa, M. J. Sanchez-Martin and M. Sanchez-Camazano, *J. Environ. Sci. Health, Part B*, **1999**, *34*, 509.
165 J. Inacio, C. Taviot-Gueho, C. Forano and J. P. Besse, *Appl. Clay Sci*., **2001**, *18*, 255.
166 C. J. Serna, J. L. White and S. L. Hern, *J. Pharm. Sci*., **1978**, *67(3)*, 324.
167 A. I. Khan, L. Lei, A. J. Norquist and D. O'Hare, *Chem. Commun*., **2001**, 2342.
168 G. Fardella, L. Perioli, U. Costantino, M. Nocchetti, V. Ambrogi and G. Grandolini, *Proc. Int. Symp. Controlled Release Bioact. Mater*., **1997**, 1033.
169 V. Ambrogi, G. Fardella, G. Grandolini and L. Perioli, *Int. J. Pharm.*, **2001**, *220*, 23.
170 M. D. Arco, E. Cebadera, S. Gutierrez, C. Martin, M. J. Montero, V. Rives, J. Rocha and M. A. Sevilla, *J. Pharm. Sci*., **2004**, *93 (6)*, 1649.
171 V. Ambrogi, G. Fardella, G. Grandolini, L. Perioli and M. C. Tiralti, *Pharm. Sci. Technol*., **2002**, *3* (3), 1.
172 C. O. Oriakhi, I. V. Farr and M. M. Lerner, *J. Mater. Chem*., **1996**, *6*, 103.
173 D. Margarita, L. B. Mar, A. Pilar, F. Leroux and R. H. Eduardo, *Chem. Mater.*, **2005**, *17(8)*, 1969.
174 F. Leroux, M. Ben Belkacem, G. Guyot, C. Taviot-Gueho, P. Leone, L. Cario, L. Desigaux and B. Pitard, *Mat. Res. Soc. Symp*., **2005**, *847*, 223.
175 J. H. Choy, S. Y. Kwak, Y. J. Jeong and J. S. Park, *Angew. Chem. Int. Ed.*, **2000**, *39 (22)*, 4042.
176 L. Vieille, C. Taviot-Gueho, J. P. Besse and F. Leroux, *Chem. Mater*., **2003**, *15*, 4369.
177 L. Vieille, El M. Moujahid, C. Taviot-Gueho, J. Cellier, J. P. Besse and F. Leroux, *J. Phys. Chem. Solids*, **2004**, *65*, 385.
178 F. Leroux, *J. Nanosci. Nanotechno*., **2006**, *6(2)*, 303.
179 F. Leroux and C. Taviot-Gueho, *J. Mater. Chem.*, **2005**, *15*, 3628.
180 D. G. Evans and X. Duan, *Chem. Commun*., **2006**, 485.
181 W. Chen and B. J. Qu, *J. Mater. Chem*., **2004**, *14*, 1705.
182 F. Leroux, El M. Moujahid, C. Roland-Swanson, L. Vieille, C. Taviot-Gueho, J. P. Besse, E. Raymundo-Pinero, F. Beguin, *Mat. Res. Soc. Symp*., **2005**, *847*, 195.

183 E. V. Starikova, V. P. Isupov, K. A. Tarasov, L. E. Chupakhina and M. M. Yulikov, *J. Struct. Chem.*, **2004**, *45*, S115.
184 A. V. Lukashin, M. V. Chernysheva, A. A. Vertegel and Yu. D. Tret'yakov, *Dokl. Chem. (Engl. Transl.)*, **2003**, *388 (1-3)*, 19.
185 A. V. Lukashin, A. A. Eliseev, N. G. Zhuraleva, S. V. Kalinin, A. A. Verfetel and Yu. D. Tret'yakov, *Dokl. Chem. (Engl. Transl.)*, **2002**, *383 (4-6)*, 93.
186 G. Schulz-Ekloff, D. Wohrle, B. Van Duffel and R. A. Schoonheydt, *Microporous Mesoporous Mater*., **2002**, *51*, 91.
187 P. Radu, S. Rouba, V. Laget, C. Hornick and M. Drillon, *J. Chem. Soc*., *Chem. Commun*., **1996**, 1107.
188 V. Laget, C. Hornick, P. Rabu, M. Drillon, and R. Ziessel, *Coord. Chem. Rev*., **1998**, *178*, 1533.
189 V. Laget, C. Hornick, P. Rabu, M. Drillon, P. Turek and R. Ziessel, *Adv. Mater.*, **1998**, *10 (13)*, 1024.
190 P. Rabu, Z. L. Huang, C. Hornick and M. Drillon, *Synth. Metals*, **2001**, *122*, 509.
191 S. Decurtins, R. Pellaux, A. Hauser, M. E. Von Arx, in O. Kahn (Ed.), *Magnetism: A Superamolecular Function*, NATO ASI Series, Vol. C8484, Kluwer Academic Publishers, Dordrecht, **1996**, P. 487.
192 H. N. Kim, S. W. Keller, T. E. Mallouk and J. Schmitt, *Chem. Mater*., **1997**, *9*, 1414.
193 S. W. Keller, H. N. Kim and T. E. Mallouk, *J. Am. Chem. Soc.*, **1994**, *116*, 8817.
194 D. M. Kaschak and T. E. Mallouk, *J. Am. Chem. Soc*., **1996**, *118*, 4222.
195 C. Sanchez and P. Gomez-Romero (Ed.), *Functional Hybrid Materials*, Wiley-VCH publishers, **2004**.
196 C. N. R. Rao, *J. Mater. Chem*., **1999**, *9*, 1.
197 A. P. Alivisatos, P. F. Barbara, A. W. Vastleman, J. Chang, D. A. Dixon, M. L. Klein, G. L. McLendon, J. S. Miller, M. A. Ratner, P. J. Rossky, S. I. Stupp and M. E. Thompson, *Adv. Mater*., **1998**, *10 (16)*, 1297.
198 R. J. Cava, F. J. DiSalvo, L. E. Brus, K. R. Dunbar, C. B. Gorman, S. M. Haile, L. V. Interrante, J. L. Musfeldt, A. Navrotsky, R. G. Nuzzo, W. E. Pickett, A. P. Wilkinson, C. Ahn, J. W. Allen, P. C. Burns, G. Ceder, C. E. D. Chidsey, W. Clegg, E. Coronado, H. J. Dai, M. W. Deem, B. S. Dunn, G. Galli, A. J. Jacobson, M. Kanatzidis, W. B. Lin, A. Manthiram, M. Mrssich, D. J. Norris, A. J. Nozik, X. G. Peng, C. Rawn, D. Rolison, D. J. Singh, B. H. Toby, S. Tolbert, U. B. Wiesner, P. M. Woodward and P. D. Yang, *Progress Solid State Chem*., **2002**, *30*, 1.
199 A. D. Pomogailo and V. N. Kestelman (ED.), *Metallopolymer Nanocomposites*, Springer publisher, **2005**.
200 S. A. Solin, *J. Mol. Catal*., **1984**, *27*, 293.
201 W. Rüdorff, *Z. Phys. Chem.*, **1940**, *45*, 42.
202 W. Rüdorff , *Chimia*, **1965**, *19*, 489.
203 N. Daumas and A. Hérold, *C. R. Acad. Sci. Paris C*, **1969**, *268*, 373.
204 N. Daumas and A. Hérold, *Synth. Met*., **1988**, *23*, 27.
205 A. M. Fogg, J. S. Dunn and D. O'Hare, *Chem. Mater.*, **1998**, *10*, 356.
206 J. C. Schon, D. Alder and G. Dresselhaus, *J. Phys. C: Solid State Phys.*, **1988**, *21*, 5595.
207 S. A. Solin, *J. Mol. Catal*,. **1987**, *27*, 293.
208 F. Kooli, I. C. Chisem, M. Vucelic and W. Jones, *Chem. Mater.*, **1996**, *8*, 1969.
209 A. M. Fogg, J. S. Dunn and D. O'Hare, *Chem. Mater.*, **1998**, *10*, 356.

210 N. Iyi, K. Kurashima and T. Fujita, *Chem. Mater.*, **2002**, *14*, 583.
211 J. Pisson, C. Taviot-Gueho, Y. Israeli, F. Leroux, P. Munsch, J. P. Itie, V. Briois, N. Morel-Desrosiers and J. P. Besse, *J. Phys. Chem. B*, **2003**, *107*, 9243.
212 T. Enoki, M. Endo and M. Suzuki, *Graphite Intercalation Compounds and Applications*, Oxford University press US, April 1 **2003**.
213 N. E. Sorokina, I. V. Nikol'skaye, S. G. Ionov and V. V. Avdeev, *Russ. Chem. Bull.*, **2005**, *54*, 1749.
214 H. Shiyama, *Synth. Met.* **2000**, *114*, 1-15.
215 Y. Mizutani, T. Abe, M. Asano and T. Harada, *J. Mater. Res.*, **1993**, *8*, 1586.
216 Y. Murkami, T. Kishimoto, H. Suematsu, R. Nishitani, Y. Sasaki and Y. Nishina, *Synth. Met.*, **1989**, *34*, 205.
217 H. Shioyama, Y. Wakukawa and Y. Sawada, *Mol. Cryst. Liq. Cryst.*, **1998**, *310*, 69.
218 T. Baker, *Chem. Ind.*, **1982**, *18*, 698.
219 F. Beguin and R. Setton, *J. Chem. Soc., Chem. Commun.*, **1976**, 611.
220 R. Schöllhorn, *Pure & Appl. Chem*., **1984**, *56(12)*, 1739.
221 J. Rouxel, in *Intercalated Layered Materials*, edited by F. Lévy, D. Reidel, Dordrecht, **1979**, p201.
222 R. Schöllhorn, in *Physics of Intercalation Compounds*, edited by L. Pietronero and E. Tosatti, Springer Verlag, Berlin/New York, **1981**, p33.
223 C. Riekel, H. G. Rezink and R. Schöllhorn, *J. Solid State Chem*., **1979**, *29*, 323.
224 T. Hibma, *J. Solid State Chem.*, **1980**, *34*, 97.
225 W. R. Mc Kinnon and R. R. Haering, *Solid State Ionics*, **1980**, *1*, 111.
226 J. R. Dahn, W. R. Mc Kinnon and R. R. Haering, *Can. J. Phys.*, **1980**, *15*, 208; J. R. Dahn and R. R. Haering, *Solid State Commun.*, **1981**, *40*, 245.
227 S. A. Safran, *Phys. Rev. Lett.*, **1980**, *44*, 937; *Synth. Met.*, **1980**, *2*, 1.
228 W. Thulke, Thesis, Universität Kiel, **1984**.
229 R. Schöllhorn and W. Schmucker, *Z. Naturforsch*, **1975**, *30b*, 975.
230 W. L. Ijdo and T. J. Pinnavaia, *J. Solid State Chem*., **1998**, *139*, 281.
231 W. L. Ijdo and T. J. Pinnavaia, *Chem. Mater.*, **1999**, *11*, 3227.
232 V. A. Drits, T. N. Sokolova, G. V. Sokolova and V. I. Cherkashin, *Clays Clay Miner.*, **1987**, *35 (6*), 401.
233 A. S. Bookin, V. I. Cherkashin and V. A. Drits, *Clays Clay Miner.*, **1993**, *4*1, 558.
234 G. R. Williams and D. O'Hare, *Chem. Mater*., **2005**, *17*, 2632.
235 G. R. Williams, A. J. Norquist and D. O'Hare, *Chem. Commun.*, **2003**, 1816.
236 G. R. Williams, A. J. Norquist and D. O'Hare, *Chem. Mater.*, **2004**, *16*, 975.
237 G. R.Williams, Thesis, University of Oxford, **2005**, September.
238 D. O'Hare, J. S. O. Evans, A. Fogg and S. O'Brien, *Polyhedron*, **2000**, *19*, 297.
239 J. S. O. Evans, S. J. Price, H. V. Wong and D. O'Hare, *J. Am. Chem. Soc.*, **1998**, *120*, 10837.
240 J. S. O. Evans, R. J. Francis, D. O'Hare, S. J. Price, S. M. Clarke, J. Flaherty, J. Gordon, A. Nield and C. C. Tang, *Rev. Sci. Instrum.*, **1995**, *66*, 2442.
241 S. M. Clarke, A. Neild, T. Rathbone, J. Flaherty, C. C. Tang, J. S. O. Evans, R. J. Francis and D. O'Hare, *Nucl. Ins. Methods*, **1995**, *97*, 98.
242 A. M. Fogg, J. S. Dunn, S. G. Shyu, D. R. Cary and D. O'Hare, *Chem. Mater.*, **1998**, *10*, 351.
243 L. Lei, R. P. Vijayan and D. O'Hare, *J. Mater. Chem*., **2001**, *11*, 3276.
244 F. Millange, R. I. Walton, L. Lei and D. O'Hare, *Chem. Mater.*, **2000**, *12*, 1990.
245 S. M. Clark, *J. Appl. Crystallogr*., **1995**, *28*, 646.

246 J. H. Sharp, G. W. Brindley and B. N. N. Achar, *J. Am. Ceram. Soc*., **1966**, *49*, 379.
247 J. D. Hancock and J. H. Sharp, *J. Am. Ceram. Soc*., **1972**, *55*, 74.
248 G. R. Williams, A. I. Khan and D. O'Hare, *Struct. Bond*., **2006**, *119*, 161.
249 W. Jander, *Z. Anorg. Chem.*, **1927**, *163*, 1927.

Chapter 2 Factors Influencing Staging during Anion-exchange Reaction in $[Zn_2Cr(OH)_6]X\cdot nH_2O$ and $[Zn_2Al(OH)_6]Cl\cdot nH_2O$ Layered Double Hydroxides

2.1 Introduction

Recently, the mechanism by which intercalation occurs in layered hosts acquired a renewed of interest with the development of multifunctional materials. In the same time, the technological and experimental advances in energy-dispersive powder X-ray diffraction (EDXRD) with synchrotron X-ray sources have provided new possibilities for the study of solid-state reaction kinetics.[1] This technique allows the simultaneous observation of a wide range of *d*-spacings for all possible species involving the intercalation reaction such as the host, any intermediate phase and the product. Particularly, the markedly higher intensity over conventional laboratory X-ray source makes it possible the acquisition of good quality spectra on time scale of seconds, hence the kinetic study of fast intercalation reactions.[2] A wide variety of intercalation reactions have been investigated using EDXRD (see **Chapter 1**). [3-9]

By means of EDXRD, in collaboration with D. O'Hare and co-workers, we intend to develop a better understanding of LDH anion-exchange mechanisms and to determine the factors influencing the formation of LDH second-stage intermediate. [1, 10-14] EDXRD technique allows reactions to be continuously monitored in situ and detailed structural data can be collected.

The work described in this chapter builds on previous work performed by C. Taviot-Gueho and co-workers[14, 15] and seeks for the conditions that prevail for the formation of LDH second-stage compounds. In the first part, the exchange reactions of chloride (Cl^-) anions by tartrate ($^-O_2C(CHOH)_2CO_2^-$)/succinate ($^-O_2C(CH_2)_2CO_2^-$) anions in Zn_2Cr-Cl and Zn_2Al-Cl were investigated by means of EDXRD. The aims here are to further confirm the formation of the second-stage intermediates between tartrate/succinate

and chloride anions, examine the influence of the addition rate of the incoming anions on the observation/detection of the intermediate and investigate the kinetics of exchange reactions (partial kinetic analysis). In a second part, the study is extended to other anions. The exchange reactions of Cl^- anions with inorganic anions including carbonate (CO_3^{2-}), sulfate (SO_4^{2-}), ferricyanide ($[Fe^{III}(CN)_6]^{3-}$), and adipate ($^-O_2C(CH_2)_4CO_2^-$) organic anions in Zn_2Cr-Cl were investigated. We also looked at the exchange of tartrate anions by Cl^- and CO_3^{2-}inorganic anions in Zn_2Cr-Tart. These studies will give us some clues regarding the occurrence of staging phenomena in LDH system.

2.2 Experimental details

2.2.1 Synthesis of the host materials

Zn_2Cr-Cl/Zn_2Al-Cl host materials were synthesized by direct coprecipitation method while Zn_2Cr-Tart material was prepared from Zn_2Cr-Cl via anion-exchange route. [14] For the synthesis by coprecipitation, 40 mL of an aqueous solution containing a mixture of $ZnCl_2$ (0.66 M) and $CrCl_3/AlCl_3$ (0.33 M) were added in a flask previously filled with 150 mL of deionized and decarbonated water by a syringe pump under vigorous stirring. A solution of sodium hydroxide (2 M) was simultaneously added. The addition was carried out at room temperature under nitrogen (N_2) atmosphere and monitored by a pH regulator *via* a pH electrode immersed in the reagent solution to fix the pH of coprecipitation at 5.5 for Zn_2Cr-Cl and 8.0 for Zn_2Al-Cl. The resulting slurries were aged for 24 h in the mother liquid, then recovered by three dispersion and centrifugation cycles in water and finally dried in air.

Table 2-1: Chemical composition of precursor compounds

LDH	M^{2+}/M^{3+}	Cl^-/M^{3+}	H_2O/M^{3+}
Zn_2Cr-Cl	1.98	1.00	1.90
Zn_2Al-Cl	1.94	0.90	1.52

The chemical analysis of these chloride precursors given in **Table 2-1** by inductively coupled plasma (ICP) emission spectroscopy corresponds to a LDH composition with a M^{2+}/M^{3+} molar ratio close to 2. The powder X-ray diffraction patterns in **Figure 2-1** further confirm the formation of pure and well crystallized LDH compounds.

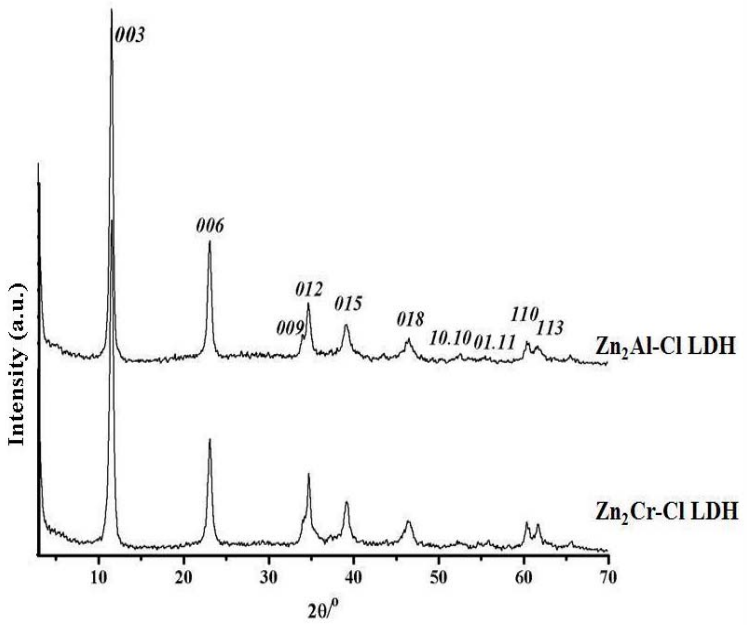

Figure 2-1: Powder X-ray diffraction patterns of Zn_2Al-Cl and Zn_2Cr-Cl prepared by coprecipitation.

Zn_2Cr-Tart was obtained by stirring about 1.5 g Zn_2Cr-Cl precursor, dispersed in a solution of sodium tartrate containing an excess of 2.5 of tartrate anions compared to the anionic exchange capacity (AEC) of Zn_2Cr-Cl precursor. The suspension was stirring for

24 h at room temperature and under nitrogen atmosphere, and then the solid was recovered by three dispersion-centrifugation cycles in water and finally dried in air. The powder XRD pattern of Zn_2Cr-Tart is displayed in **Figure 2-2**. The crystallinity of Zn_2Cr-Tart is lower than that of Zn_2Cr-Cl as often reported for tartrate containing LDH and attributed to the complexing power of tartrate anions reacting with metal cations from the hydroxide layer. [16]

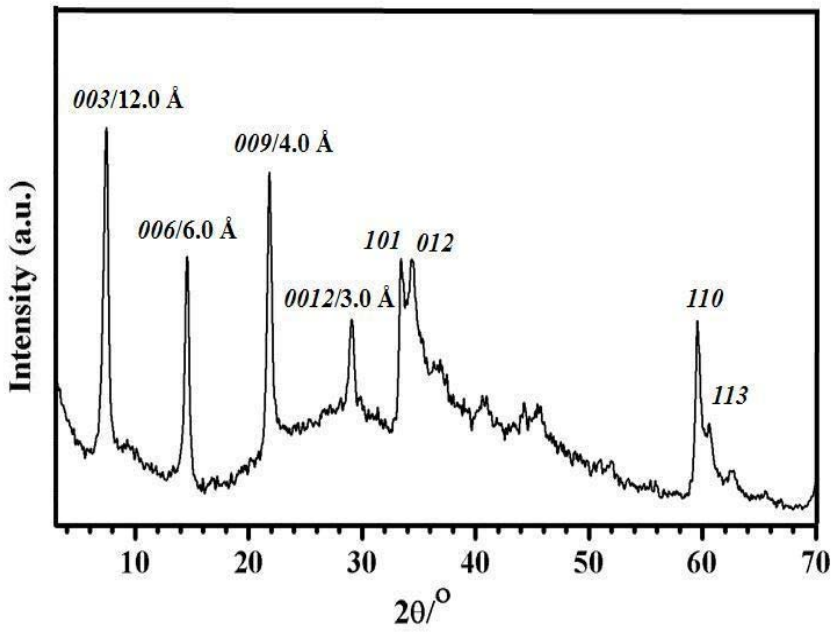

Figure 2-2: Powder X-ray diffraction patterns of Zn_2Cr-Tart from Zn_2Cr-Cl *via* anion-exchange route.

2.2.2 Time-resolved in situ energy-dispersive X-ray diffraction (EDXRD) measurements

The experiments were performed on Station 16.4 of the U. K. Synchrotron radiation source (SRS) at the Daresbury Laboratory using the same experimental setup as reported by O'Hare *et al.*.[1, 10] A photo of this equipment is given in **Figure 2-3**. A wide range of

d-spacing from *ca.* 109 – 3.8 Å can be observed while our interest in the present study focuses on the range of 20 – 3.8 Å.

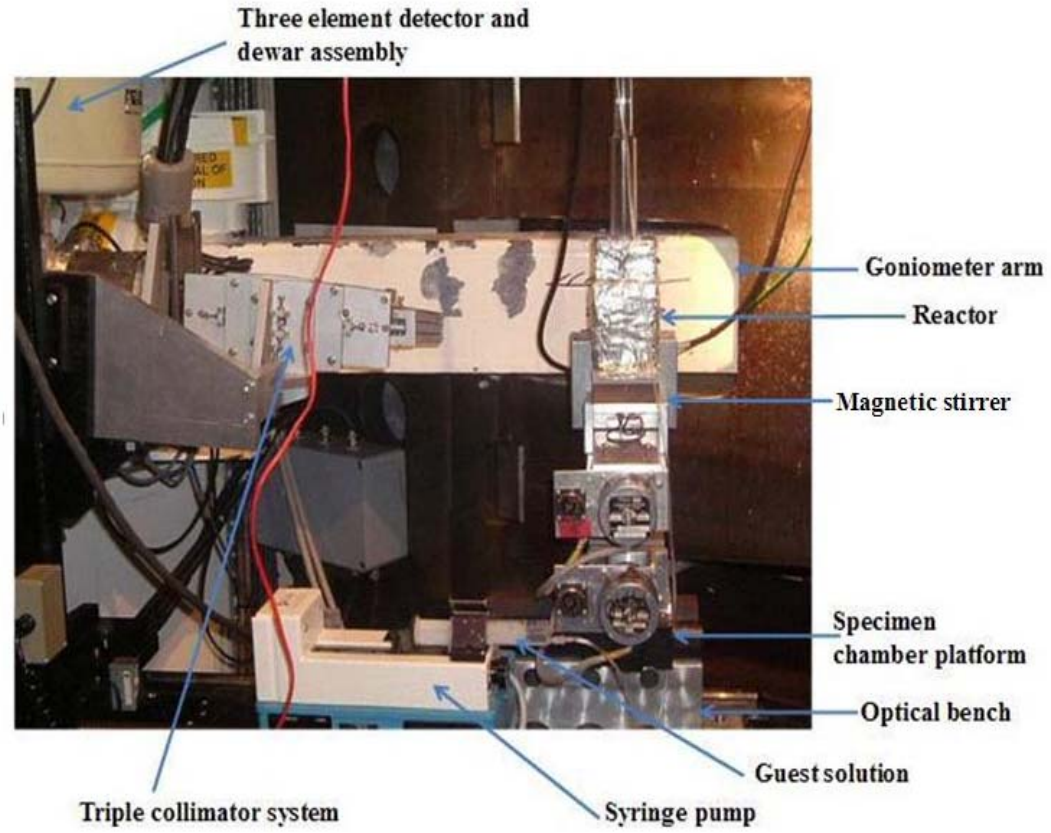

Figure 2-3**:** EDXRD experimental setup on station 16.4 at the UK SRS, Daresbury Laboratory used for studying in situ the anion-exchange reaction in LDH system.

An aqueous solution containing the incoming anions (different concentrations depending on the anions: 0.2 M for tartrate ($^{-}OOC(CHOH)_2COO^{-}$), succinate ($^{-}OOC(CH_2)_2COO^{-}$), adipate ($^{-}OOC(CH_2)_4COO^{-}$), CO_3^{2-} and SO_4^{2-} anions, 0.15 M for ferricyanide ($[Fe^{III}(CN)_6]^{3-}$) anions, and 1.6 M for Cl^- anions) was added by a syringe pump system into 10 mL of a suspension (25 g· L^{-1}) of LDH (Zn_2Cr-Cl, Zn_2Al-Cl, Zn_2Cr-Tart) in water. Two addition rates of the incoming anions solution were applied: 0.059 mL· min^{-1} and 1.0 mL· min^{-1}. The EDXRD spectra were collected at a fixed

detector angle of 1.625 ^{o} (2θ) with an acquisition time varying from 10 s to 60 s depending on the crystallinity of the system. The amount of incoming anions added into the suspension as a function of time was converted into a theoretical exchange rate based on the AEC of LDH starting phase. The EDXRD data collected by the program "PINCER" were converted into an available format for input into the Xfit peak profiling program using the program DLConverter.

2.2.3 Kinetic analysis of EDXRD data

The Xfit program was used to obtain the peak integrated areas of the Bragg reflections I_{hkl}, considering Gaussian curves.[17] These values were subsequently converted into the extent of reaction α at time *t* defined as:

$$\alpha(t) = I_{hkl}(t)/I_{hkl}(max) \quad (1)$$

where $I_{hkl}(t)$ is the area of a given *hkl* peak at a certain time *t* and $I_{hkl}(max)$ is the maximum area of this peak.

Information on reaction mechanism can be deduced from the kinetic equation of Avrami and Erofe'ev and the corresponding parameters k (the rate constant) and n (Avrami exponent) were calculated based on the Sharp and Hancock method[18]. The detailed analysis and kinetic models are introduced in Section **1.7.2**.

2.2.4 Powder X-ray diffraction (PXRD).

A Philips X-Pert Pro diffractometer was used for the X-ray diffraction analysis of the powders. The diffractometer was equipped with a Cu X-ray tube, graphite monochromator and Ar-filled proportional counter. Divergence and receiving slits were 1/16° and 1 mm, respectively. Powders were back-loaded in an aluminum sample holder

to produce a good sample surface and avoid preferential orientation effects. Data were collected in a step mode with a step size of 0.03° (2θ) and a counting time of 10 sec/step.

2.3 Anion-exchange Reaction of Cl^- Anions by Tartrate or Succinate Anions in Zn_2Cr-Cl and Zn_2Al-Cl LDHs

2.3.1 Formation of second-stage intermediates

2.3.1.1 In Zn_2Cr-Cl system

The exchange reactions in LDH system occur very vapidly; in a few minutes at room temperature we observed the formation of the fully exchanged phase. So, in order to study these reactions in detail, it is necessary to slow down the reaction rate by adding the anion solution in a dropwise manner. However, this slow addition of guest anions prevents a full quantitative kinetic analysis of the data.

Figure 2-4 shows the anion-exchange reaction of Zn_2Cr-Cl with tartrate anions for a slow addition (0.059 mL · min^{-1}) of the tartrate anion solution (0.2 M). Individual spectra were collected with an acquisition time of 60 s. The amount of guest anions added in the suspension of Zn_2Cr-Cl is converted into a theoretical anion exchange capacity (AEC) given on the right scale.

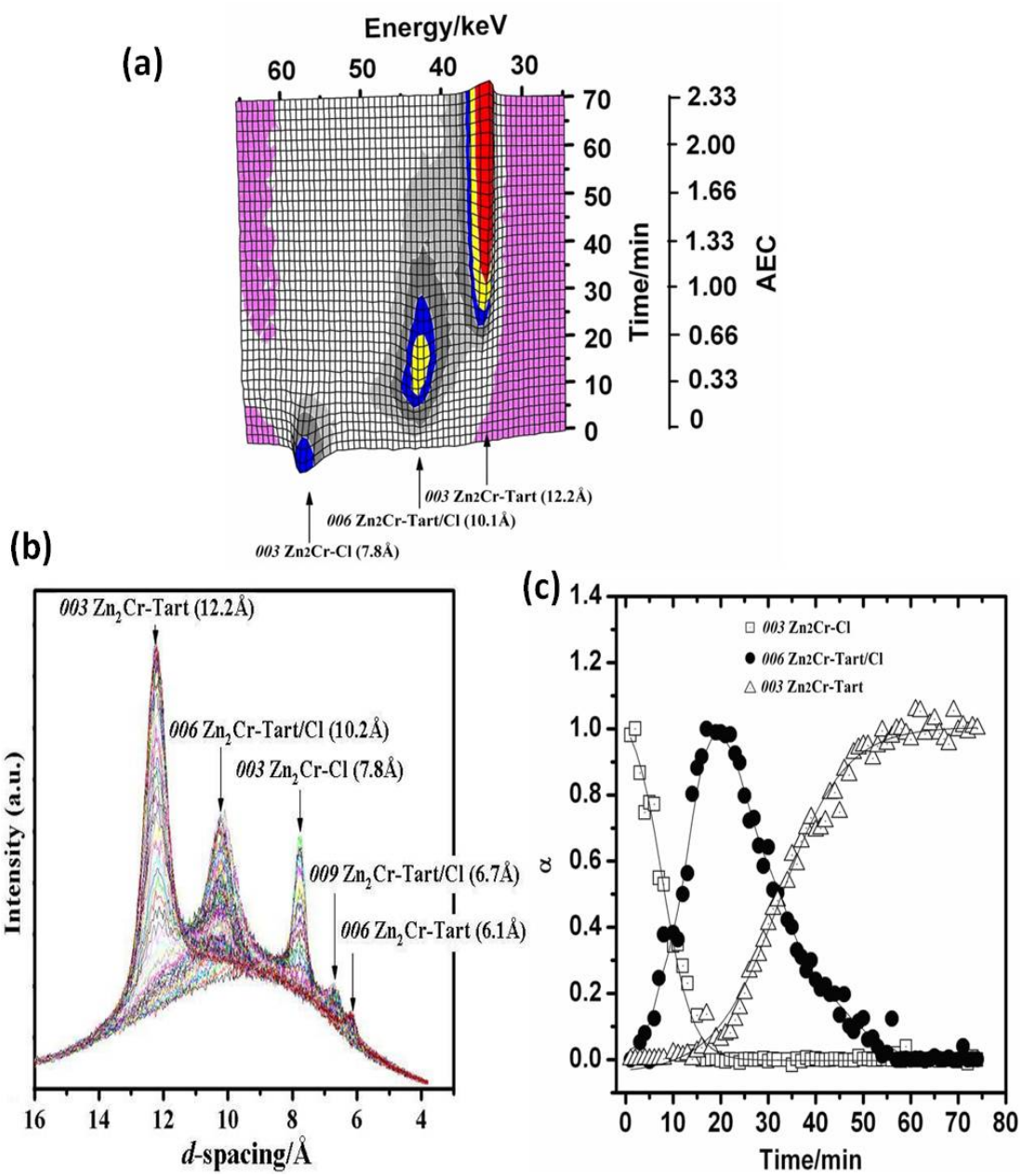

Figure 2-4**:** EDXRD data showing the course of the exchange reaction of Zn_2Cr-Cl with tartrate at room temperature. (a) 3D stacked plot showing the evolution of Zn_2Cr-Cl host *003*, Zn_2Cr-Tart/Cl intermediate *006*, and Zn_2Cr-Tart product *003* Bragg reflections as a function of time; (b) 2D stacked plot showing the same; (c) Extent of reaction (α) *vs.* time curves for host *003*, intermediate *006* and product *003* Bragg reflections.

Three successive Bragg reflections were observed with different *d*-spacings as a

function of time indicating a two-step exchange reaction process. The first peak at 7.8 Å corresponds to the *003* reflection of Zn_2Cr-Cl host; the immediate decay of this peak following the addition of the tartrate solution is accompanied by the growth of a new reflection at 10.1 Å attributed to the *006* reflection of the second-stage intermediate Zn_2Cr-Tart/Cl. The growth of the fully exchanged phase Zn_2Cr-Tart at 12.2 Å is not observed until the intermediate phase has gone through its maximum and the host has decayed completely. However, the present experimental setup cannot allow us to observe the *003* reflection of Zn_2Cr-Tart/Cl, only the second harmonic *006* reflection is visible at *ca.* 10.1 Å. This value multiplied by two exactly corresponds to the sum of the interlayer distance of the two anions, chloride and tartrate anions, as depicted in **Figure 2-5**.

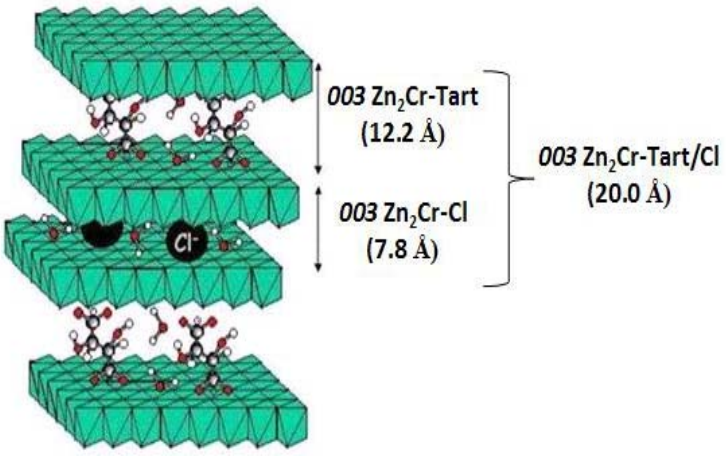

Figure 2-5**:** Idealized structure of Zn_2Cr-Tart/Cl second-stage compound with alternate interlayers occupied by chloride and tartrate anions.

From the variation of the intensity of the Bragg reflections, it is possible to calculate the extent of reaction noted alpha (α) as a function of time for each phase. The crossing for the host (Zn_2Cr-Cl) and the product (Zn_2Cr-Tart) at α = 0 indicates that the reaction is a two-step process implying the presence of an intermediate phase (**Figure 2-4** (c)).

Besides, the crossing at α = 0.5 for the intermediate (Zn_2Cr-Tart/Cl) and the product curves as well as for the intermediate and the product curves indicates a conversion of the host to the intermediate followed by the conversion of the intermediate to the product.

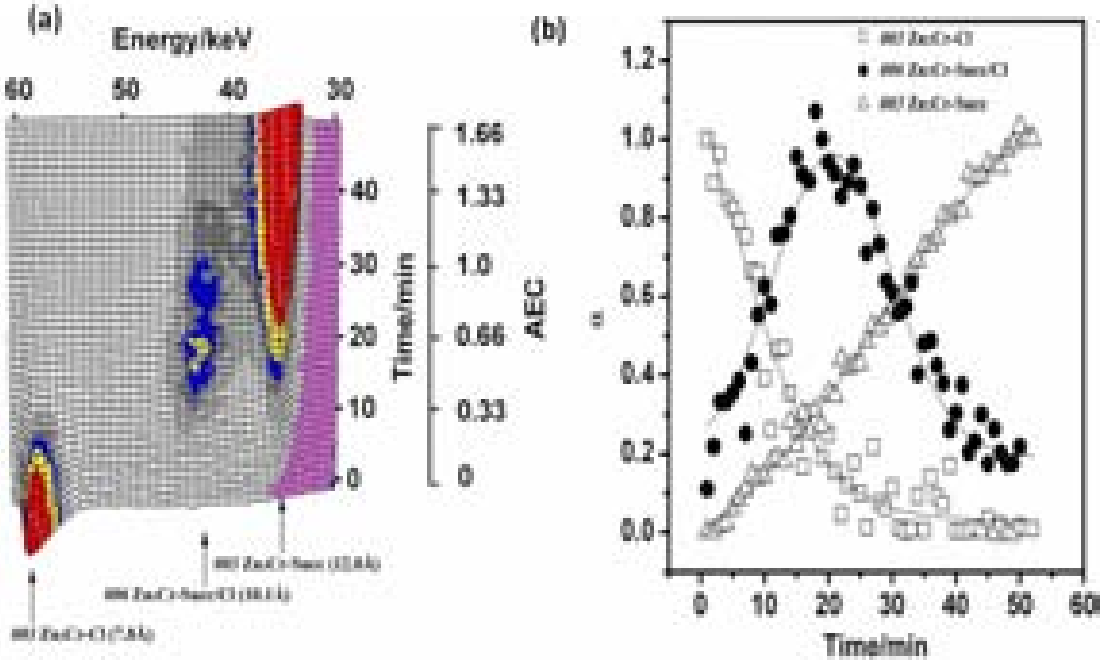

Figure 2-6**:** EDXRD data showing the course of the exchange reaction of Zn_2Cr-Cl with succinate at room temperature. (a) 3D stacked plot showing the evolution of Zn_2Cr-Cl host *003*, Zn_2Cr-Succ/Cl intermediate *006*, and Zn_2Cr-Succ product *003* Bragg reflections as a function of time and (b) extent of reaction *vs.* time curves for host *003*, intermediate *006* and product *003* Bragg reflections. The guest succinate anion solution (0.2 M) was added at a rate of 0.059 mL· min^{-1}.

Figure 2-6 shows the intercalation of succinate anions into Zn_2Cr-Cl. Three Bragg reflections are again observed at 7.8 Å *003* Zn_2Cr-Cl, 10.1 Å *006* Zn_2Cr-Succ/Cl and 12.0 Å *003* Zn_2Cr-Succ. However, in this case, the fully exchanged phase is observed almost at the same time as the second-stage intermediate, suggesting parallel processes with a route probably going through the intermediate as well as a direct transformation from the host to the fully exchanged phase. This result is different from that observed by O'Hare *et al.*[10]

in the case of the intercalation of succinate anions in $LiAl_2(OH)_6Cl{\cdot}H_2O$, for which a consecutive process was observed. The simultaneous presence of the intermediate and the fully exchanged phases also prevents isolation of Zn_2Cr-Succ/Cl second-stage compound.

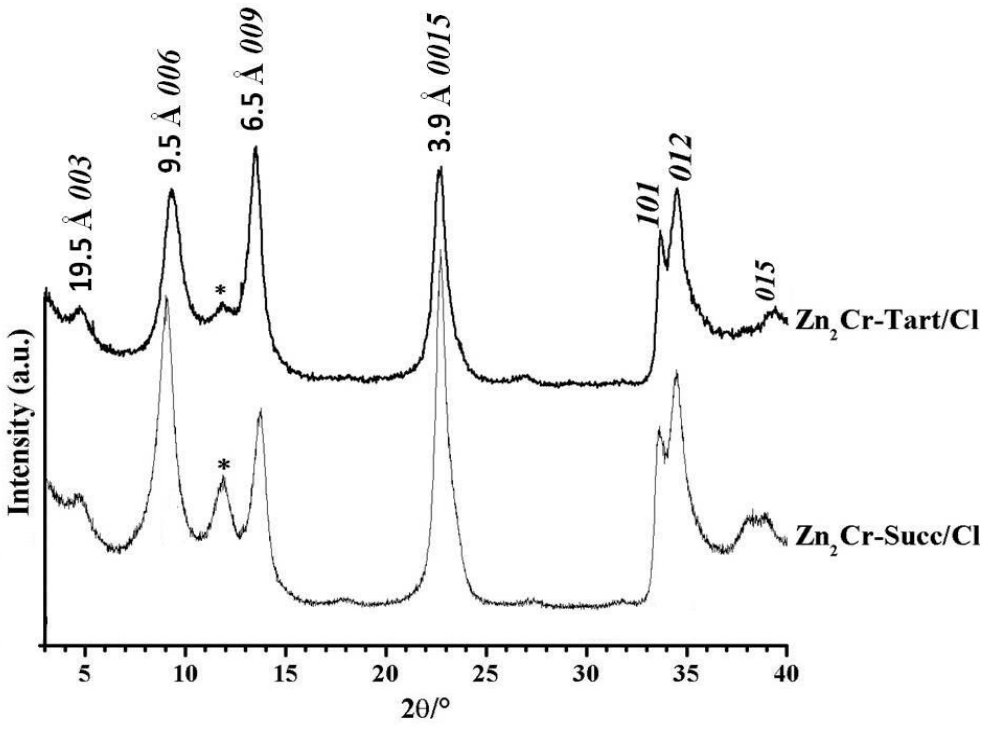

Figure 2-7**:** Ex situ powder X-ray diffraction patterns for the second-stage phases: Zn_2Cr-Succ/Cl and Zn_2Cr-Succ/Cl. Reflections marked with * correspond to the Zn_2Cr-Cl host.

In **Figure 2-7** are presented the PXRD patterns of the second-stage materials isolated in the laboratory by repeating EDXRD experiments (i.e. 0.2 M the solution of tartrate or succinate anions was added dropwise into 10 mL a suspension (25 $g \cdot L^{-1}$) of Zn_2Cr-Cl), and quenching the reaction where the concentration of the intermediate is expected to be the greatest,[19] i.e. for Zn_2Cr-Tart/Cl, at a reaction time *ca.* 18 min corresponding to the crossing point of α(t) curves of the host and the product at α = 0, and for Zn_2Cr-Succ/Cl at a reaction time *ca.* 20 min corresponding to the crossing point at *ca.* α = 0.3. As expected,

Zn_2Cr-Tart/Cl appears almost as a pure phase with low trace of Zn_2Cl-Cl. Conversely, Zn_2Cr-Succ/Cl sample is actually a mixture of Zn_2Cr-Succ/Cl and Zn_2Cr-Cl. In the case of Zn_2Cr-Succ/Cl, the powder does not exactly reflect the composition of the reaction matrix at the time of quenching since we expected a mixture of Zn_2Cr-Succ/Cl and Zn_2Cr-Succ and not Zn_2Cr-Cl. The equilibrium between phases must have been displaced during the centrifugation/washing/drying steps.

2.3.1.2 **In Zn_2Al-Cl system**

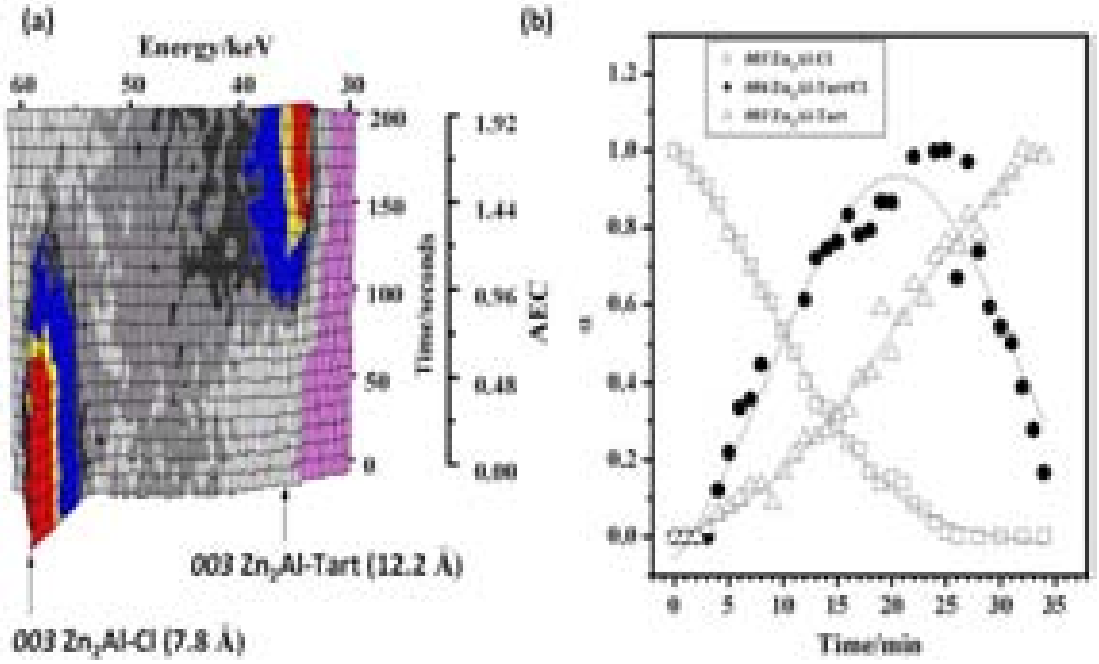

Figure 2-8**:** EDXRD data showing the course of the exchange reaction of Zn_2Al-Cl with tartrate anions at room temperature. (a) 3D stacked plot showing the evolution of Zn_2Al-Cl host *003*, Zn_2Al-Tart/Cl intermediate *006* and Zn_2Al-Tart product *003* Bragg reflections as a function of time. (b) Extent of reaction *vs.* time curves for host *003*, intermediate *006* and product *003* Bragg reflections. The guest tartrate anions solution (0.2 M) was added at a rate of 0.059 mL· min^{-1}.

The same exchange reactions were carried out with Zn_2Al-Cl. Plots showing the course of the exchange reactions of Zn_2Al-Cl with tartrate and succinate anions are

present in **Figure 2-8** and **Figure 2-9**, respectively. Compared to Zn_2Cr-system, Zn_2Al-system displays a lower crystallinity which makes detection of the second-stage intermediate rather difficult, particularly in the case of tartrate exchange reaction. In the present conditions, the intercalation of tartrate and succinate anions appear to proceed the same way i.e. *via* parallel processes. Yet, owing to the low crystallinity of the system, we cannot go further in the interpretation of the data nor in the comparison with Zn_2Cr-system.

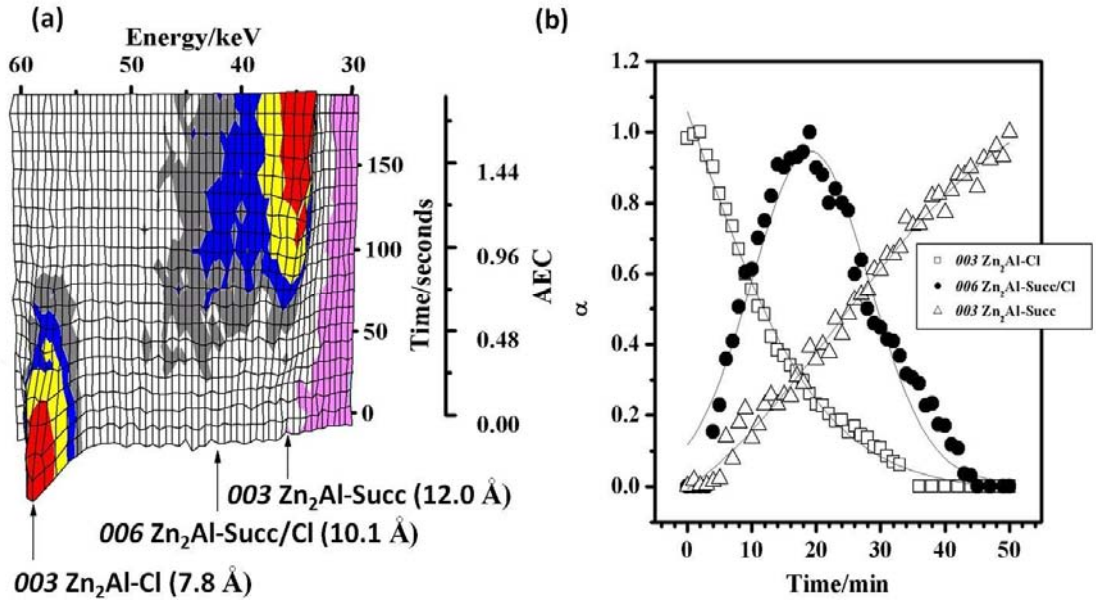

Figure 2-9**:** EDXRD data showing the course of the exchange reaction of Zn_2Al-Cl with succinate anions at room temperature. (a) 3D stacked plot showing the evolution of Zn_2Al-Cl host *003*, Zn_2Al-Succ/Cl intermediate *006* and Zn_2Al-Succ product *003* reflections, and (b) extent of reaction *vs.* time curves for host *003*, intermediate *006* and product *003* Bragg reflections. The succinate anion solution (0.2 M) was added at a rate of 0.059 mL· min^{-1}.

This results are consistent with those we previously obtained; the better quality of Zn_2Cr data allows us to confirm the trends highlighted in this previous work, in particular the existence of different exchange pathways depending on the nature of the incoming

organic anions.

2.3.2 Effect of the addition rate of the incoming anions on the observation of second-stage intermediates

In **Figure 2-10**, are compared the exchange reactions of tartrate anions with Zn_2Cr-Cl conducted at two different addition rates:

(a) Slow addition rate of 0.059 mL · min^{-1} with acquisition time of 60 s;

(b) High addition rate of 1.0 mL · min^{-1} with acquisition time of 10 s.

For the high addition rate, EDXRD patterns are less resolved and the intermediate and the product appear almost at the same time. For the lower addition rate, the second-stage intermediate has reached its maximum after *ca.* 18 min which corresponds to a theoretical anion exchange level of 0.60 AEC, while the fully exchanged phase is the only phase present after 50 min i.e. 1.65 AEC. For the high addition rate, the maximum intensity for Zn_2Cr-Tart/Cl is observed after *ca.* 1.8 min i.e. 1.03 AEC and for the product after 4 min i.e. 2.28 AEC. These measurements clearly show that the rate of the exchange reaction is dependent on the addition rate of the guest anion solution. One can say that the exchange reaction in LDH system occur very rapidly in a few minutes and to study these reactions in detail, observe and eventually isolate intermediate phases, it is necessary to add the incoming anion solution dropwise at a low addition rate. This experimental constraint on the addition rate prevents a full quantitative kinetic analysis of the data. However, assuming a rather negligible effect on the reaction rate for the high addition rate of 1.0 mL · min^{-1}, we attempted to extract kinetic information from the α(t) plots recorded in these conditions.

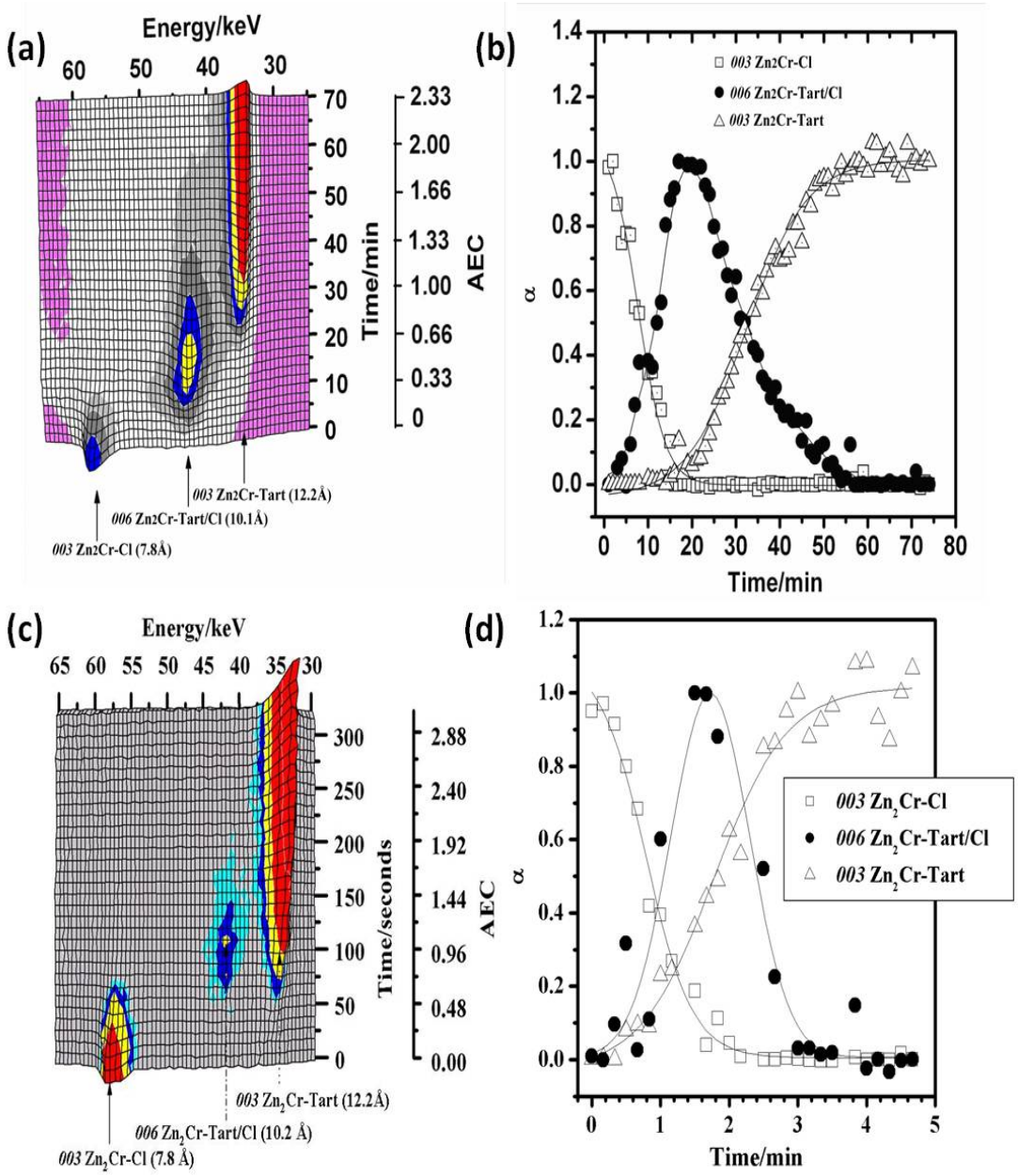

Figure 2-10: EDXRD data showing the course of the exchange reaction of Zn_2Cr-Cl with tartrate (0.2 M) at room temperature. 3D stacked plots showing the evolution of Zn_2Cr-Cl host *003*, Zn_2Cr-Tart/Cl intermediate *006* and Zn_2Cr-Tart product *003* Bragg reflections as a function of time (a) at an addition rate of 0.059 mL· min^{-1} with an acquisition time of 60 s and (c)1.0 mL· min^{-1} with 10 s, respectively; Extent of reaction *vs.* time curves for host *003*, intermediate *006* and product *003* Bragg reflections (b) at the high addition rate and (d) at the low addition rate.

2.3.3 Kinetic analysis

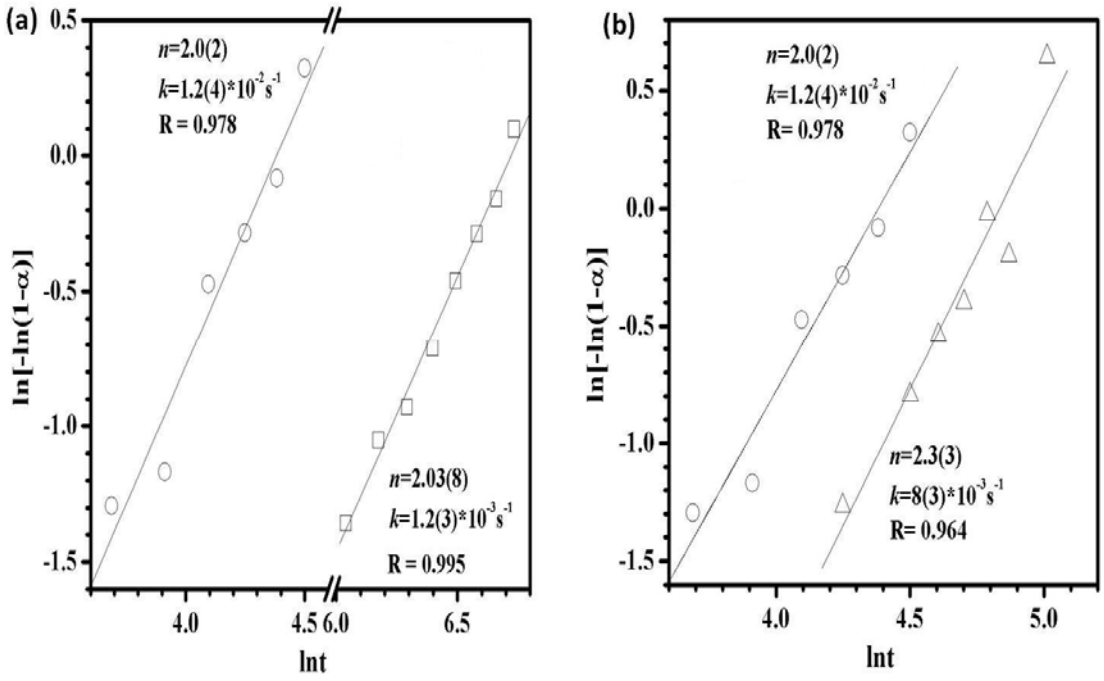

Figure 2-11: Sharp-Hancock plots of ln[-ln(1-α)] *vs.* ln(time) for the transformation (a) from Zn_2Cr-Cl to Zn_2Cr-Tart/Cl at the two different addition rates of tartrate anions into Zn_2Cr-Cl system: at 0.059 mL· min^{-1} (□) and 1.0 mL· min^{-1} (○); (b) from Zn_2Cr-Cl to Zn_2Cr-Tart/Cl (○) and from Zn_2Cr-Tart/Cl to Zn_2Cr-Tart (Δ) at the addition rate of 1.0 mL · min^{-1}. *R* presents the linear correlation factor.

From the α(t) plots, it is possible to extract kinetic data *via* the Sharp-Hancock method corresponding to the Log-linearized form of the Avrami and Erofe'ev equation[20]as follows:

$$\ln(-\ln(1-\alpha)) = n\ln k + n\ln t \qquad \textbf{Equation } 2\text{-}1$$

where *k* is the rate constant and *n* is the Avrami exponent as described in the **Section 1.7.2**. **Figure 2-11** (a) gives the Sharp-Hancock analysis for the Zn_2Cr-Cl~ Zn_2Cr-Tart/Cl transformation at the two addition rates (0.059 mL· min^{-1} and 1.0 mL· min^{-1}). As expected,

the rate constant *k* increases with the addition rate of tartrate anions: $1.2(3)*10^{-3}s^{-1}$ for 0.059 mL· min^{-1} and $1.2(4)*10^{-2}$ s^{-1} for 1.0 mL· min^{-1} at 25 ℃. This latter value is comparable with rate constants reported elsewhere for intercalation reactions in other layered materials [2] and for the intercalation of phenylphosphonic (PPA) anions into $[LiAl_2(OH)_6]Cl{\cdot}H_2O$ ($3.5 \times 10^{-3}\ s^{-1}$ at 26.5 ℃) [11]. The *n* value derived from the slope is the same for the two addition rate and equal to 2.0, indicating the same reaction mechanism whatever the addition rate.

Table 2-2**:** Nuclei growth models for solid state reactions. Values possible for intercalation into a layered host are highlighted in *bold.* See ref. 20.

Dimension of growth (λ)	**Nucleation rate (β)**	**Exponent value**	
		Phase boundary controlled (*n*)	Diffusion controlled (*m*)
1	Zero (instantaneous)	1	0.5
	Deceleratory	**1-2**	**0.5-1.5**
	Constant	2	1.5
2	**Zero (instantaneous)**	**2**	**1**
	Deceleratory	**2-3**	**1-2**
	Constant	3	2
3	Zero (instantaneous)	3	1.5
	Deceleratory	3-4	1.5-2.5
	Constant	4	2.5

For a layered materials like LDH, it is expected that the growth is in two dimension (λ = 2) corresponding to the movement of the anions between LDH hydroxide layers. [21] The intercalation sites are the edges of the layers. As the exchange reaction proceeds, some of the layers are filled leading to a decrease of the number of nucleation site. Thus

one might expect exchange reaction in LDH to be 2D process with **deceleratory nucleation** (β) as described in **Table 2-2**. Following nucleation, the reaction then may be either phase boundary or diffusion controlled. The value of *n* obtained from Sharp-Hancock analysis i.e. 2-3 (**Figure 2-11** (b)) is in favor of a phase boundary controlled process i.e. the reaction rate is limited by the expansion of the interlayer space necessary to accommodate tartrate anions.

2.3.4 Refinement of Zn_2Cr-Tart/Cl second-stage intermediate

The refinement was performed using the Fullprof program[22, 23]. The collected PXRD data were treated for profile matching in the space group *R-3m* using the TCH pseudo-Voigt-profile function according to procedures described elsewhere[24]. In order to take into account the instrumental broadening, the PXRD pattern of a silicon standard specimen (U = 0.064902, V= -0.369403, W= 0.095556, X= 0.042914, Y= 0.041991) was fitted by the convolution to the experimental TCH pseudo-Voigt function. A mathematical model based on linear combinations of spherical harmonics was used to treat anisotropic size broadening while anisotropic size effects were described by the phenomenological model suggested by Stephens[25, 26]. Size and strain parameters were refined one-by-one due to the small number of reflections, also because no structure constraint was applied.

The diffraction peaks were indexed based on a hexagonal unit cell with the space group *P3*. As evidenced from the position of the reflection markers shown at the bottom of the XRD pattern in **Figure 2-12**, Zn_2Cr-Tart/Cl appear as “pure” sample. In particular, the observation of the *003* reflection at *ca.* 19.5 Å makes no doubt of the formation of the second-stage compound. A profile refinement was attempted using the TCH pseudo-Voigt profile function; the poor quality of the fitting is visible on the plot but allow us to give

the following cell parameters: a = 3.101(1) Å and c = 19.83(1) Å. The size parameters derived from the profile refinement indicate a small crystallite size of ~100 Å with an anisotropy of ~ 30 Å in agreement with the hexagonal platelet-like morphology of LDH materials. Such a small size of the coherent domain which corresponds to the stacking of only five repeat units of Zn_2Cr-Tart/Cl, may explain the fact that higher stage phases could not be detected by X-ray diffraction technique even if they exist.

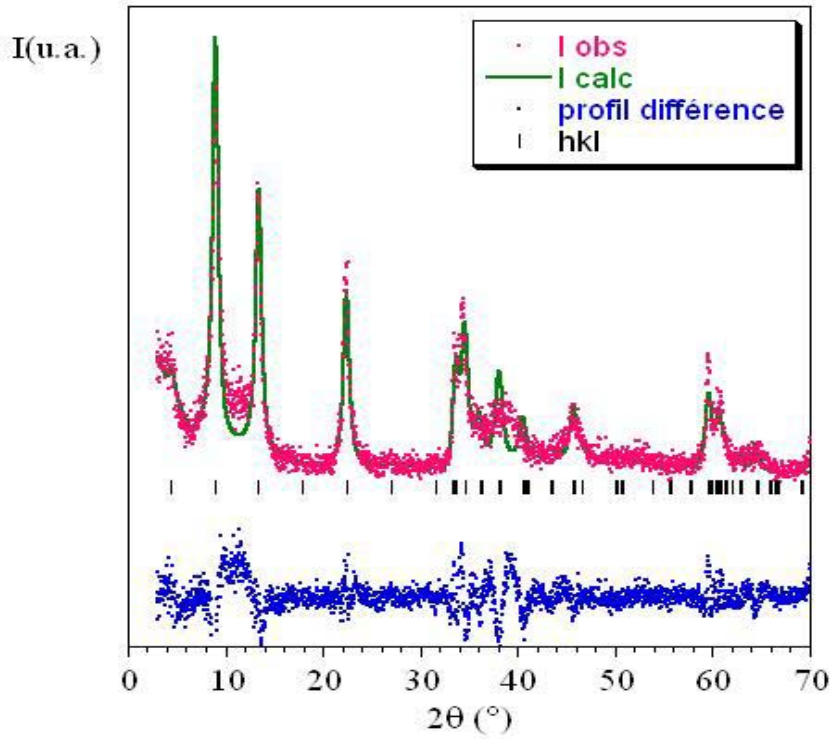

Figure 2-12**:** Profile matching of the X-ray powder diffraction diagram of Zn_2Cr-Tart/Cl: experimental data (points), calculated (line) and Bragg reflections (ticks) and difference profile.

2.4 Effect of nature of initial interlayer anions (X) and incoming anions on the formation of second-stage intermediate

From the previous work by Taviot-Gueho *et al.* [14, 15] and Iyi *et al.* [12], the staging in LDH system is a peculiarity of organic-inorganic exchange reactions since staging has been never observed for inorganic-inorganic exchange reaction so far, except the mineral in the composition of $[Mg_8Al_4(OH)_{24}][M^+_{0.5}(SO_4)_{1.25}(CO_3)_{1.0}\cdot 9H_2O]$[27, 28]. However, it is not all organic anions which can form staging structure with inorganic anions. Yet, the number of inorganic anions already investigated is quite limited (Cl^-, Br^- and NO_3^-).[1] In the following, we consider first the exchange of CO_3^{2-}, SO_4^{2-} and $[Fe^{III}(CN)_6]^{3-}$ inorganic anions with Zn_2Cr-Cl, then the exchange of adipate anions with Zn_2Cr-Cl and finally the exchange of Cl^- and CO_3^{2-} anions with Zn_2Cr-Tart.

2.4.1 Inorganic-inorganic exchange reactions: Cl^- anions by CO_3^{2-}, SO_4^{2-} and $[Fe(CN)_6]^{3-}$ anions in Zn_2Cr-LDH

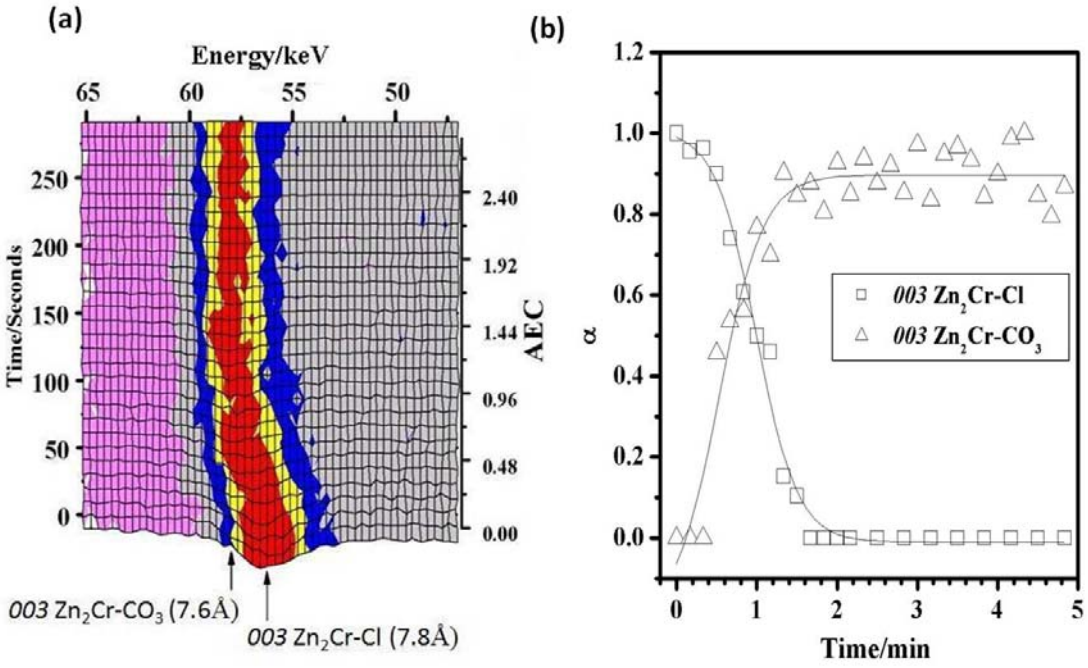

Figure 2-13: EDXRD data showing the course of the exchange reaction of Zn_2Cr-Cl with carbonate (CO_3^{2-}) anions at room temperature. (a) Three-dimension stacked plot showing the evolution of Zn_2Cr-Cl host *003* and Zn_2Cr-CO_3 product *003* Bragg reflections as a function of time, and (b) extent of reaction *vs*. time curves for host *003* and product *003* Bragg reflections. The carbonate guest anion solution (0.2 M) was added at a rate of 1.0 mL· min^{-1} and individual spectra were collected with an acquisition time of 10 s.

The exchange of Cl^- anions by CO_3^{2-} and SO_4^{2-} anions presented in **Figure 2-13** and **2-14** show only two reflection peaks corresponding to the *003* Bragg reflection of the host (Zn_2Cr-Cl at 7.8 Å) and the *003* reflection of the final product (Zn_2Cr-CO_3 at 7.6 Å and Zn_2Cr-SO_4 at 11.0 Å), respectively. In the both cases, there is no intermediate peak observed. Although, one must say that the small difference between the interlamellar distance of Zn_2Cr-Cl (7.8 Å) and Zn_2Cr-CO_3 (7.6 Å) would make it difficult to observe an

intermediate compound if it existed. However, the intersection of α(t) curves again occurs at α ≈ 0.6 in **Figure 2-13** (b), thus confirming the occurrence of a one-step process. The *d*-value of Zn_2Cr-SO_4 at 11.0 Å is consistent with data reported elsewhere[29] and observed at very high humidity (RH > 50%).

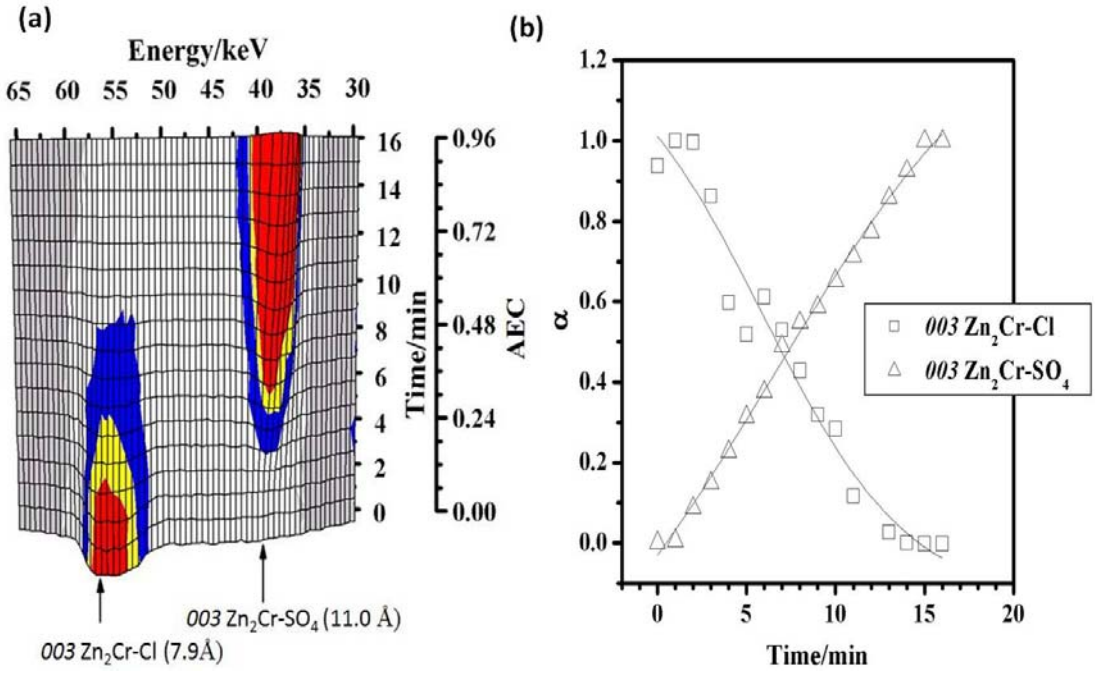

Figure 2-14: EDXRD data showing the course of the exchange reaction of Zn_2Cr-Cl with sulfate anions (SO_4^{2-}) at room temperature. (a) 3D stacked plot and (b) extent of reaction *vs.* time curves showing the evolution of Zn_2Cr-Cl *003* and Zn_2Cr-SO_4 *003* Bragg reflections as a function of time. The sulfate anion solution (0.2 M) was added at a rate of 0.059 mL· min^{-1}.

Figure 2-15 shows the exchange reaction of Cl^- anions by $[Fe^{III}(CN)_6]^{3-}$ anions in Zn_2Cr-Cl. Only two Bragg reflection peaks were detected at 7.8 Å corresponding to *003* Zn_2Cr-Cl (the host) and at 10.88 Å assigned to *003* Zn_2Cr-$Fe(CN)_6$, a value close to 11.1 Å generally reported for hexacyanoferrate-containing LDH.[30, 31]Similarly, the α(t) curves for Zn_2Cr-Cl and Zn_2Cr-$Fe(CN)_6$ cross at α ≈ 0.5, indicating a direct conversion from the host to the fully exchanged phase.

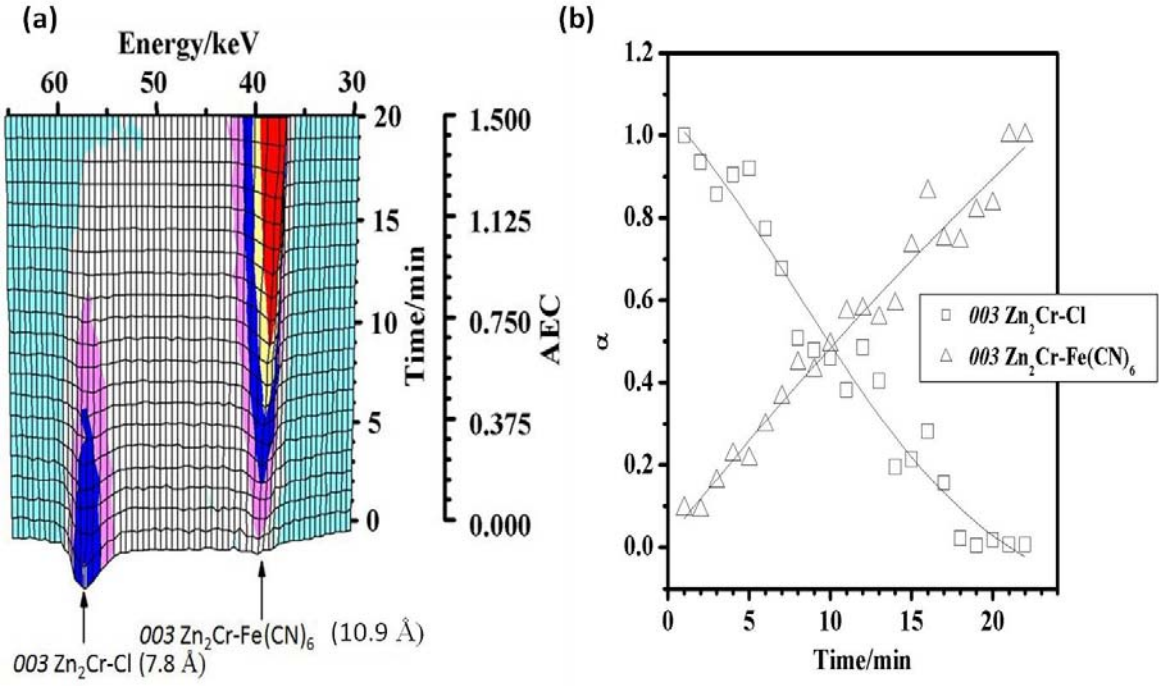

Figure 2-15**:** EDXRD data showing the course of the exchange reaction of Zn_2Cr-Cl with ferricyanide ($[Fe(CN)_6^{3-}]$) at 55 ℃.(a) Three-dimension stacked plot and (b) extent of reaction *vs.* time curves showing the evolution of Zn_2Cr-Cl host *003* and Zn_2Cr-$Fe(CN)_6$ product *003* Bragg reflections as a function of time. The ferricyanide guest anion solution (0.15 M) was added at a rate of 0.118 $mL \cdot min^{-1}$.

These findings further indicate that inorganic-inorganic anion exchange reactions proceed one-step with a direct transformation from the host to the fully exchanged product. This supports the above assumption of inorganic/organic segregation responsible for staging in LDH system. Additionally, the fact that no staging was observed between Cl^- (d_{003} = 7.8 Å) and $[Fe(CN)_6]^{3-}$ (d_{003} = 10.9 Å) anions, of a similar size compared with tartrate anions (d_{003} = 12.2 Å), may indicate that size effect does not play a prominent role in staging phenomena in LDH system.

2.4.2 Organic-inorganic exchange reactions in Zn_2Cr-LDH

2.4.2.1 Cl^- anions exchanged by adipate anions

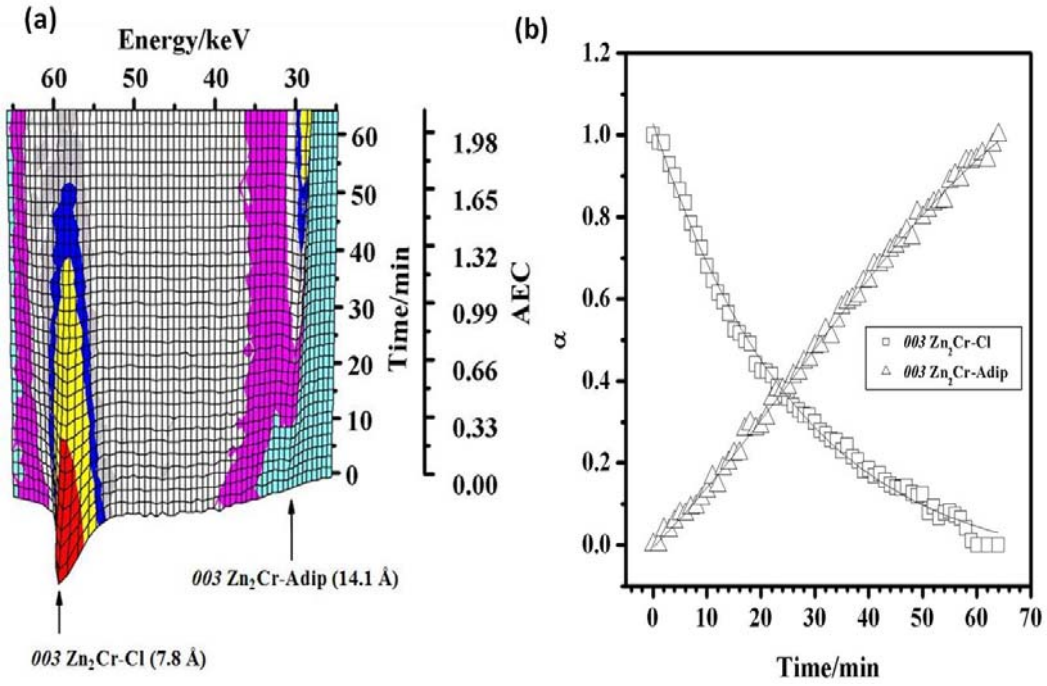

Figure 2-16**:** EDXRD data showing the course of the exchange reaction of adipate ($^-O_2C(CH_2)_4CO_2^-$) with Zn_2Cr-Cl at room temperature. (a) Three-dimensional stacked plot showing the evolution of Zn_2Cr-Cl host *003* and Zn_2Cr-Adip product *003* Bragg reflections as a function of time. and (b) extent of reaction *vs.* time curves for host *003* and product *003* Bragg reflections. The adipate guest anion solution (0.2 M) was added at a rate of 0.059 mL· min^{-1}.

Figure 2-16 shows the exchange reaction of Cl^- anions by adipate anions in Zn_2Cr-Cl. Again only two Bragg reflections are observed, at 7.8 Å assigned to the *003* reflection of the host Zn_2Cr-Cl and at 14.1 Å corresponding to the *003* reflection of the first stage product Zn_2Cr-Adip. The crossing point of the α(t) curves for the host and the first stage product occurs at α ≈ 0.4 (**Figure 2-16** (b)) indicating a direct transformation from the host to the product. However, ex situ powder X-ray diffraction patterns

presented in **Figure 2-17** indicate the presence of a poor crystalline second-stage phase formed at a theoretical exchange rate of 0.6. The reflection at *ca.* 22.2 Å can be assigned with no doubt to the *003* reflection of Zn_2Cr-Adip/Cl second-stage, being equal to the sum of the *d*-spacings of Zn_2Cr-Cl host (7.8 Å) and Zn_2Cr-Adip product (14.1 Å) and very close to the *d*-spacing reported for $LiAl_2$-Adip/Cl (22.0 Å)[10]. It is noteworthy that the intensities of both *003* and *006* diffraction peaks of Zn_2Cr-Adip/Cl are very weak, explained why they are not detected in solution by EDXRD.

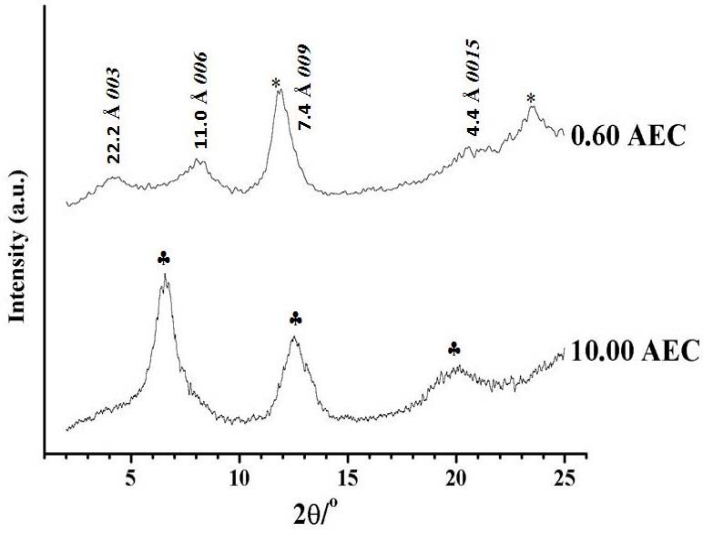

Figure 2-17**:** Ex situ powder X-ray diffraction patterns showing the exchange reaction of Zn_2Cr-Cl with adipate anions at theoretical exchange rates of 0.60 and 10.00. Reflections marked with * correspond to the Zn_2Cr-Cl host and with ♣ present the Zn_2Cr-Adip product.

2.4.2.2 Tartrate anions exchanged by Cl^- and CO_3^{2-}anions

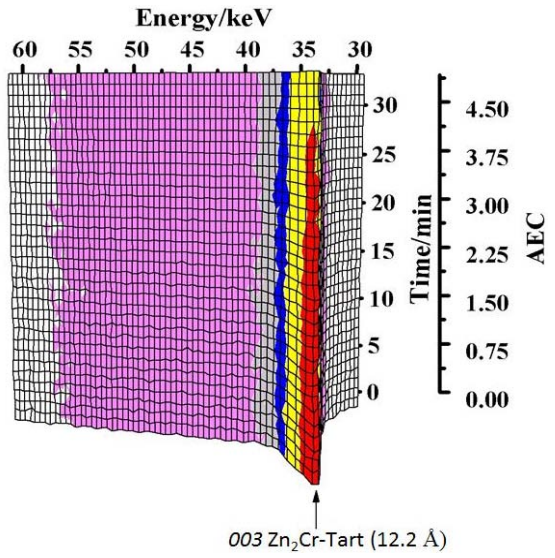

Figure 2-18: EDXRD data showing the course of the exchange reaction of Zn_2Cr-Tart with chloride (Cl^-) at room temperature. Three-dimension stacked plot showing the evolution of Zn_2Cr-Tart *003* Bragg reflections as a function of time. The guest chloride anion solution (1.6 M) was added at a rate of 0.059 $mL \cdot min^{-1}$.

In the case of chloride anion exchange (in **Figure 2-18**), only the *003* reflection of Zn_2Cr-Tart host at 12.2 Å is observed even for an excess of chloride anions representing 20 times the AEC.

On the contrary, CO_3^{2-} anions can exchange with tartrate anions in Zn_2Cr-Tart (**Figure 2-19** (a)) and three Bragg reflections are observed, corresponding to *003* Zn_2Cr-Tart host at 12.2 Å, *006* Zn_2Cr-Tart/CO_3 second-stage intermediate centered at 9.6 Å and *003* Zn_2Cr-CO_3 product at *ca.* 7.9 Å. The immediate decay of the *003* Zn_2Cr-Tart following the addition of carbonate anions is accompanied by the growth of the *006* reflection of Zn_2Cr-Tart/CO_3. Then, the final product Zn_2Cr-CO_3 is not observed until the intermediate has disappeared completely. The gradual shift of the position of the

intermediate peak from 10.2 Å to 8.56 Å upon carbonate-tartrate exchange may be explained by a variation of the number of the layers intercalated by CO_3^{2-} as reported for staged fluorohectorite clays[32]. In this case, we assume the existence of staging of higher order than 2, which has never been reported so far. In **Figure 2-19** (b) are presented the α(t) curves for the *003* reflection of Zn_2Cr-Tart host and the *003* reflection of Zn_2Cr-CO_3 final product; owing to the variation of the interlayer distance for *006* the intermediate, it was impossible to obtain the corresponding α(t) curve. The intersection point at α = 0 confirms the existence of Zn_2Cr-Tart/CO_3 intermediate. EDXRD measurements were repeated in the laboratory. The PXRD patterns of Zn_2Cr-Tart/CO_3 isolated after 15 min (**Figure 2-20** (a)) and 25 min (**Figure 2-20** (b)). They appear as pure phases but with a different cell parameter *c*. This is in total agreement with a variation of the number of layer intercalated by CO_3^{2-} anions as described above. For the sample after 15 min (**Figure 2-20** (a)), the cell parameter *c* is equal to 2×9.5 (d_{006}) = 19.0 Å ≈ 12.0 (d_{003}, Tart) + 7.5 (d_{003}, CO_3^{2-}) in agreement with the *006* Bragg reflection of a second-stage phase Zn_2Cr-Tart/CO_3; for the sample obtained after 25 min (**Figure 2-20** (b)), the cell parameter *c* can be assumed as $27 \text{ Å} = 3 \times 9.0$ ($\approx 6.6 \times 4$) = 12.0 (d_{003}, Tart) + 7.5 (d_{003}, CO_3^{2-}) + 7.5 (d_{003}, CO_3^{2-}) indicating a possible third stage phase Zn_2Cr-CO_3/Tart/CO_3.

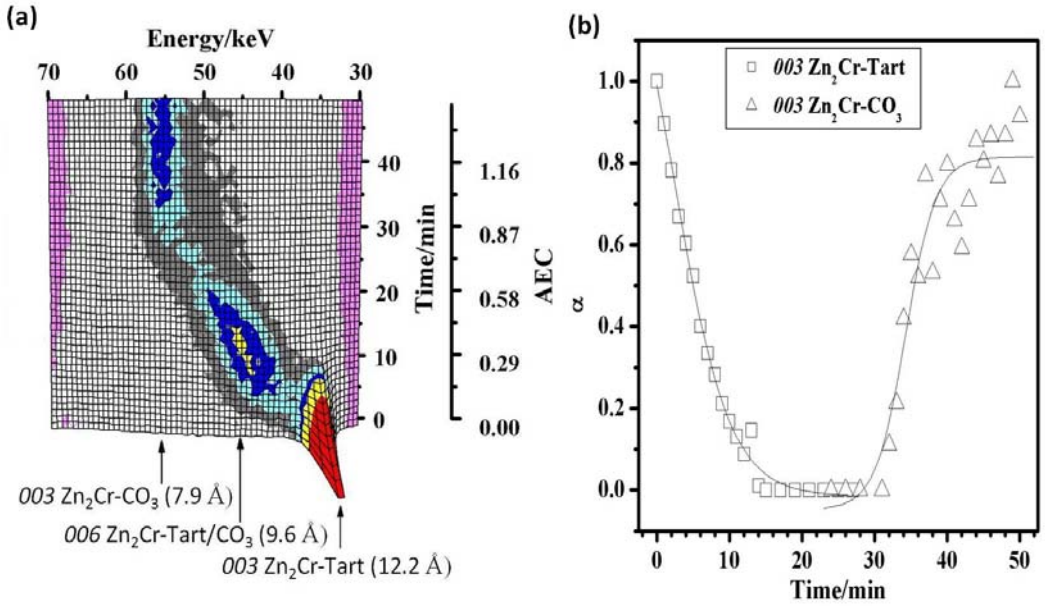

Figure 2-19: EDXRD data showing the course of the exchange reaction of carbonate anions with Zn_2Cr-Tart at room temperature. (a) Three-dimension stacked plot showing the evolution of Zn_2Cr-Tart host *003*, Zn_2Cr-Tart/CO_3 intermediate *006* and Zn_2Cr-CO_3 product *003* Bragg reflections as a function of time; (b) extent of reaction *vs.* time curves for host *003* and product *003* Bragg reflections. The carbonate guest anion solution (0.2 M) was added at a rate of 0.059 mL· min^{-1}.

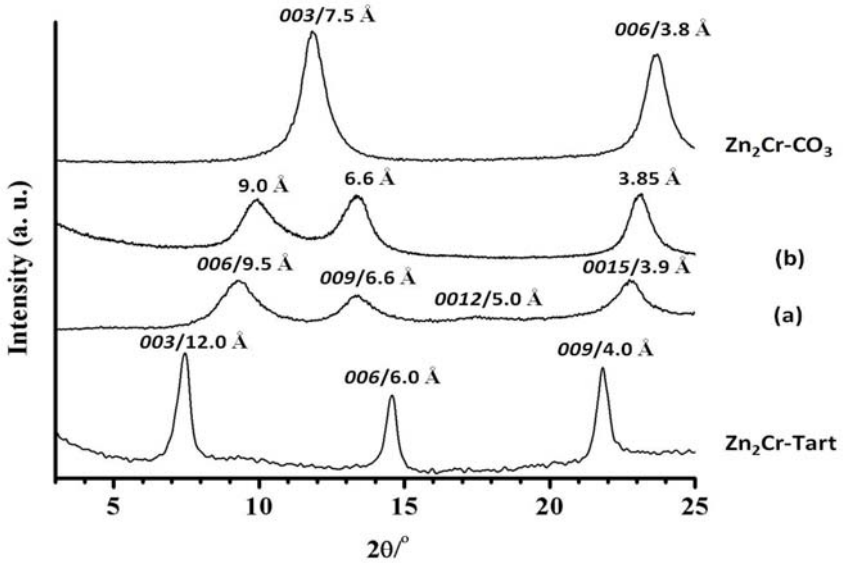

Figure 2-20: Ex situ powder X-ray diffraction patterns for the host Zn_2Cr-Tart, the intermediate Zn_2Cr-Tart/CO_3 ((a) quenched at 15 min, (b) quenched at 25 min) and the fully exchanged product Zn_2Cr-CO_3.

2.5 Conclusions

These results show that the observation of LDH second-stage intermediate during anion-exchange reactions by means of in situ EDXRD technique depends on the addition rate applied for the incoming guest anion solution. A slow addition rate of guest anions delays the exchange reaction making it possible to observe and isolate second-stage compounds. The formation of LDH second-stage is determined by the nature of both initial and incoming guest anions. No staging was observed for the exchange of Cl^- anions by CO_3^{2-}, SO_4^{2-} and $[Fe^{III}(CN)_6]^{3-}$ *i.e.* for purely inorganic exchange reactions. These results provide other evidences for the previous assumption [12] we made on the occurrence of staging phenomena as a result of inorganic/organic separation, though not all organic anions can form staging with inorganic anions.

2.6 References

1 G. R. Williams and D. O'Hare, *Chem. Mater*., **2005**, *17*, 2632.
2 J. S. O. Evans, S. J. Price, H.-V. Wong and D. O'Hare, *J. Am. Chem. Soc.*, **1998**, *120*, 10837
3 F. Rey, G. Sankar, J. M. Thomas, P. A. Barrett, D. W. Lewis, C. R. A. Catlow, S. M. Clark and G. N. Greaves, *Chem. Mater.*, **1995**, *7*, 1435.
4 F. Rey, G. Sankar, J. M. Thomas, P. A. Barrett, D. W. Lewis, C. R. A. Catlow and G. N. Greaves, *Chem. Mater.*, **1996**, *8*, 590.
5 S. J. Price, J. S. O. Evans, R. J. Francis and D. O'Hare, *Adv. Mater.*, **1996**, *8*, 582.
6 A. T. Davies, G. Sankar, C. R. A. Catlow and S. M. Clark, *J. Phys. Chem. B*, **1997**, *101*, 10115.
7 R. I. Walton, T. Loiseau, D. O'Hare and G. Ferey, *Chem. Mater.*, **1999**, *11*, 3201.
8 R. I. Walton, A. J. Norquist, S. Neeraj, S. Natarajan, C. N. R. Rao, J. S. O. Evans, R. J. Francis and D. O'Hare, *Chem. Commun*., **2001**, *19*, 1990.
9 A. J. Norquist and D. O'Hare, *J. Am. Chem. Soc*., **2004**, *126*, 6673.
10 A. M. Fogg, J. S. Dunn and D. O'Hare, *Chem. Mater.*, **1998**, *10*, 356.
11 G. R. Williams, A. J. Norquist and D. O'Hare, *Chem. Mater*., **2004**, *16*, 975.
12 N. Iyi, K. Kurashima and T. Fujita, *Chem. Mater.*, **2002**, *14*, 583.
13 F. Kooli, I. C. Chisem, M. Vucelic and W. Jones, *Chem. Mater.*, **1996**, *8*, 1969.

14 J. Pisson, C. Taviot-Gueho, Y. Israeli, F. Leroux, P. Munsch, J. P. Itie, V. Briois, N. Morel-Desrosiers and J. P. Besse, *J. Phys. Chem. B*, **2003**, *107*, 9243.
15 C. Taviot-Gueho, F. Leroux, C. Payen and J. P. Besse, *Appl. Clay Sci.*, **2005**, *28*, 111.
16 V. Prevot, C. Forano and J. P. Besse, *Inorg. Chem*., **1998**, *37*, 4293.
17 S. M. Clark, *J. Appl. Crystallogr.*, **1995**, *28*, 646.
18 J. D. Hancock and J. H. Sharp, *J. Am. Ceram. Soc.*, **1972**, *55*, 74.
19 S. M. Clark, *J. Appl. Cryst*., **1995**, *28*, 646.
20 J. D. Hancock and J. H. Sharp, *J. Am. Ceram. Soc*., **1972**, *55*, 74.
21 G. R. Williams, A. I. Khan and D. O'Hare, *Struct. Bond*., **2006**, *119*, 161.
22 J. Rodriguez-Carvajal, "FULLPROF: A program for Rietveld Refinement and Pattern Matching Analysis", Abstract of the Satelitte Meeting on Powder Diffraction of the XVth Congress International Union of Crystallogrphy Toulouse, France (1990), p127.
23 J. Rodriguez-Carvajal, Fullprof computer program ; http//www-llb.cea.fr/.
24 P. Thompson, D. E. Cox and J. B. Hastings, *J. Appl. Cryst.*,**1987**, *20*, 79.
25 J. Rodriguez-Carvajal, Newsletter of the Powder Diffraction Commission of the International Union of Crystallography **2001**, *n.26*, 12.
26 P. W. Stephen, *J. Appl. Crystallogr.*, **1999**, 32, 281.
27 V. A. Drits, T. N. Sokolova, G. V. Sokolova and V. I. Cherkashin, *Clays Clay Miner.*, **1987**, *35*, 401.
28 A. S. Bookin, V. I. Cherkashin and V. A. Drits, *Clays Clay Miner.*, **1993**, *41*, 558.
29 K. El Malki, A. de Roy and J. P. Besse, *Eur. J. Solid State Inorg. Chem*., **1989**, *26*, 339.
30 I. Carpani, M. Berrettoni, M. Giorgetti, and D. Tonelli, *J. Phys. Chem. B*, **2006**, *110*, 7265.
31 I. Carpani, M. Berrettoni, B. Ballarin, M. Giorgetti, E. Scavetta, D. Tonelli, *Solid State Ionics*, **2004**, *168*, 167.
32 W. L. Ijdo and T. J. Pinnavaia, *J. Solid State Chem*., **1998**, *139*, 281.

Chapter 3 Selective Anion-Exchange Properties of Second-Stage Layered Double Hydroxides

3.1 Introduction

LDH second-stage materials consist of regularly stacked organic and inorganic gallery sequences. Combining the hydrophobic and hydrophilic properties of organic and inorganic LDH intercalates in a single heterostructured phase will produce amphiphilic materials, which may have novel anion-exchange properties.

The aim of the study described in this chapter was thus to investigate the anion-exchange properties of the second-stage intermediate phases, i.e. $[Zn_2Cr(OH)_6]Cl_{0.5}$-$(succinate)_{0.25}{\cdot}nH_2O$ (Zn_2Cr-Succ/Cl) and $[Zn_2Cr(OH)_6]Cl_{0.5}(tartrate)_{0.25}{\cdot}nH_2O$ (Zn_2Cr-Tart/Cl), which were isolated under the conditions described in the **Chapter 2**. The two second-stage materials as starting phases were separately treated with adipate and fluoride anions and the reactions were monitored by time-resolved, in situ, energy-dispersive X-ray diffraction (EDXRD), using the same setup as presented in **Chapter 2**. Selective anion-exchange reactions were observed as a result of the difference in the polarity between the two successive interlayer spaces.

3.2 Experimental Section

3.2.1 Time-resolved in situ energy-dispersive X-ray diffraction (EDXRD) measurements

EDXRD experimental setup is the same as described in **Section 2.2.2**. The reactions were conducted in glass ampules contained within a temperature-controlled block; individual spectra were collected at a fixed detector angle of (2θ) 1.625°, with acquisition times ranging from 10 s to 60 s. In a typical experiment, a solution of the guest species (at a concentration of 0.15 or 0.2 M for adipate/$O_2C(CH_2)_4CO_2^-$anions, and 0.4 M for fluoride anions) was

added dropwise to 10 mL of a suspension of the LDH (25 g· L^{-1}) at a rate of 0.046 or 0.059 mL· min^{-1} using a syringe pump. Spectra were thus recorded at different anion/LDH ratios in solution converted into theoretical exchange rates expressed in AEC (anionic exchange capacity) of the starting phase.

In **chapter 2**, a better crystallinity was observed in the case of the Zn_2Cr system, which led us to choose this composition for the present work; the synthesis and chemical composition of Zn_2Cr-Cl are given in **Section 2.2.1** close to $Zn_2Cr(OH)_6Cl{\cdot}2H_2O$ (356.26 g· mol^{-1}).

3.2.2 Data analysis

An automated Gaussian fitting routine was used to obtain the peak areas of the Bragg reflections.[1] These values are then converted to the extent of reaction at time t. The latter is defined as $\alpha(t) = I_{hkl}(t)/I_{hkl}(max)$, where $I_{hkl}(t)$ is the area of a given peak at time t, and $I_{hkl}(max)$ is the maximum area of this peak.

3.2.3 Powder X-ray diffraction

Quenched compositions were analyzed in our laboratory by PXRD after centrifugation and drying in order to get more structural information. The powder X-ray diffraction patterns were recorded on an X'Pert Pro Philips diffractometer using Cu Kα radiation, as described in **Section 2.2.4**.

3.3 Formation and Isolation of Second-Stage Zn_2Cr-Succ/Cl and Zn_2Cr-Tart/Cl Materials

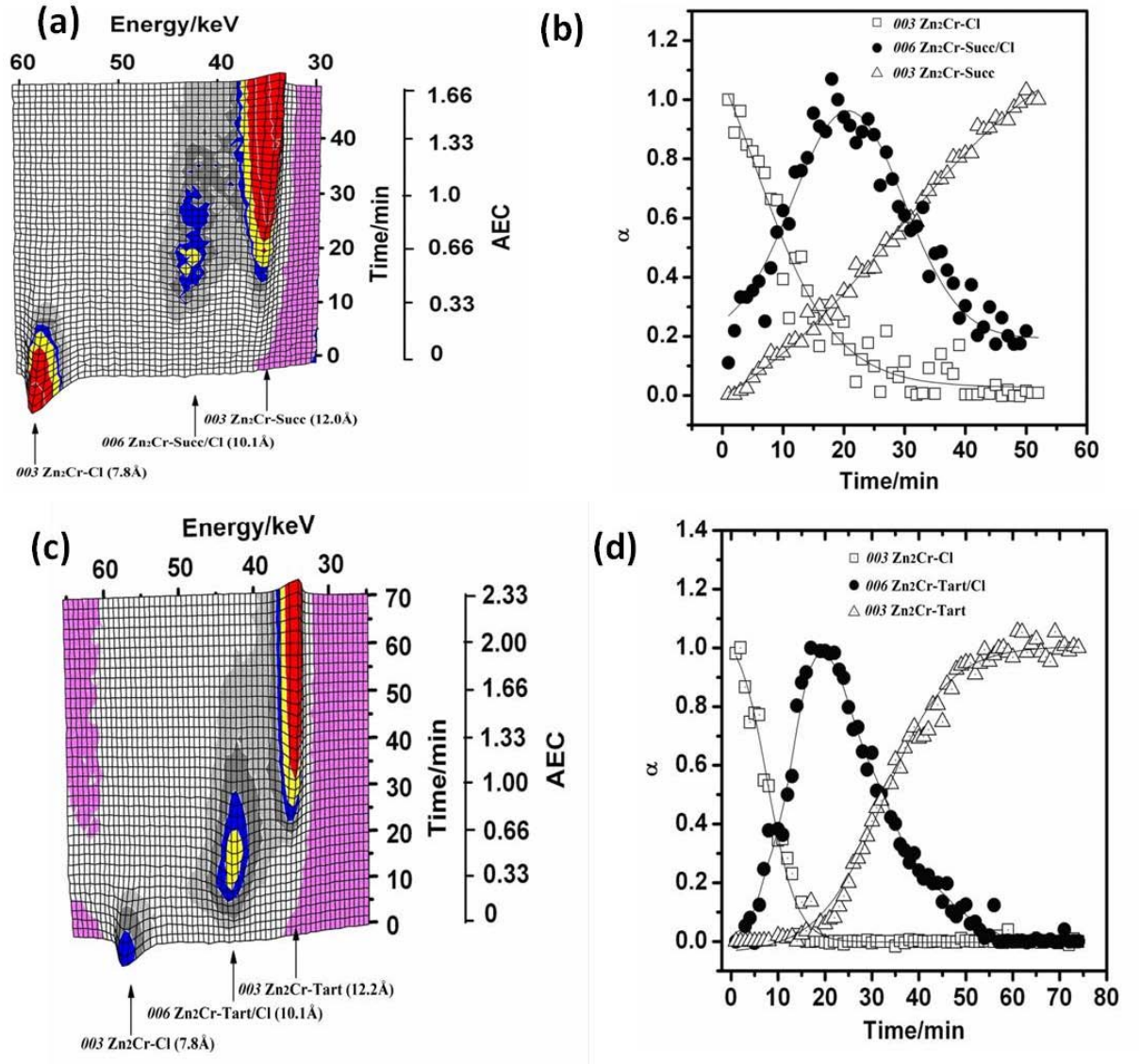

Figure 3-1**:** 3D stacked plots from EDXRD data showing the course of the exchange reactions of Zn_2Cr-Cl with: (a) succinate anions and (c) tartrate anions as a function of time and the corresponding α(t) curves (b) and (d) showing the best conditions for isolating the stage phases: Zn_2Cr-Succ/Cl and Zn_2Cr-Tart/Cl.

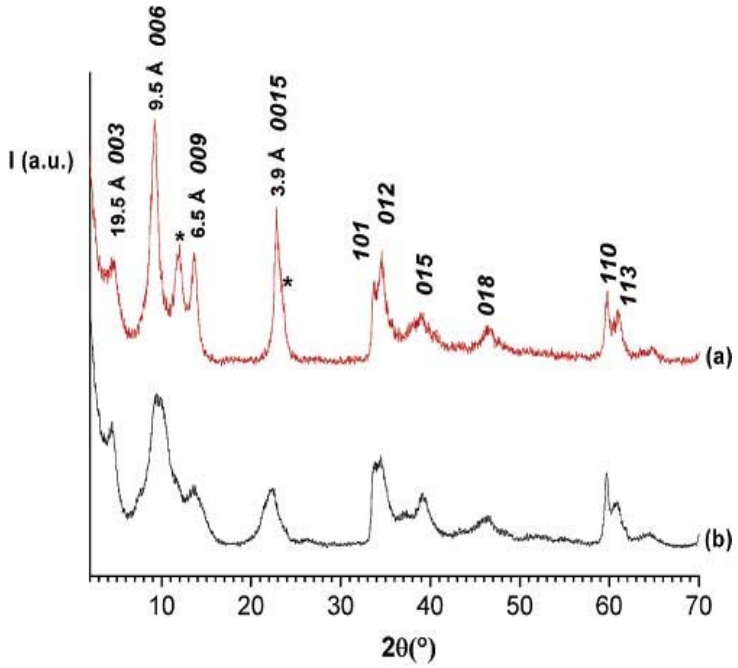

Figure 3-2**:** Powder X-ray diffraction patterns for the second-stage phases: (a) Zn_2Cr-Succ/Cl and (b) Zn_2Cr-Tart/Cl. Reflections marked with an asterisk correspond to the Zn_2Cr-Cl host.

For the in situ study of the anion-exchange properties of Zn_2Cr-Succ/Cl and Zn_2Cr-Tart/Cl, both second-stage phases were prepared in the laboratory by repeating the EDXRD experiments described above and quenching the reactions when solely the second-stage phases are present, where the concentration of the intermediate is expected to be greatest[2] i.e. in the case of Zn_2Cr-Succ/Cl when α(t) curves for the host Zn_2Cr-Cl and the product Zn_2Cr-Succ cross at α = 0.2 and for Zn2Cr-Tart/Cl when the crossing point of α(t) curves for the host Zn_2Cr-Cl and the product Zn_2Cr-Tart occurs at α = 0. The powder X-ray diffraction patterns of the quenched materials are shown in **Figure 3-2**. As can be seen, the Zn_2Cr-Succ/Cl sample is not a pure phase but consists of a mixture with Zn_2Cr-Cl. It is worthwhile to note that with reaction time scales on the order of 1-2 min, it is difficult to isolate second-stage intermediates, and products quenched after drying do not necessarily reflect the reaction matrix observed in situ, as diffusion process may continue to occur when the addition of organic molecule has been stopped. In contrast, Zn_2Cr-Tart/Cl appears as a

pure phase. Another very important point is the detection of the *003* reflection at *ca.* 19.5 Å in each case, providing irrefutable proof that second-stage materials are really formed.

3.4 Anion-exchange Properties of Second-stage Materials

The as-prepared second-stage materials (Zn_2Cr-Succ/Cl and Zn_2Cr-Tart/Cl) were then resuspended in water (25 g · L^{-1}), and EDXRD experiments were performed to follow the exchange reactions with adipate and fluoride anions, under the same conditions as those described in **Chapter 2**.

In our first attempts, we successively monitored in one experiment the the formation of Zn_2Cr-Succ/Cl or Zn_2Cr-Tart/Cl intermediates followed by the exchange reactions with fluoride or adipate anions. Yet, under these conditions, the crystallinity of the system decreased dramatically and it was impossible to analyze the data. This failure can be attributed to a combination of factors: first, a dilution factor, which makes detection difficult, and second, a competition between anions in solution, which may hinder their intercalation.

Plots showing the time evolution of the exchange reactions with adipate anions are presented in **Figure 3-3** for Zn_2Cr-Succ/Cl, **Figure 3-4** (at room temperature) and **Figure 3-5** (at 55 ℃) for Zn_2Cr-Tart/Cl, respectively, and those corresponding to the exchange with fluoride anions are presented in **Figure 3-6** and **Figure 3-7**. In all cases, the reactions are observed to proceed in two steps and new second-stage intermediate phases are identified that result from the selective replacement of either succinate or tartrate anions by adipate anions, or Cl^- anions by F^-anions. The exchange reactions are described in details in the following sections.

3.4.1 Exchange reactions with adipate anions

For the exchange reaction of adipate anions with Zn_2Cr-Succ/Cl host (panels a and b of **Figure 3-3**), a crystalline intermediate phase was detected at *ca.* 12.2 Å that can be assigned

to a new second-stage intermediate, Zn_2Cr-Adip/Cl. This phase has alternate layers occupied by chloride and adipate anions, and hence has a predicted basal spacing d_{003} =7.8 +14.1=21.9 Å, and hence a d_{006} of *ca.* 11 Å. This latter value is slightly different from that observed (12.2 Å), but the low crystallinity of Zn_2Cr-Adip/Cl intermediate makes the determination of the exact position of the Bragg reflection rather difficult. Additionally, the poor crystallinity and the partial overlap between Bragg reflections complicate the integration of the diffraction intensities, thus explaining the relatively poor resolution for α-time curves.

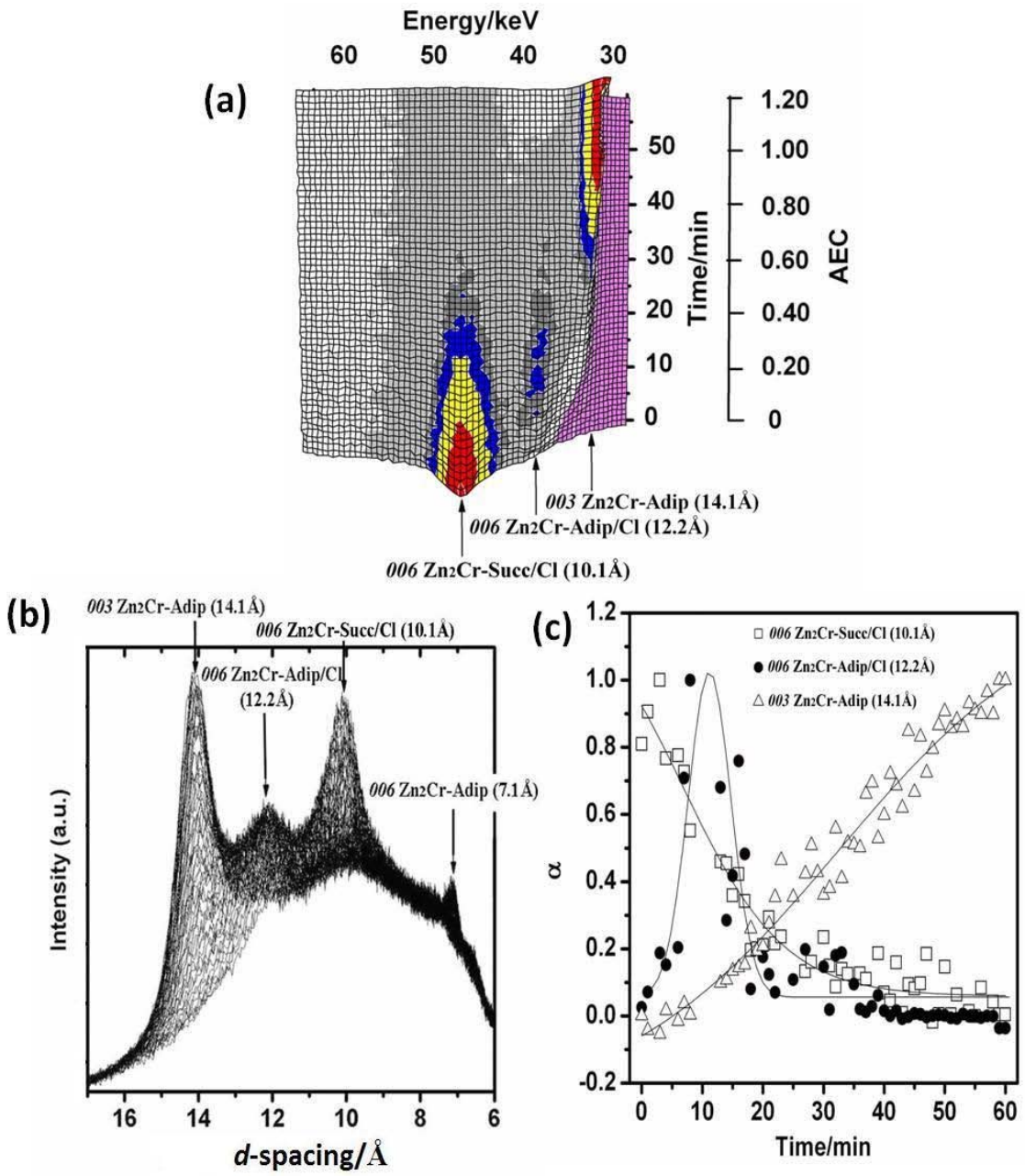

Figure 3-3: EDXRD data showing the course of the exchange reaction of adipate ($^{-}O_2C(CH_2)_4CO_2^{-}$) with Zn_2Cr-Succ/Cl at room temperature. (a) 3D stacked plot showing the evolution of Zn_2Cr-Succ/Cl host *006*, Zn_2Cr-Adip/Cl intermediate *006*, and Zn_2Cr-Adip product *003* Bragg reflections as a function of time, (b) 2D stacked plot showing the same, and (c) extent of reaction *vs*. time curves for host *006*, intermediate *006* and product *003* Bragg reflections. The adipate anion solution (0.15 M) was added at a rate of 0.046 $mL \cdot min^{-1}$.

For the exchange reaction of adipate anions with the Zn_2Cr-Tart/Cl host, the intermediate was initially very hard to observe and only the fact that the extent of the reaction *vs.* time curves of the Zn_2Cr-Tart/Cl host and Zn_2Cr-Adip product cross at α close to 0 suggested the presence of an intermediate in **Figure 3-4**. However, performing the reaction at 55 °C allowed us to improve the detection and unequivocally observe the growth of a Bragg reflection at the same distance as for the Zn_2Cr-Succ/Cl host, i.e., 12.2 Å (panels a and b of **Figure 3-5**). This coincidence in position strongly suggests a similar composition for the intermediate phase, *i.e.*, Zn_2Cr-Adip/Cl, in both cases. Yet, the effect of temperature in the case of the Zn_2Cr-Tart/Cl host reveals differences in reactivity between Zn_2Cr-Succ/Cl and Zn_2Cr-Tart/Cl compounds, probably with higher activation energy for the exchange reaction of tartrate with adipate than that of succinate. Additionally, there is a difference in the induction time, before the reaction begins. Indeed, for the Zn_2Cr-Tart/Cl host, the Zn_2Cr-Adip/Cl intermediate is not detected until the theoretical exchange rate has reached a value of *ca.* 0.6, whereas for the Zn_2Cr-Succ/Cl host, Zn_2Cr-Adip/Cl is detected at the initial stages of adipate addition, at a theoretical exchange rate of *ca.* 0.15. The conditions for the appearance of the Zn_2Cr-Adip product are also different, with the coexistence of Zn_2Cr-Adip/Cl and Zn_2Cr-Adip in the case of the Zn_2Cr-Tart/Cl host, whereas Zn_2Cr-Adip is not observed until Zn_2Cr-Adip/Cl has disappeared in the case of the Zn_2Cr-Succ/Cl host. The persistence of the Zn_2Cr-Adip/Cl intermediate in the former case might indicate a random filling of the Cl-containing layers after alternate layers have been exchanged with adipate anions. Conversely, for the Zn_2Cr-Succ/Cl host, the direct transformation from the Zn_2Cr-Adip/Cl intermediate to the Zn_2Cr-Adip product would arise from an ordered replacement of the Cl-containing layers, supported by the fact that the corresponding α *vs.* time curves cross at $\alpha \approx 0.5$ (**Figure 3-3** (c)). Another explanation could be differences in the anion-exchange affinities, the exchange between tartrate and adipate anions being energetically less favorable than the exchange between succinate and adipate anions; this is consistent with the effect of the temperature showing that the activation energy is higher in the former case.

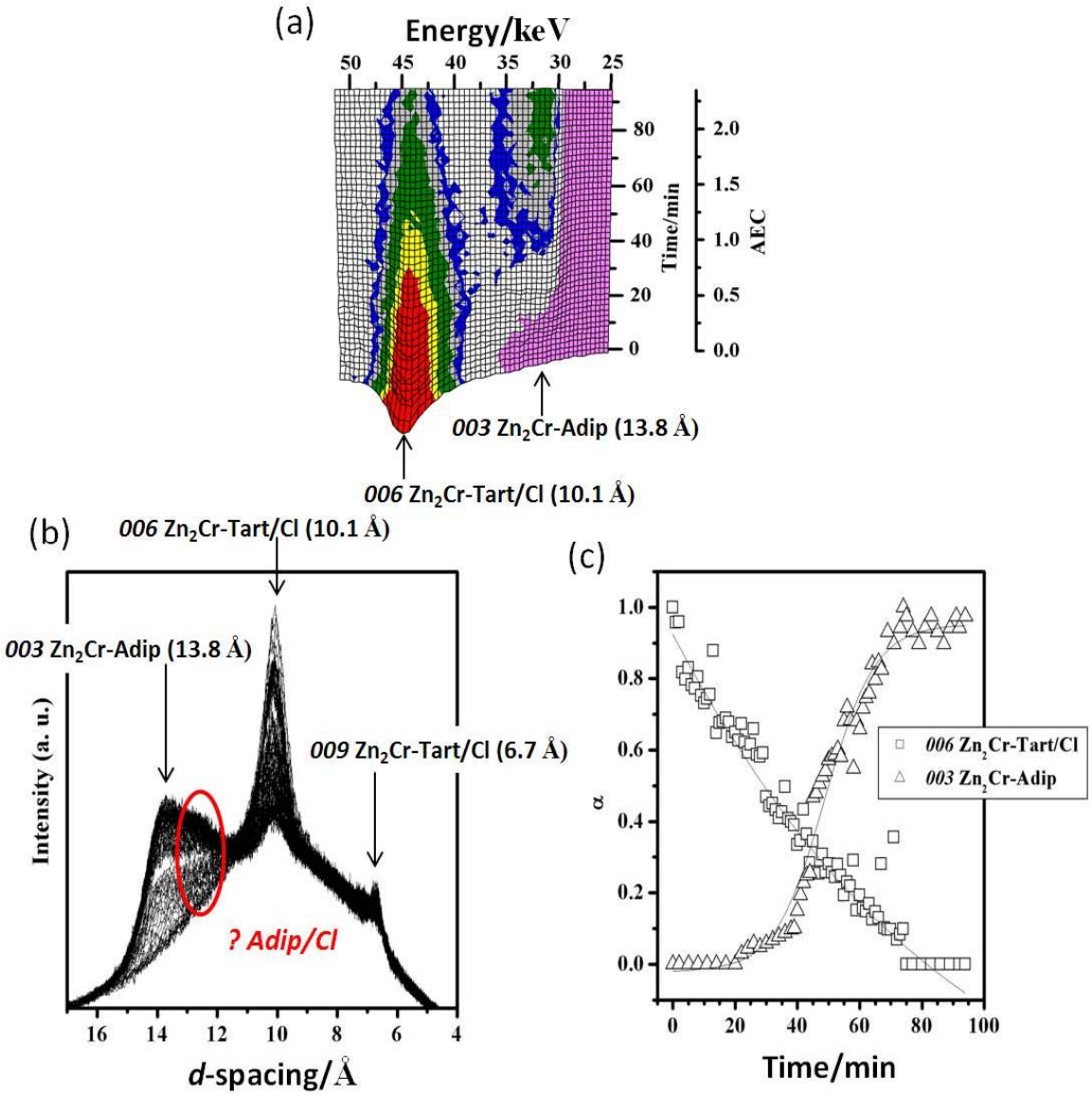

Figure 3-4**:** EDXRD data showing the course of the exchange reaction of Zn_2Cr-Tart/Cl with adipate anions at room temperature. (a) 3D stacked plot showing the evolution of Zn_2Cr-Tart/Cl host *006*, Zn_2Cr-Adip product *003* Bragg reflections as a function of time, (b) 2D plot showing the same, and (c) extent of reaction *vs.* time curves for host *006* and product *003* Bragg reflections. The adipate guest anions solution (0.2 M) was added at 0.059 mL · min^{-1}.

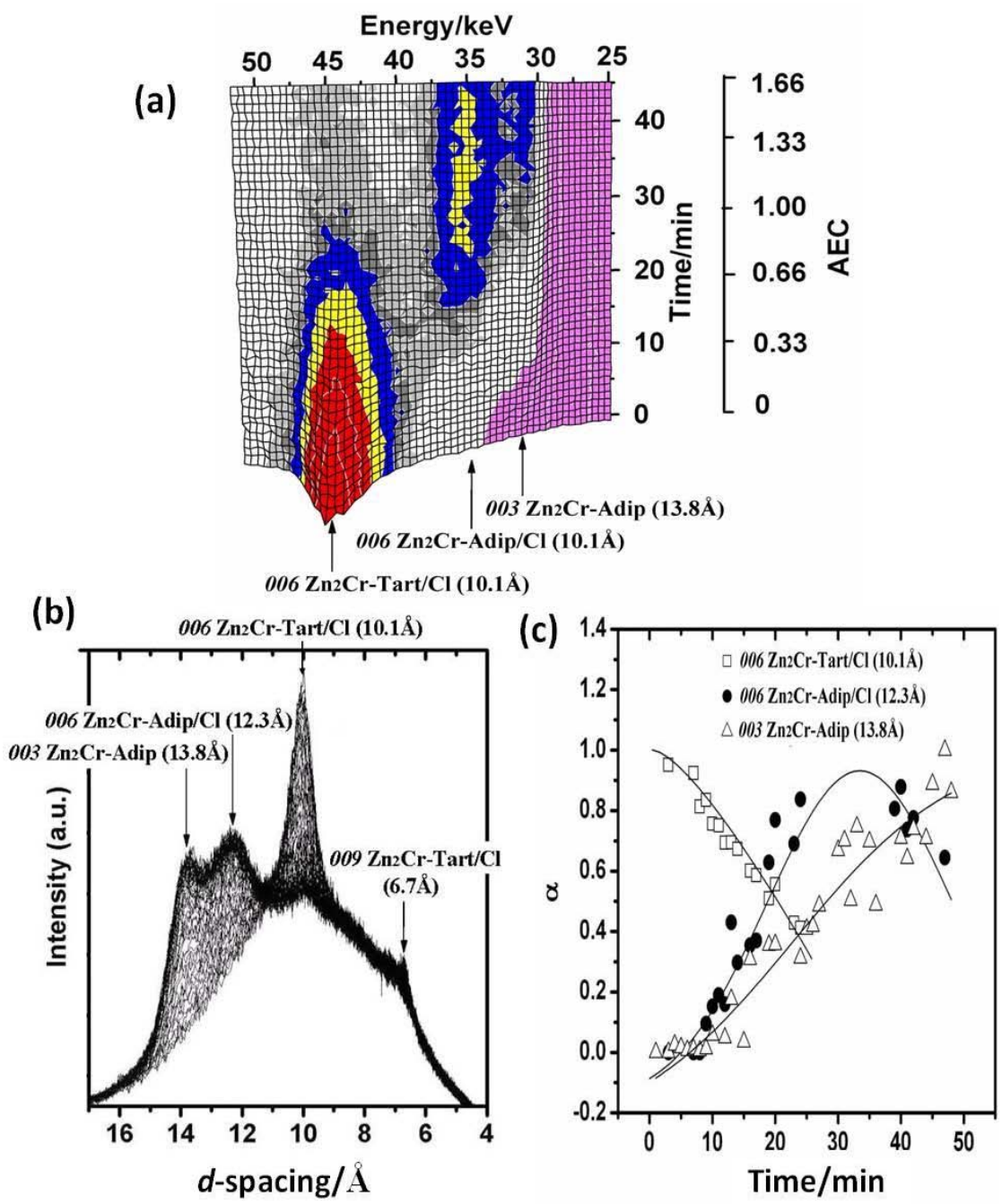

Figure 3-5: EDXRD data showing the course of the exchange reaction of adipate with Zn_2Cr-Tart/Cl at 55 °C. (a) 3D stacked plot showing the evolution of Zn_2Cr-Tart/Cl host *006*, Zn_2Cr-Adip/Cl intermediate *006*, and Zn_2Cr-Adip product *003* Bragg reflections as a function of time, (b) 2D stacked plots showing the same, and (c) extent of reaction *vs.* time curves for host *006*, intermediate *006* and product *003* Bragg reflections. The adipate solution (0.2 M) was added at a rate of 0.059 mL· min^{-1}.

3.4.2 Exchange reactions with fluoride anions

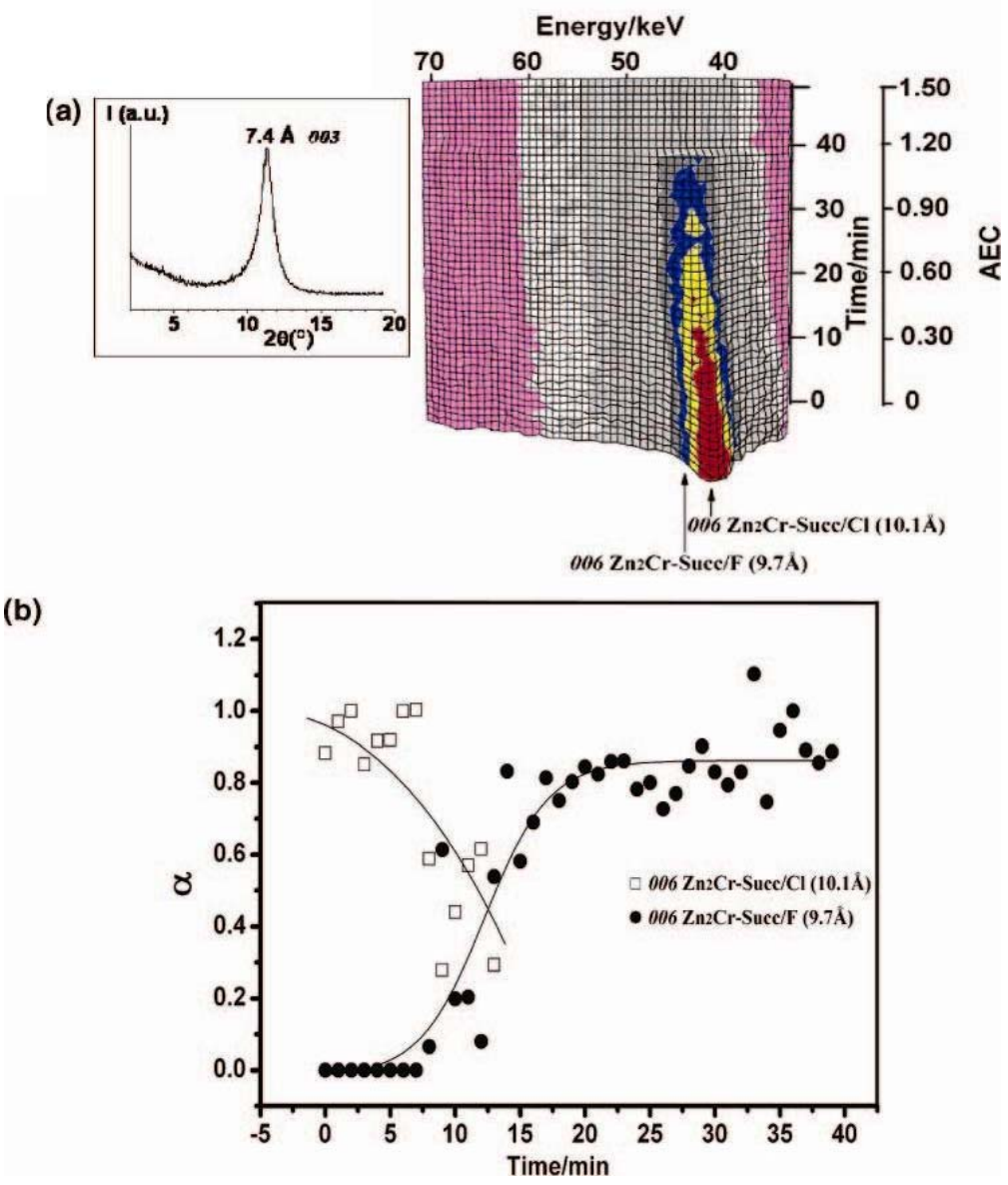

Figure 3-6: Time-resolved diffraction data showing the course of the exchange reaction of fluoride with Zn_2Cr-Succ/Cl at room temperature. (a) 3D stacked plot showing the evolution of Zn_2Cr-Succ/Cl host *006* and intermediate Zn_2Cr-Adip/F *006* Bragg reflections as a function of time and (b) extent of reaction *vs.* time curves for host and intermediate *006* Bragg reflections. The fluoride anion solution (0.4 M) was added at a rate of 0.046 mL· min^{-1}. Inset figure gives the powder X-ray diffraction pattern of the final solid recovered after centrifugation and drying.

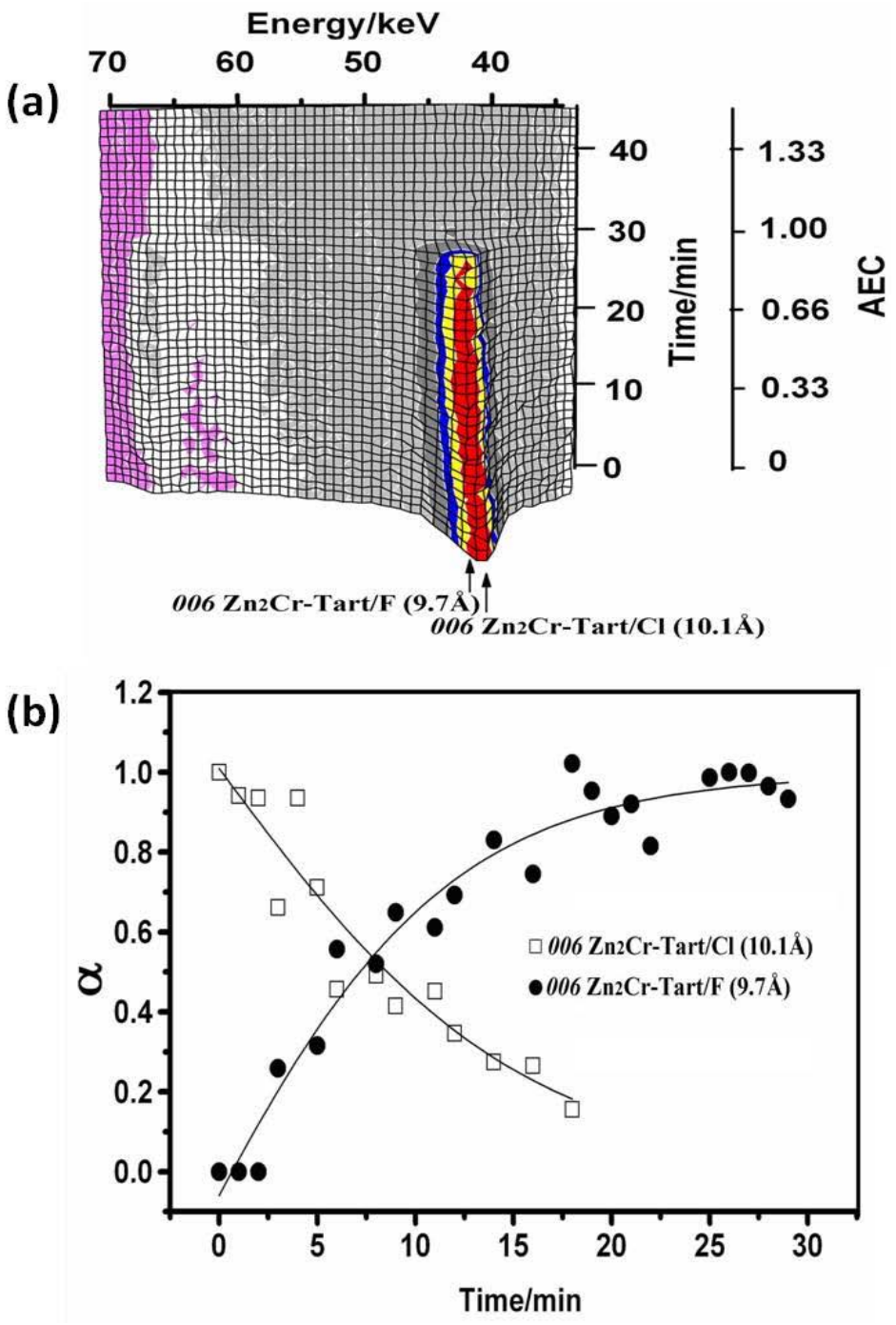

Figure 3-7: EDXRD data showing the course of the exchange reaction of fluoride with Zn_2Cr-Tart/Cl at room temperature. (a) 3D stacked plot showing the evolution of Zn_2Cr-Tart/Cl host *006* and Zn_2Cr-Adip/F intermediate *006* Bragg reflections as a function of time and (b) extent of reaction *vs.* time curves for host and intermediate *006* Bragg reflections. The fluoride anion solution (0.4 M) was added at a rate of 0.059 $mL \cdot min^{-1}$.

For the exchange reactions with fluoride anions (**Figure 3-6** and **Figure 3-7** for Zn_2Cr-Succ/Cl and Zn_2Cr-Tart/Cl, respectively), a gradual displacement of the *006* reflection of Zn_2Cr-Succ/Cl and Zn_2Cr-Tart/Cl hosts from 10.1 to 9.7 Å is observed in each case. This is in total agreement with the formation of new second-stage phases, Zn_2Cr-Succ/F and Zn_2Cr-Tart/F, both resulting from the replacement of Cl^- by F^- anions in Zn_2Cr-Succ/Cl and Zn_2Cr-Tart/Cl, respectively. Because of the small difference between the interlamellar distances for chloride (7.8 Å) and fluoride (7.4 Å) anions, only a small displacement of the *006* Bragg reflection of the second-stage phases to lower *d* values is expected upon the exchange of chloride by fluoride. The Zn_2Cr-Succ/F intermediate therefore has a predicted d_{003} =12.1 +7.4 =19.6 Å, leading to a d_{006} of 9.8 Å; the same calculation for Zn_2Cr-Tart/F gives d_{006} = 9.9 Å. This is in excellent agreement with the EDXRD data. A deconvolution of the EDXRD patterns in the range 9−11 Å (by considering two contributions centered at 10.1 and 9.7 Å, attributed to Zn_2Cr-Succ/Cl and Zn_2Cr-Succ/F or Zn_2Cr-Tart/Cl and Zn_2Cr-Tart/F), allows us to draw the α(*t*) curves presented in **Figure 3-6** (b) and **Figure 3-7** (b). Again, the crossing of these curves at α = 0.5 is consistent with a direct conversion of Zn_2Cr-Succ/Cl or Zn_2Cr-Tart/Cl hosts to Zn_2Cr-Succ/F or Zn_2Cr-Tart/F intermediates. In both cases, for a theoretical exchange rate approaching the anion-exchange capacity, the intermediate phase disappears. The fully exchanged phase Zn_2Cr-F with d_{003} = 7.4 Å is not observed, probably because it is too poorly crystalline and cannot be resolved. Nevertheless, the powder XRD analysis of the final solid product recovered after centrifugation and drying unambiguously shows the formation of Zn_2Cr-F with the *003* Bragg reflection at ca. 7.4 Å (inset of **Figure 3-6** (a)).

3.5 Conclusions

These results demonstrate a segregation between organic and inorganic anions, leading to selective exchange reactions governed by this. The reaction of the second-stage compounds Zn_2Cr-Succ/Cl and Zn_2Cr-Tart/Cl with either fluoride or adipate anions initially occurs with preferential replacement of the hydrophilic Cl ion with F or replacement of the hydrophobic succinate or tartrate anions with adipate as shown in **Figure 3-8**. This result has

major implications for the intercalation chemistry of LDH. Another important point to note is that attempts to prepare Zn_2Cr-Tart/F second-stage materials by direct synthesis failed. Indeed, no staging was observed for the exchange of tartrate by fluoride in Zn_2Cr-Tart, which suggests that the present phases can be prepared starting only from second-stage structures such as Zn_2Cr-Tart/Cl. Possibly, this property can be used to synthesize a new kind of staging compounds containing desired anions with specific properties as discussed in the next chapter.

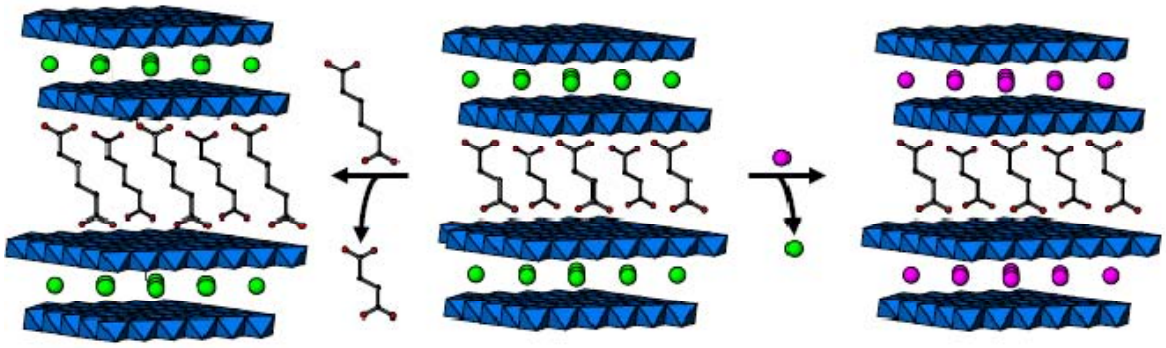

Figure 3-8: Schematic anion-exchange reactions of the second-stage LDH materials (Zn_2Cr-Succ/Cl or Zn_2Cr-Tart/Cl) with organic adipate and inorganic fluoride anions.

3.6 References

1 J. S. O. Evans, R. J. Francis, D. O'Hare, S. J. Price, J. Flaherty, A. Gordon, A. Nield, C. C. Tang, *Rev. Sci. Instrum.*, **1995**, *66*, 2442.

2 S. M. Clark, *J. Appl. Cryst.*, **1995**, *28*, 646.

Chapter 4 Staging Behaviors of Styrene-4-sulfonate Anions and Ferricyanide Anions in Layered Double Hydroxides

As already said several times in this manuscript, the formation of LDH heterostructures is of major interest for future developments in LDH intercalation chemistry, particularly in the direction of multifunctional materials.

For this purpose, the intercalation of vinyl benzene sulfonate (VBS) monomer and hexacyanometal complex ($Fe(CN)_6^{3-}$) into Zn_2Cr-Cl or Zn_2Al-Cl first stage phases and Zn_2Cr-Tart/Cl second-stage compound have been investigated using time resolved, in situ energy-dispersive synchrotron X-ray diffraction (EDXRD).

I. Exchange reaction with VBS

4.1 Introduction

In the past two decades, a lot of attention has been devoted to the study of nanocomposites built from the assembly of a lamellar inorganic host structure and a polymer.[1-6] These systems may find applications in a large number of fields such as those emphasizing the mechanical enhancement, gas permeably, fire-retardant or membrane. [7-9]

LDH-polymer assemblies have been largely studied in our group by F. Leroux et al.[10, 11]. The incorporation of polymer into LDH can be achieved *via* different synthesis routes. An interesting route is the in situ thermal polymerization of pre-intercalated monomers as reported for aspartate into Mg_2Al, [12] anilimine sulfonate into Cu_2Cr [13] and more recently VBS into Zn_2Al LDH [14-16].

In this latter case, the in situ polymerization upon a thermal treatment at 200 ℃ was evidenced by in situ high temperature powder X-ray diffraction (HTXRD) with a contraction of the lamellar structure from d_{003} = 18.04 Å to 14.46 Å (**Figure 4-1**) and by

^{13}C NMR with the disappearance of the resonance peak of the vinyl bond (**Figure 4-2**).

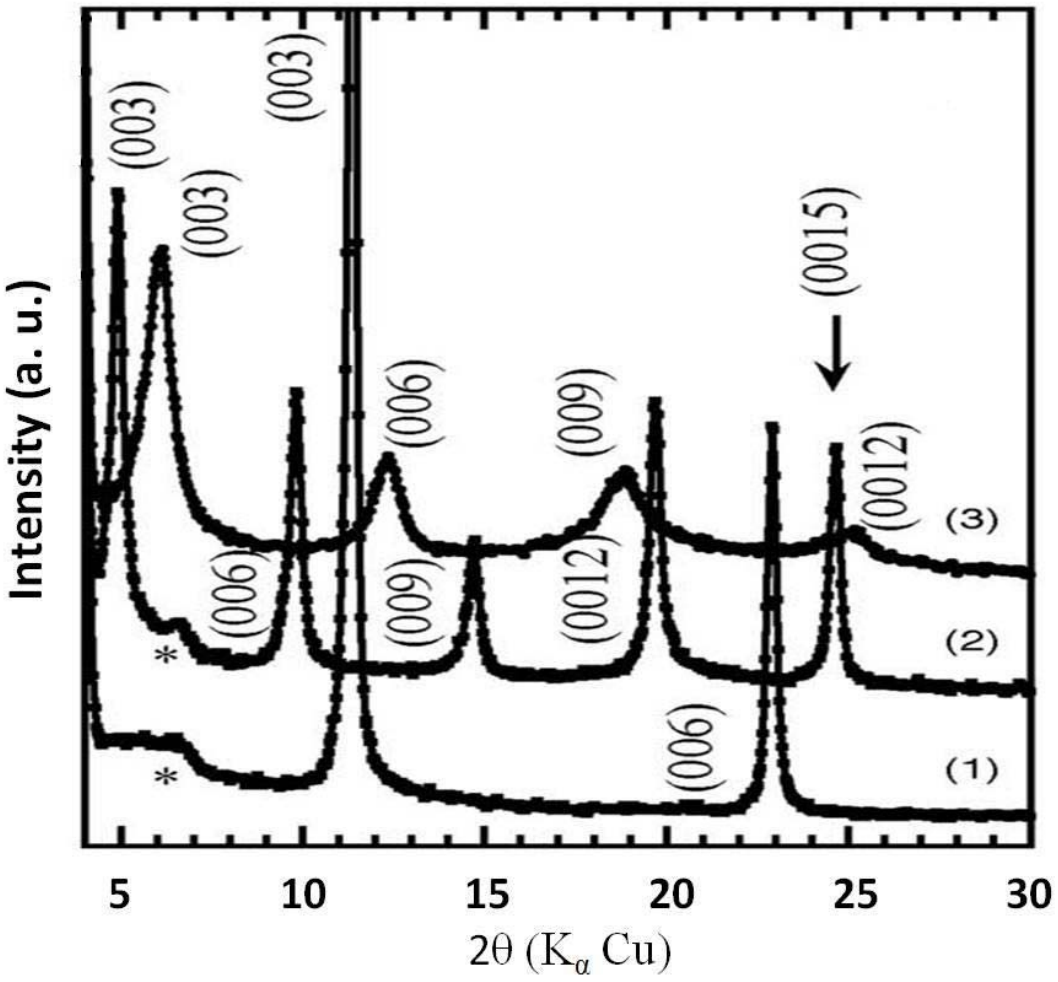

Figure 4-1: In situ PXRD patterns of (1) LDH pristine and monomer derivatives at (2) 25 ℃ and (3) 200 ℃ for Zn_2Al-VBS. The asterisk corresponds to PSD system. The miller indexing is given. See ref. 16.

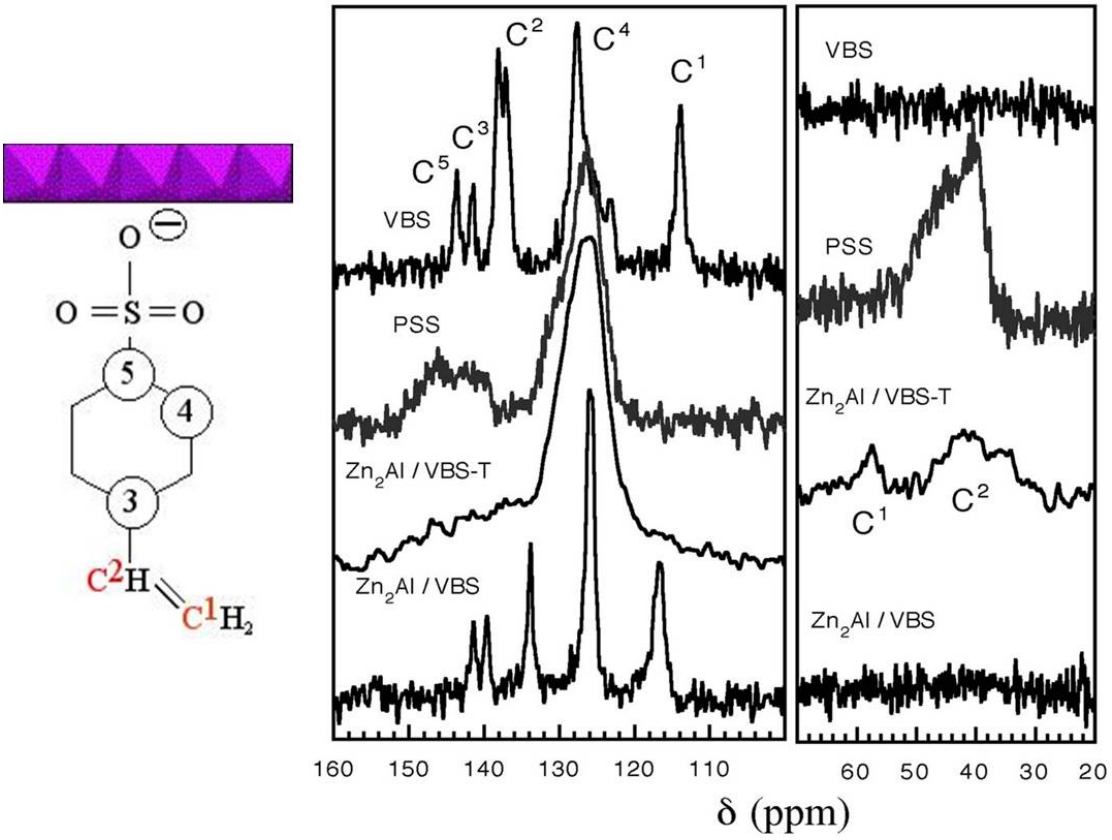

Figure 4-2**:** ^{13}C CP-MAS spectra of VBS, PSS, Zn_2Al/VBS-T (after in situ thermal treatment at 200 ℃) and Zn_2Al/VBS (at 25 ℃) samples, from top to bottom. See ref. 16.

In the following, the intercalation of VBS into Zn_2Cr-Cl, Zn_2Al-Cl LDH and Zn_2Cr-Tart/Cl second-stage LDH was examined by means of EDXRD. The in situ thermal polymerization of VBS into PSS was then investigated using in situ HTXRD technique.

4.2 Experimental

4.2.1 Synthesis and characterization of host materials

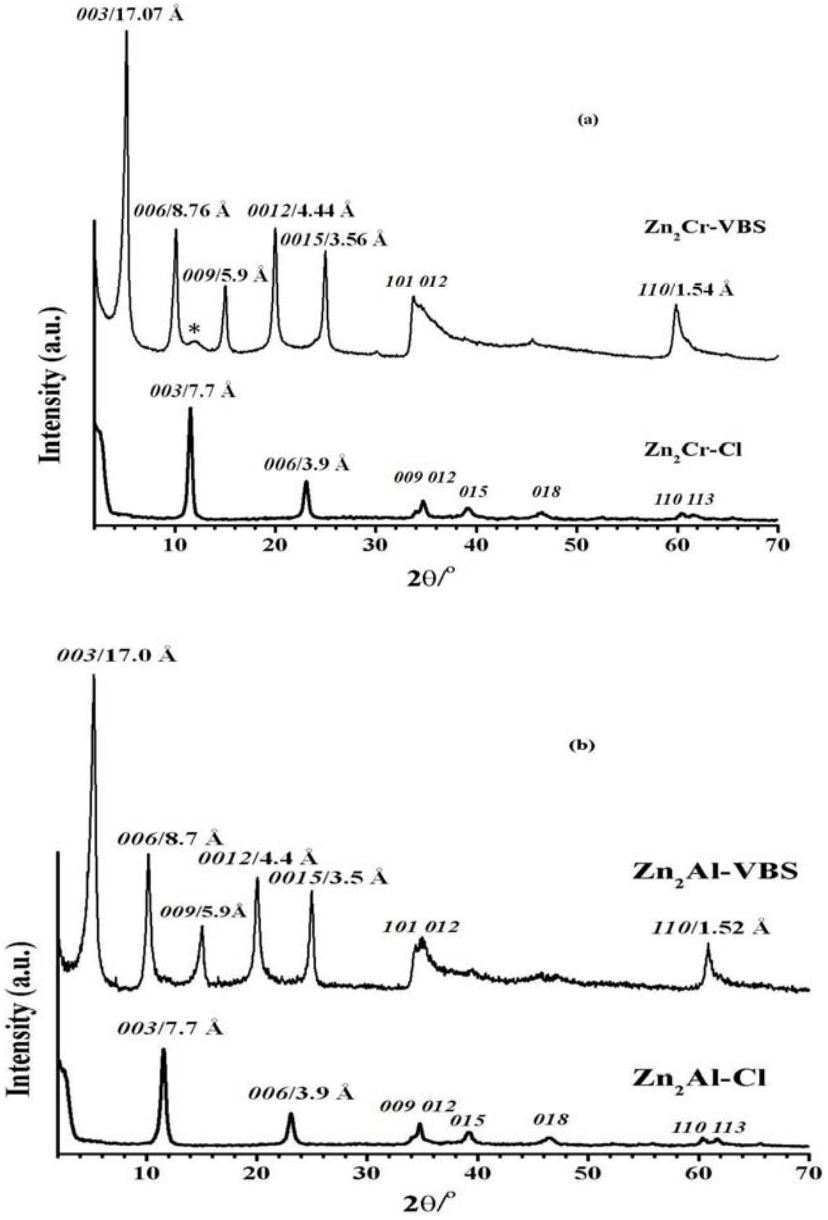

Figure 4-3**:** Powder X-ray diffraction patterns of the first stage host materials: (a) Zn_2Cr-Cl and Zn_2Cr-VBS, (b) Zn_2Al-Cl and Zn_2Al-VBS. The measurement conditions are described in **Section 2.2.4**. The mark * indicates the presence of Zn_2Cr-Cl precursor.

Zn_2Cr-Cl and Zn_2Al-Cl host materials were synthesized by the coprecipitation method while Zn_2Cr-VBS and Zn_2Cr-Tart/Cl as well as Zn_2Al-VBS were prepared by the anion-exchange route using Zn_2Cr-Cl and Zn_2Al-Cl precursors as described in the **section 2.2.1** in detail.

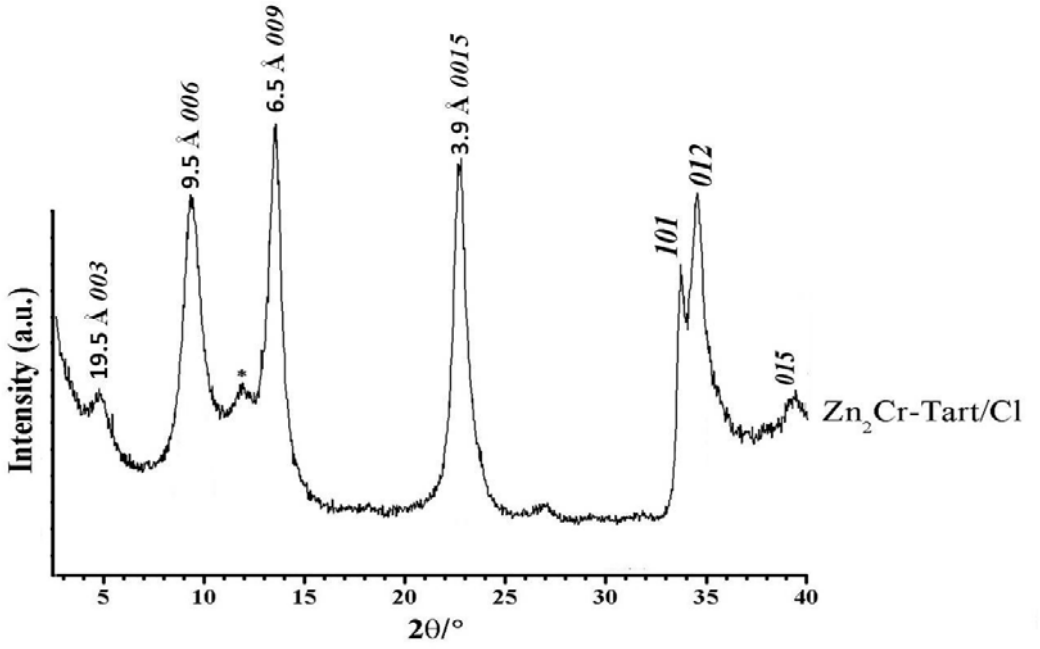

Figure 4-4: Powder X-ray diffraction patterns of Zn_2Cr-Tart/Cl second-stage host materials. The mark * indicates the presence of Zn_2Cr-Cl precursor.

The powder X-ray diffraction patterns of the first-stage host materials(a) Zn_2Cr-Cl and Zn_2Cr-VBS and (b) Zn_2Al-Cl and Zn_2Al-VBS are presented in **Figure 4-3**. The interlayer distances are calculated from the position of the first diffraction peak corresponding to the *003* Bragg reflection (in the space group $R\bar{3}m$); the values obtained for VBS containing LDH are in agreement with those reported elsewhere [15]. In **Figure 4-4** are presented the PXRD patterns of Zn_2Cr-Tart/Cl second-stage host material.

4.2.2 *In situ* EDXRD measurements

The same EDXRD experimental setup was used as described in **Section 2.2.2**. The solution of VBS guest anions at a concentration of 0.2 M was added dropwise to 10 mL of a suspension (25 g· L^{-1}) of Zn_2Cr-Cl, Zn_2Al-Cl or Zn_2Cr-Tart/Cl at room temperature and at the rate of 0.059 mL· min^{-1}, using a syringe pump. The exchange reaction with Zn_2Cr-Tart/Cl was also investigated but at 55 ℃ with an addition rate of 0.118 mL· min^{-1} of the VBS anion solution. Similarly, 0.2 M CO_3^{2-} anions solution was added into 10 mL of a suspension (25g/L) of Zn_2Al-VBS at room temperature at the rate of 1.0 mL· min^{-1}. The EDXRD spectra were collected at a fixed detector angle of 1.625 ^{o} (2θ) with an acquisition time of 60 s, except 10 s in the case of carbonate exchange. The amounts of guest anions added into LDH suspension as a function of time was converted into theoretical exchange rates expressed in anionic exchange capacity (AEC).

4.2.3 *In situ* HTXRD measurement

In situ High Temperature Powder X-ray Diffraction (HTXRD) patterns were recorded on X'Pert Pro Philips diffractometer using a high temperature chamber (Anton Paar HTK-16) and a PSD- 50m Braun detector (aperture on 2 ^{o}, 155 channels). Measurement were carried out in static air atmosphere at these different temperatures i.e. 25 ℃, 100 ℃ and 200 ℃ after 30 min equilibration at each temperature and the heating rate was 10 ℃/min. Scans were recorded in the range from 3 to 26^o (2θ) with a step of 0.02^o and a counting time per step of 9 s.

4.3 Exchange of Cl^- Anions in Zn_2Cr-Cl and Zn_2Al-Cl by VBS Anions

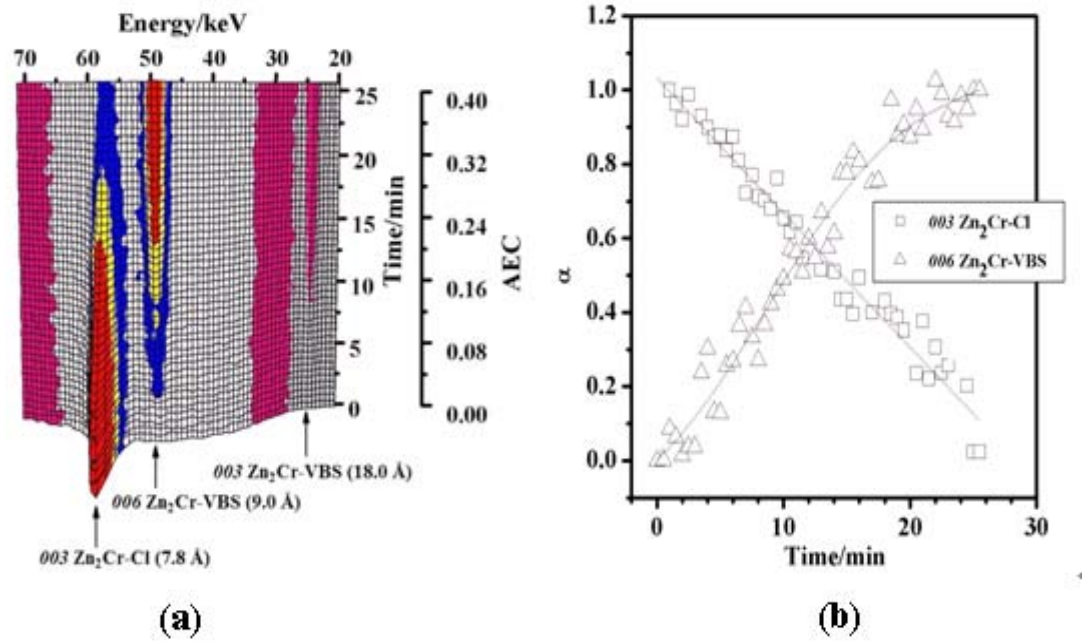

Figure 4-5: EDXRD data showing the course of the exchange reaction of Zn_2Cr-Cl with VBS at room temperature. (a) 3D stacked plot showing the evolution of Zn_2Cr-Cl host *003* and Zn_2Cr-VBS product *006* Bragg reflections as a function of time; (b) extent of reaction *vs.* time curves for host *003* and product *006* Bragg reflections. The guest VBS anion solution (0.2 M) was added at a rate of 0.059 $mL \cdot min^{-1}$.

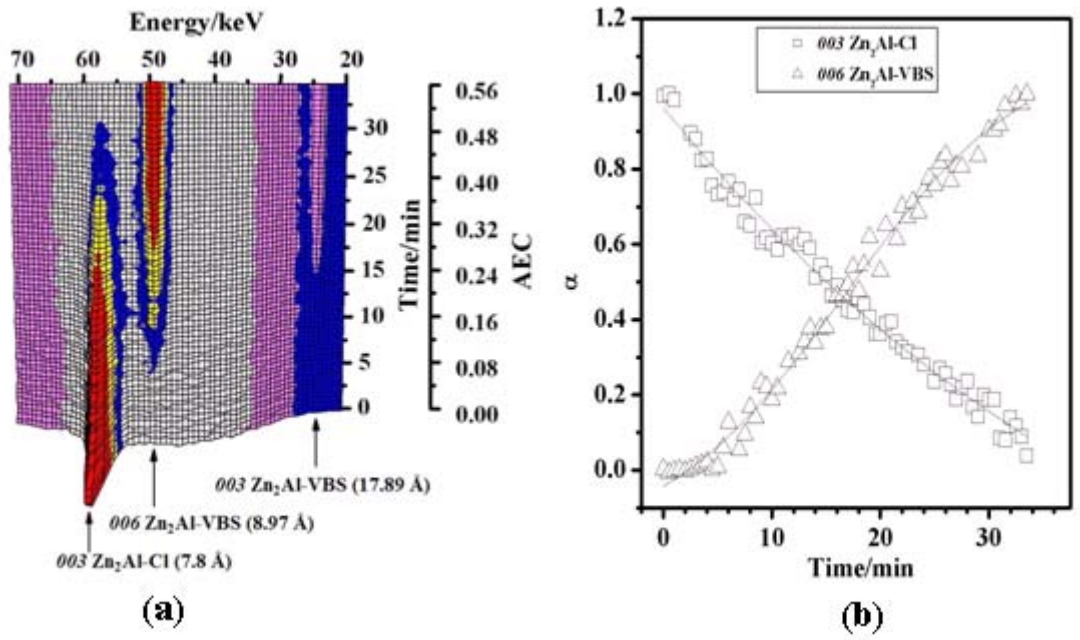

Figure 4-6**:** EDXRD data showing the course of the exchange reaction of Zn_2Al-Cl with VBS at room temperature. (a) 3D stacked plot showing the evolution of Zn_2Al-Cl host *003* and Zn_2Al-VBS product *006* Bragg reflections as a function of time; (b) extent of reaction *vs.* time curves for host *003* and product *006* Bragg reflections. The VBS guest anion solution (0.2 M) was added at 0.059 mL· min^{-1}.

Figures 4-5 and **4-6** show the reaction of Zn_2Cr-Cl and Zn_2Al-Cl respectively with VBS anions. In both cases, the reaction was observed to proceed directly from the host material to the fully exchanged phase. The EDXRD data show only the *003* Bragg reflections of the Cl-containing hosts and two reflections for VBS- products: *003* reflection at *ca.* 18.0 Å and *006* reflection at *ca.* 9.0 Å. The extent of reaction (α) *vs.* time curves of the Cl- hosts and the VBS-products (*006* reflection) are seen to cross at α = 0.5 in total agreement with a direct conversion of the hosts to the products in the absence of intermediate phase.

4.4 Exchange Reaction of Zn_2Cr-Tart/Cl with VBS Anions

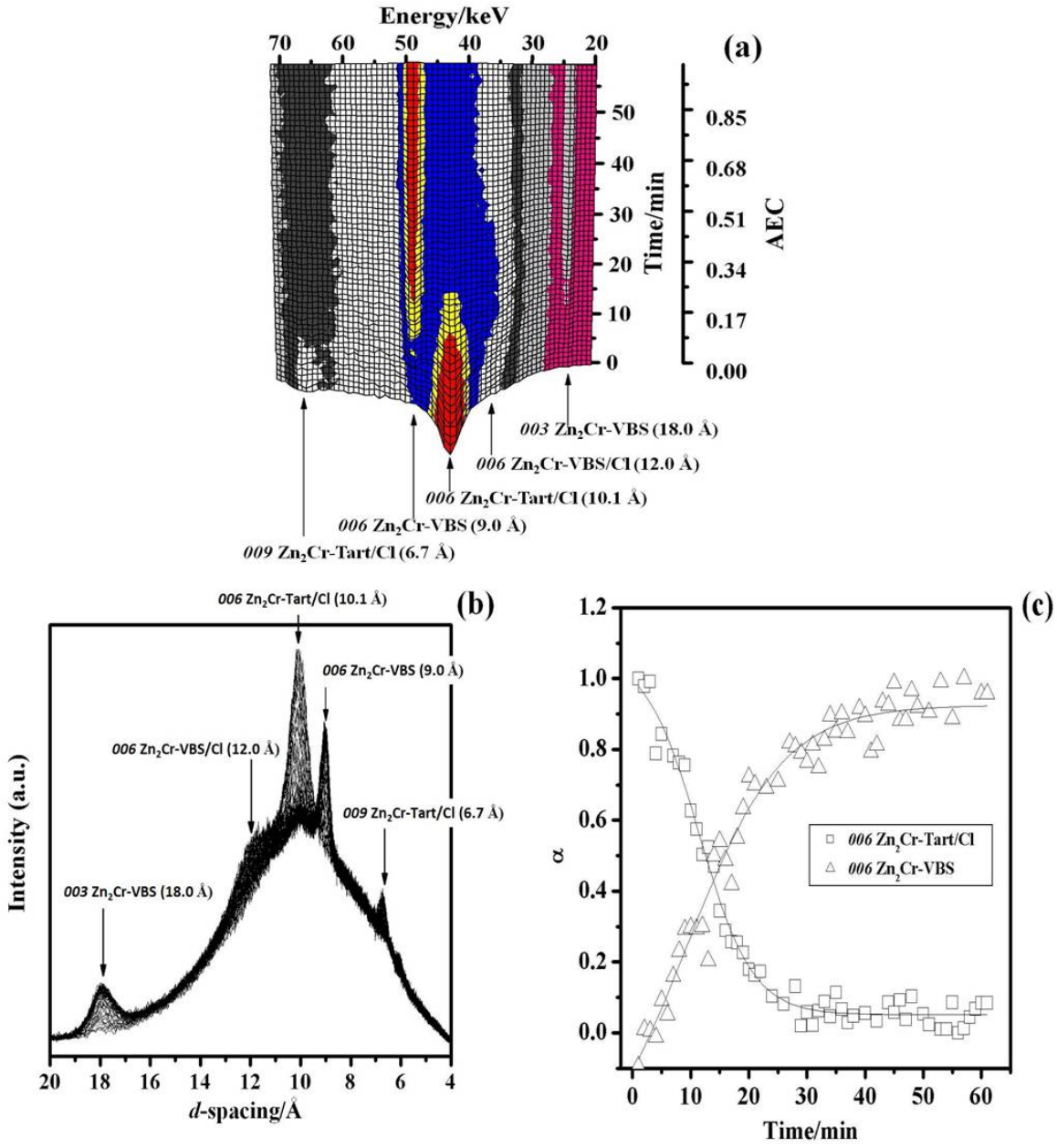

Figure 4-7**:** EDXRD data showing the course of the exchange reaction of Zn_2Cr-Tart/Cl with VBS at room temperature. (a) 3D stacked plot showing the evolution of Zn_2Cr-Tart/Cl host *006* and Zn_2Cr-VBS product *006* Bragg reflection as a function of time, (b) 2D stacked plot showing the same, (c) extent of reaction *vs.* time curves for host *006* and product *006* Bragg reflections. The VBS guest anion solution (0.2 M) was added at 0.059 mL· min^{-1}.

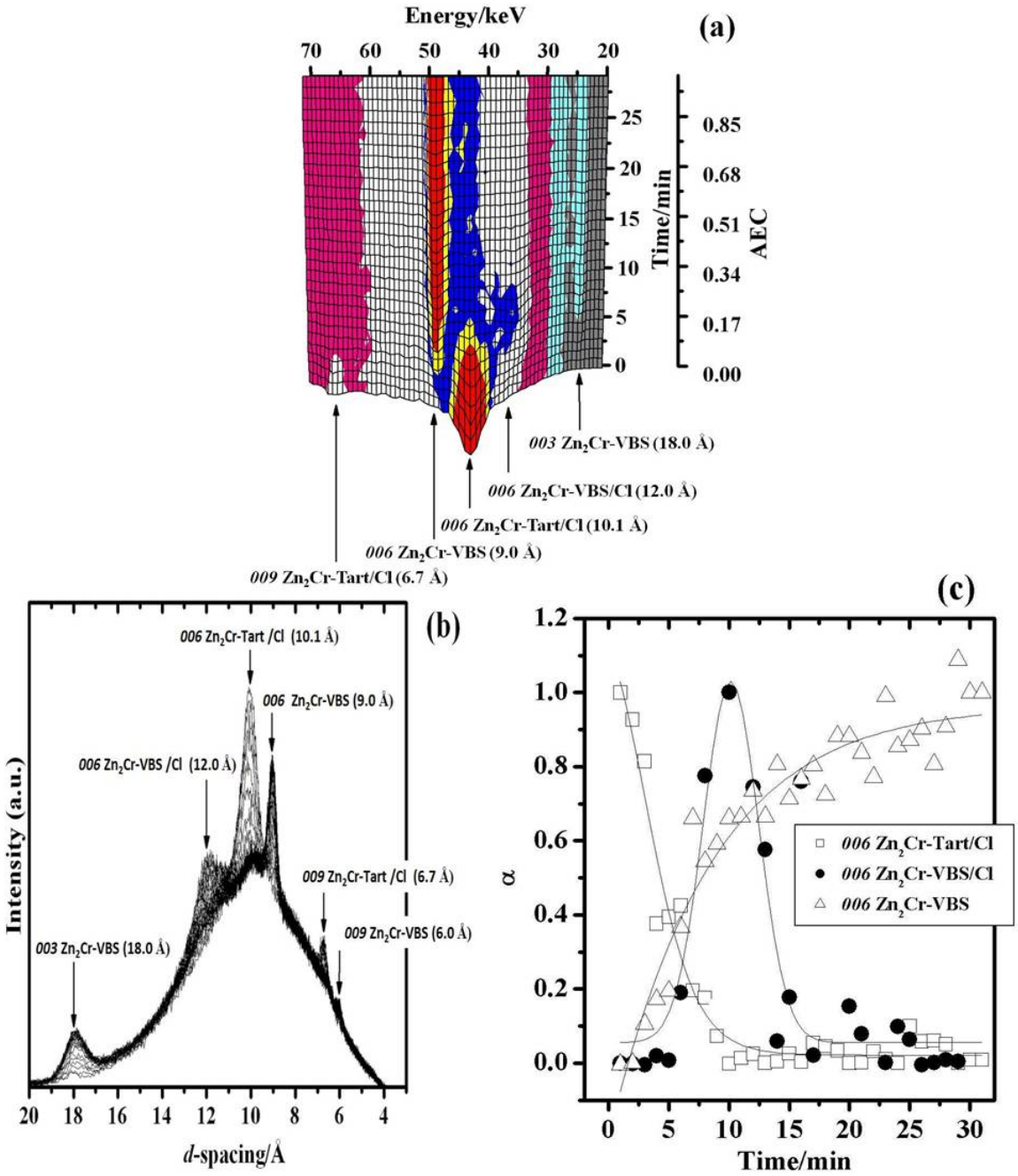

Figure 4-8**:** EDXRD data showing the course of the exchange reaction of Zn_2Cr-Tart/Cl with VBS at 55 ℃. (a) 3D stacked plot showing the evolution of Zn_2Cr-Tart/Cl host *006*, Zn_2Cr-VBS/Cl intermediate *006* and Zn_2Cr-VBS product *006* Bragg reflection as a function of time, (b) 2D stacked plot showing the same, (c) extent of reaction *vs.* time curves for host, intermediate and product *006* Bragg reflections. The VBS anion solution (0.2 M) was added at 0.118 mL· min^{-1}.

In **Figures 4-7** are presented EDXRD data showing the exchange reaction of

Zn_2Cr-Tart/Cl with VBS at room temperature. For this exchange reaction, the presence of an intermediate was initially difficult to established and it took painstaking analysis of the data to spot the shoulder at ca. 12.0 Å. Yet, performing the reaction at 55 ℃ (**Figure 4-8**) allowed us to clearly observe the growth of a reflection at 12.0 Å assigned to the *006* Bragg reflection of Zn_2Cr-VBS/Cl second-stage compound. This compound has a predicted d_{003} = 18.0 (*003* VBS) + 7.8 (*003* Cl) = 25.8 Å leading to a d_{006} of 12.9 Å. This value is slightly higher than that observed 12.0 Å but the low intensity of the corresponding peak makes the determination of its exact position rather difficult.

One can note that α(t) curves for the host and the product do not cross at α = 0. This suggests parallel process with probably a route going through the intermediate and also a direct transformation of the host, as observed in the case of the exchange reaction of Zn_2Cr-Tart/Cl with adipate (**Chapter 3**). The crossing point difference at room temperature α = 0.45 and at 55 ℃ α = 0.35, cannot be attributed to differences in data resolution. The decrease of α between room temperature and 55 ℃ is effective and may indicate that staging phenomenon in this case is thermally activated.

4.5 Exchange Reaction of Zn_2Al-VBS with CO_3^{2-} Anions

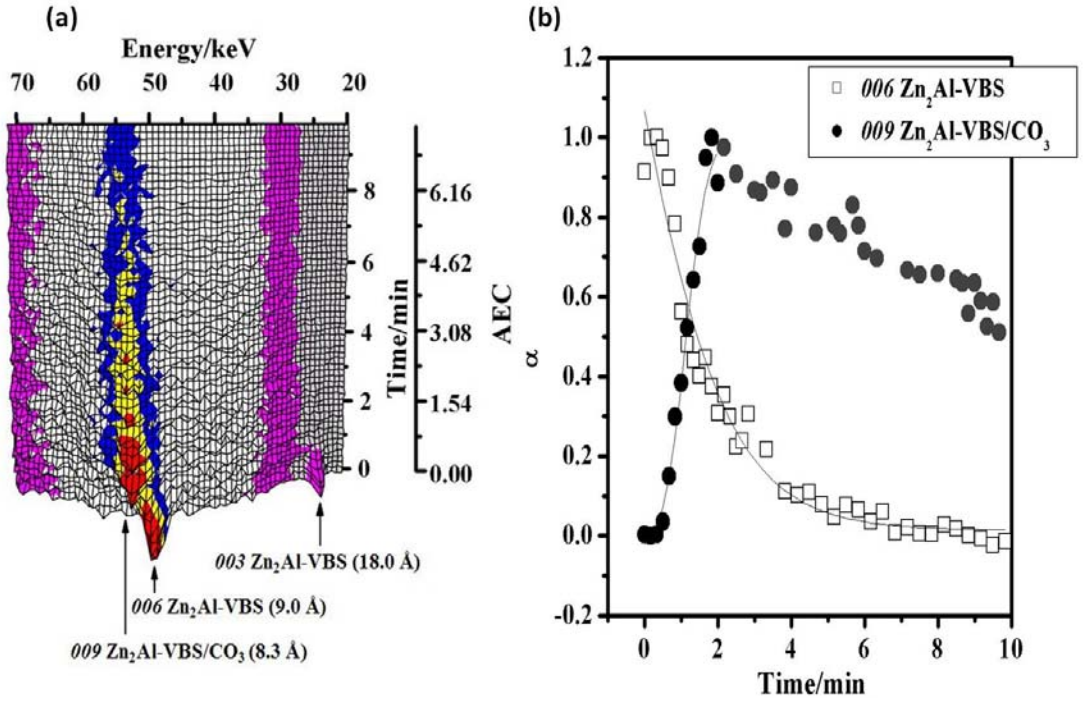

Figure 4-9**:** EDXRD data showing the course of the exchange reaction of Zn_2Al-VBS with carbonate anions at room temperature. (a) 3D stacked plot showing the evolution of Zn_2Al-VBS host *006* and Zn_2Al-VBS/CO_3 intermediate *009* Bragg reflections as a function of time, (b) extent of reaction *vs.* time curves for host and intermediate *006* Bragg reflections. Carbonate guest anions solution (0.2 M) was added at 1.0 mL· min^{-1}.

For the exchange reaction of Zn_2Al-VBS with CO_3^{2-} anions (**Figure 4-9**), a gradual decrease of the *003* (18.0 Å) and *006* (9.0 Å) reflections is first observed. This decay is accompanied with the growth of a new reflection at *ca.* 8.3 Å attributed to the *009* reflection of Zn_2Al-VBS/CO_3 second-stage compound. This compound has a predicted d_{003} = 18.0 (*003* VBS) + 7.5 (*003* CO_3^{2-})= 25.5 Å leading to a d_{009} of 8.5 Å, in agreement with EDXRD data. The α(t) curves presented **Figure 4-9** (b) calculated from the *006* Bragg reflection of host Zn_2Al-VBS and *009* reflection of intermediate Zn_2Al-VBS/CO_3 cross at $\alpha \approx 0.5$ indicating a direct conversion from the host to the intermediate.

After 2 min, corresponding to a theoretical exchange rate of 1.54, the reflection of the intermediate becomes very weak and one can consider that it is disappearing. However, the fully exchanged phase was not observed probably because it is too low crystalline.

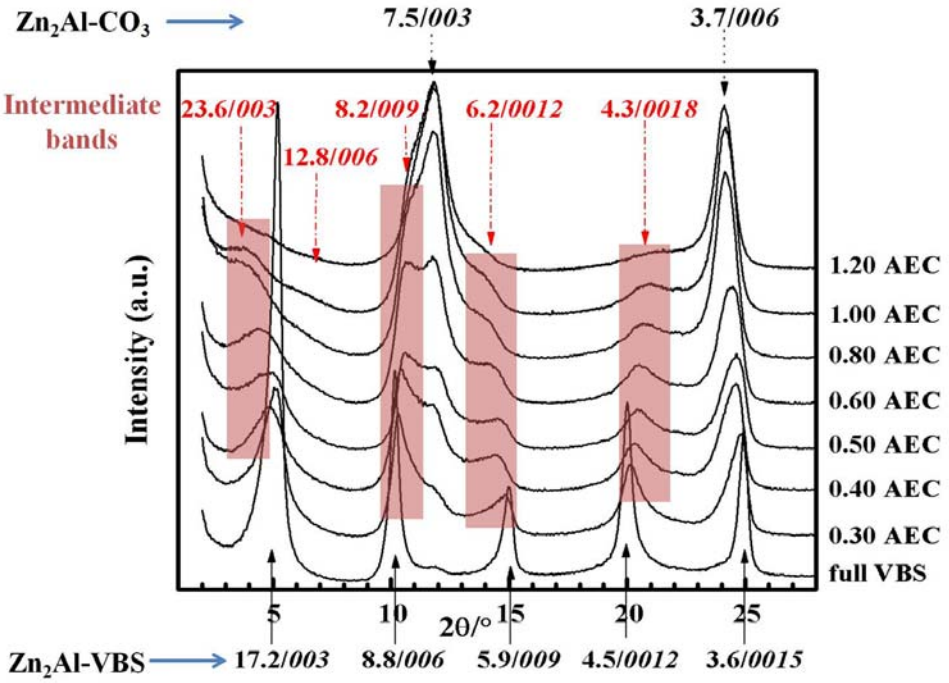

Figure 4-10: Ex situ PXRD data showing the course of the exchange reaction of Zn_2Al-VBS with CO_3^{2-} for intercalation products obtained at different theoretical exchange rates.

The same exchange reaction was repeated in the laboratory and quenched products obtained at different theoretical exchange rate were analyzed by PXRD; the patterns are given in **Figure 4-10**. The interlayer distance for Zn_2Al-VBS as a powder sample d_{003} =17.2 Å differs a little from that in solution d_{003} = 18.0 Å and this difference can be easily explained by a larger amount of interlayer water molecules for the water-suspended sample.

Contrary to EDXRD experiments, the formation of the fully exchanged phase

Zn_2Al-CO_3 is detected at a theoretical exchange rate of 0.3, giving a shoulder at *ca.* 7.5 Å and corresponding to the position of the *003* reflection of Zn_2Al-CO_3. At the same time, the formation of the second-stage intermediate Zn_2Al-VBS/CO_3 is observed. It is first marked by the gradual shift of the *006* reflection of Zn_2Al-VBS to higher 2θ angle from *ca.* 8.7 Å (0.3 AEC) to *ca.* 8.2 Å (1.0 AEC), similar to that observed by EDXRD from 9.0 Å to 8.3 Å; this displacement is associated with the appearance of the *009* reflection of Zn_2Al-VBS/CO_3. The formation of Zn_2Al-VBS/CO_3 becomes more evident with the appearance of a broad and weak reflection at *ca.* 23.6 Å attributed to the *003* reflection of the intermediate; this value is indeed very close to the sum of the interlayer distance of the two anions: 17.2 (VBS) + 7.5 (CO_3^{2-}) = 24.7 Å (within the experimental error). Besides, the weak shoulder centered at *ca.* 6.2 Å as well as the broad and weak reflection at *ca.* 4.3 Å can also be attributed to the *0012* and the *0018* reflections of the intermediate, respectively. For a theoretical exchange rate of 1.2 , the fully exchanged phase is the major phase present. Broad diffraction lines are observed indicating a poor crystallinity consistently with EDXRD data.

4.6 In Situ Thermal Polymerization of Zn_2Cr-VBS/Cl Second-stage Compound

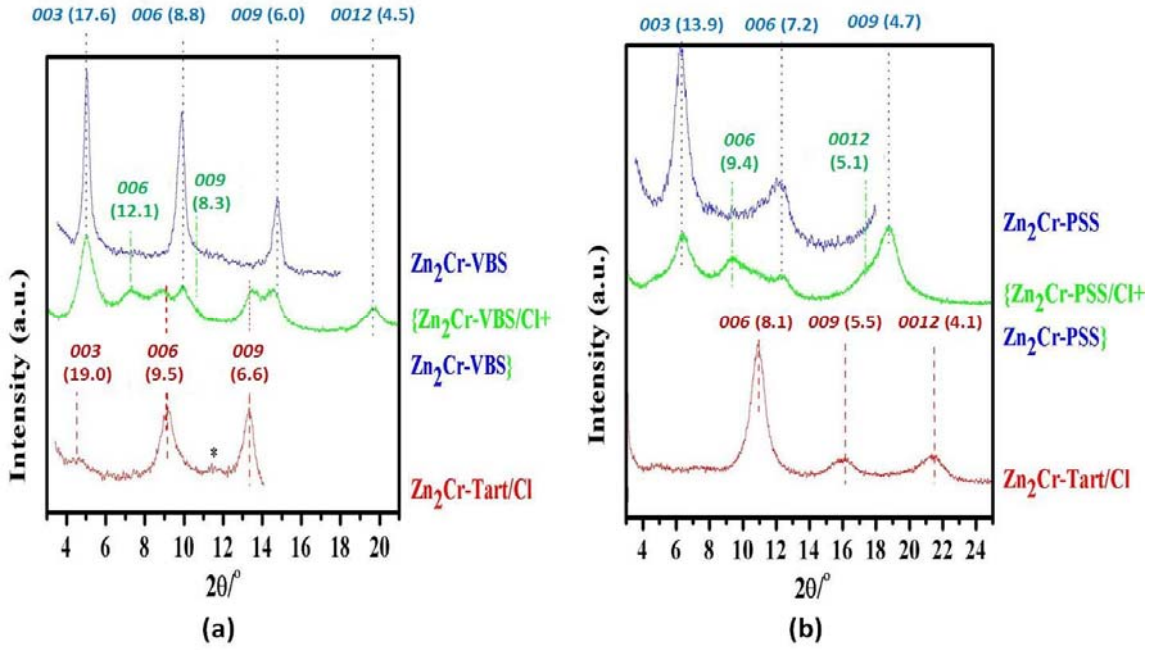

Figure 4-11**:** Powder X-ray diffraction patterns of Zn_2Cr-Tart, Zn_2Cr-Tart/Cl, Zn_2Cr-VBS/Cl and Zn_2Cr-VBS compounds in the HTK experiments: (a) 25 ℃; (b) 200 ℃. The mark * indicates the presence of Zn_2Cr-Cl.

Based on the previous reports concerning the conditions of in situ thermal polymerization of Zn_2Al-VBS, [15] high temperature in situ XRD experiments were carried out at 25 ℃ to 200 ℃ on Zn_2Cr-VBS/Cl second-stage material. Zn_2Cr-VBS/Cl was prepared in the laboratory by repeating the EDXRD experiment at 55 ℃. As can be seen in **Figure 4-11** (a), Zn_2Cr-VBS/Cl is not a pure phase but consists of a mixture of Zn_2Cr-VBS/Cl, Zn_2Cr-Tart/Cl and Zn_2Cr-VBS. Therefore, the thermal behavior of Zn_2Cr-VBS/Cl is compared to those of Zn_2Cr-Tart/Cl and Zn_2Cr-VBS as shown in **Figure 4- 11** (b).

In the case of Zn_2Cr-VBS, the thermal treatment at 200 ℃ leads to a contraction of the interlayer distance from *ca.* 17.6 Å (Zn_2Cr-VBS) to 13.9 Å (Zn_2Cr-PSS). This contraction is close to that reported for the in situ thermal polymerization process of Zn_2Al-VBS, from 18.2 Å to 14.5 Å. In the same time, the *006* reflection of Zn_2Cr-VBS/Cl is shifted to higher 2θ angle from 12.2 Å to 9.4 Å. This contraction is a little smaller than that expected i.e. 10.2 Å ($=\frac{1}{2}[13.9\ (d_{003\ PSS}) + 7.5\ (d_{003\ Cl})]$Å) for the *006* reflection of Zn_2Cr-PSS/Cl. Zn_2Cr-Tart/Cl host also shows a contraction from 9.5 Å to 8.1 Å corresponding to the reorientation of the tartrate anions in a flat position after the removal of interlayer water molecules.

II Exchange Reaction with $[Fe(CN)_6]^{3-}$ Ferricyanide Anions

4.7 Introduction

The intercalation of hexacyanoferrate (II) and (III) into LDH is of interest for several reasons. First, it has implication in electrochemistry with the formation of LDH modified electrodes able to perform electron transfer, energy conversion and molecular recognition functions.[17-19] On the other hand, hexacyanoferrate intercalated LDH form rare examples of pillared LDH, these anions acting as pillaring species creating interlayer microporosity. For instance, $Mg_{3.3}Al$-$Fe(CN)_6$ LDH displays a Langmuir surface area of 499 $m^2 \cdot g^{-1}$ originated from pores smaller than 0.71 nm. [20] Finally, hexacyanoferrate anions are also magnetic species. [21]

This wide range of properties associated with the intercalation of hexacyanoferrate anions into LDH can also be used as different probes to gain further insight into the process taking place in the interlayer space i.e. staging phenomena. In the following, are

described the anion-exchange reaction of Zn_2Cr-Cl, Zn_2Cr-Tart and Zn_2Cr-Tart/Cl with $[Fe(CN)_6]^{3-}$ investigated by means of EDXRD.

4.8 In situ EDXRD measurements

The solution of hexacyanoferrate guest anions was added dropwise to 10 mL of suspension (25 g· L^{-1}) of LDH at 55 ℃ at a rate of 0.118 mL· min^{-1} and a concentration 0.15 M in the case of Zn_2Cr-Cl host, 0.035 mL· min^{-1} and 0.075 M in the case of Zn_2Cr-Tart and Zn_2Cr-Tart/Cl hosts. The EDXRD spectra were collected at a fixed detector angle of 1.625 º (2θ) with acquisition time of 60 s.

4.9 Exchange Reaction of Cl^- Anions in Zn_2Cr-Cl by Ferricyanide Anions

Figure 4-12 shows the course of the exchange reaction of Zn_2Cr-Cl with ferricyanide anions. Only two reflection peaks were observed at a *d*-value of 7.8 Å corresponding to the *003* reflection of Zn_2Cr-Cl host and 10. 9 Å assigned to the *003* reflection of the fully exchanged phase Zn_2Cr-$Fe(CN)_6$. The latter value is close to those reported elsewhere for Mg_2Cr-LDH (10.45 Å) [22], $Mg_{1.5}Al$-LDH (11.10 Å) [22] and Mg_2Fe(III)-LDH (10.8 Å) [23]. The size of the ferricyanide anions is close to 11 Å along the C_4 axis, 8.7 Å along the C_2 axis and 6.51 Å along the C_3 axis. [24] The present gallery height (6.1 Å) means that the ferricyanide anions are oriented with the C_3 axis perpendicular to the hydroxide sheets.

Furthermore, the crossing point in α(t) curves occurring at α = 0.5 (**Figure 4-12** (c)) confirms the one-step process with a direct transformation from the host to the product.

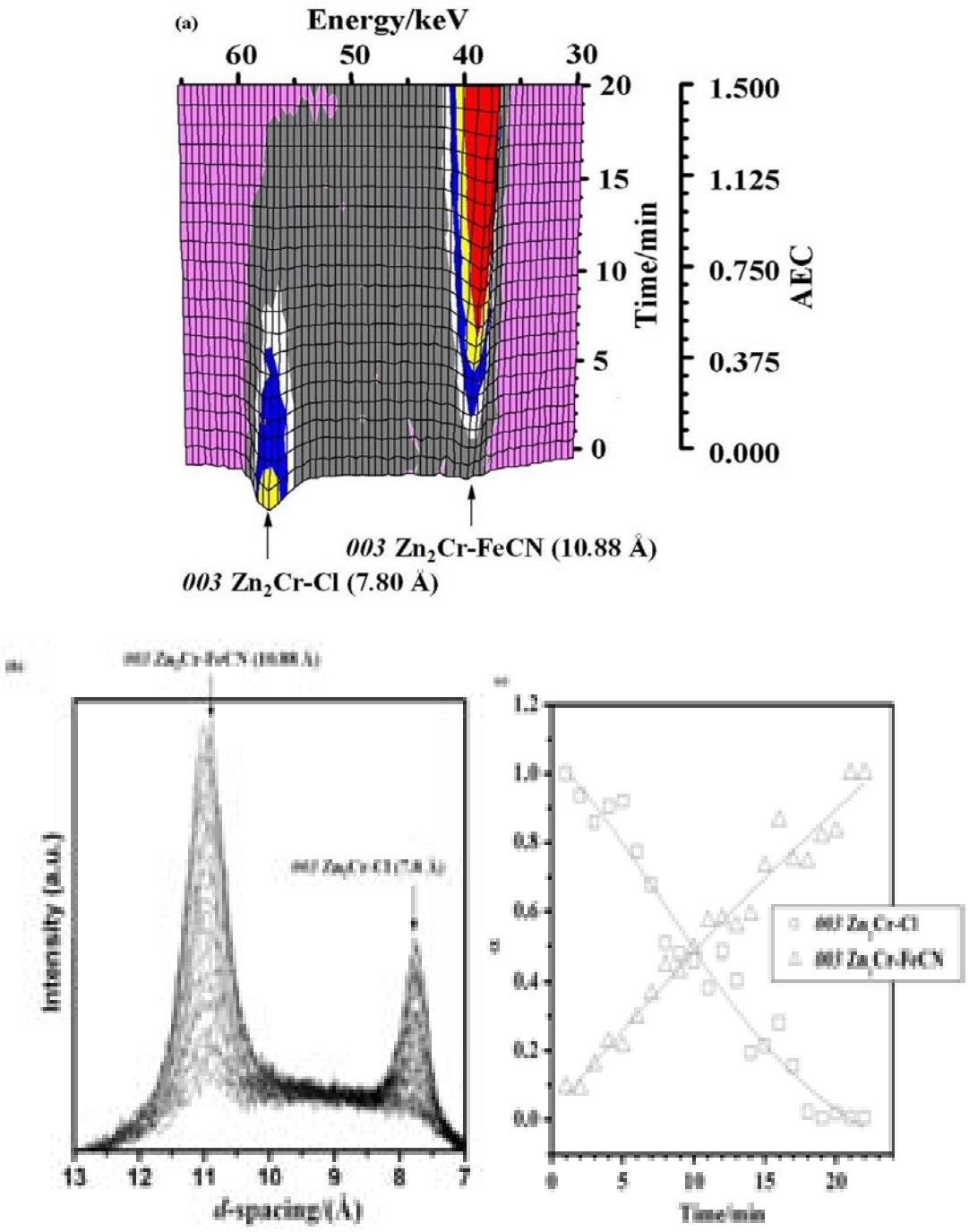

Figure 4-12**:** EDXRD data showing the course of the exchange reaction of Zn_2Cr-Cl with ferricyanide anions at 55℃. (a) 3D stacked plot showing the evolution of Zn_2Cr-Cl host *003* and Zn_2Cr-FeCN product *003* Bragg reflections as a function of time, (b) 2D plots showing the same reflections, (c) extent of reaction *vs.* time curves for host *003* and product *003* Bragg reflections.

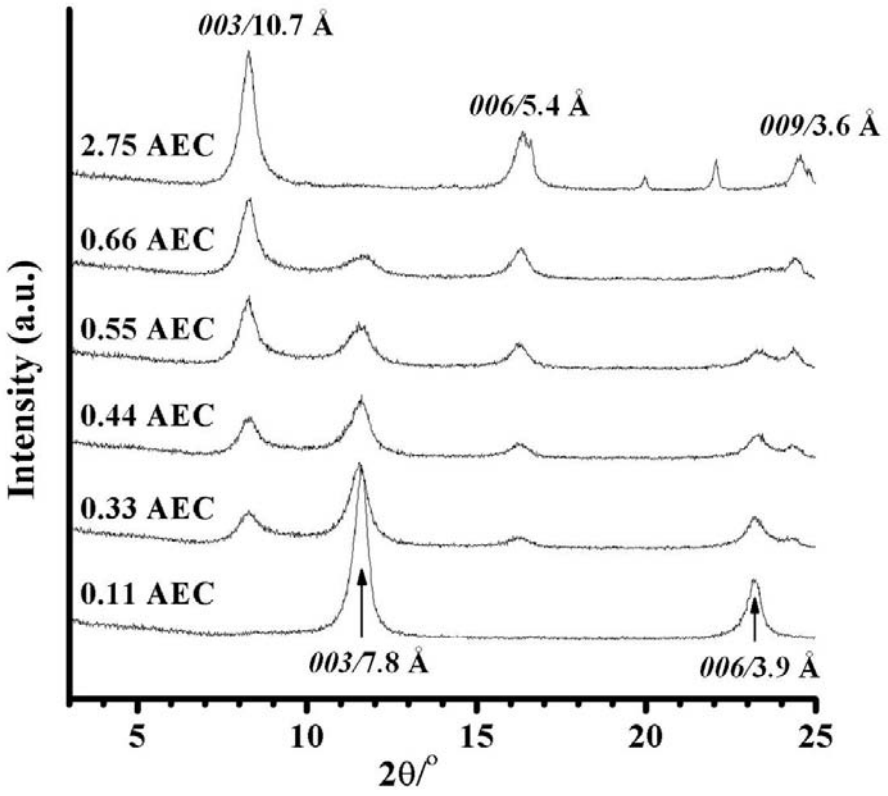

Figure 4-13: Ex situ PXRD data showing the course of the exchange reaction of $[Fe(CN)_6]^{3-}$ anions with Zn_2Cr-Cl: PXRD patterns of the intercalation products obtained at different theoretical exchange rate: 2.75 AEC, 0.66 AEC, 0.55 AEC, 0.44 AEC, 0.33 AEC and 0.11 AEC from top line to bottom.

The same experiment was also performed in the laboratory and PXRD patterns of the products quenched at different theoretical exchange rates are shown in **Figure 4-13**. These data are in total agreement with EDXRD data. Since only one product is formed i.e. Zn_2Cr-$Fe(CN)_6$ and the growth of Zn_2Cr-$Fe(CN)_6$ is correlated to the decay of Zn_2Cr-Cl host.

4.10 Exchange Reaction of Ferricyanide Anions with Zn_2Cr-Tart

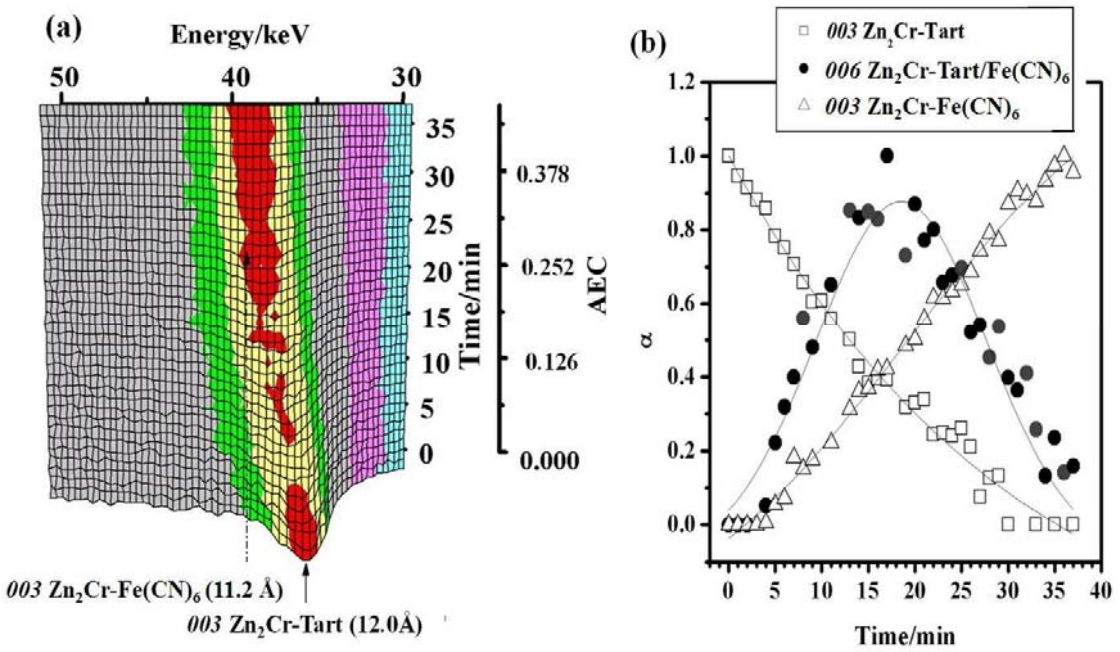

Figure 4-14: EDXRD data showing the course of the exchange reaction of Zn_2Cr-Tart with ferricyanide anions at 55 ℃. (a) 3D stacked plot showing the evolution of Zn_2Cr-Tart host *003* and Zn_2Cr-FeCN product *003* Bragg reflections as a function of time. (b) extent of reaction *vs.* time curves for host *003*, intermediate *006* and product *003* Bragg reflections. The guest ferricyanide anions solution (0.075 M) was added at a rate of 0.035 mL · min^{-1}.

For the exchange reaction of Zn_2Cr-Tart with ferricyanide, a gradual displacement of the *003* reflection of Zn_2Cr-Tart from 12.0 Å to 11.2 Å is observed (**Figure 4-14**). This last value is that expected for Zn_2Cr-$Fe(CN)_6$. A deconvolution of the EDXRD patterns was first attempted by considering two contributions centered at 12.0 Å and 11.2 Å (**Figure 4-14** (a)). A better **Figure 4-14** (b) was obtained by considering an additional peak at 11.6 Å corresponding to the *006* reflection of Zn_2Cr-Tart/$Fe(CN)_6$. This peak has a predicted d_{003} = 12.00 Å + 11.2 Å = 23.2 Å and hence a d_{006} of *ca.* 11.6 Å.

4.11 Exchange reaction of Zn_2Cr-Tart/Cl with Ferricyanide Anions

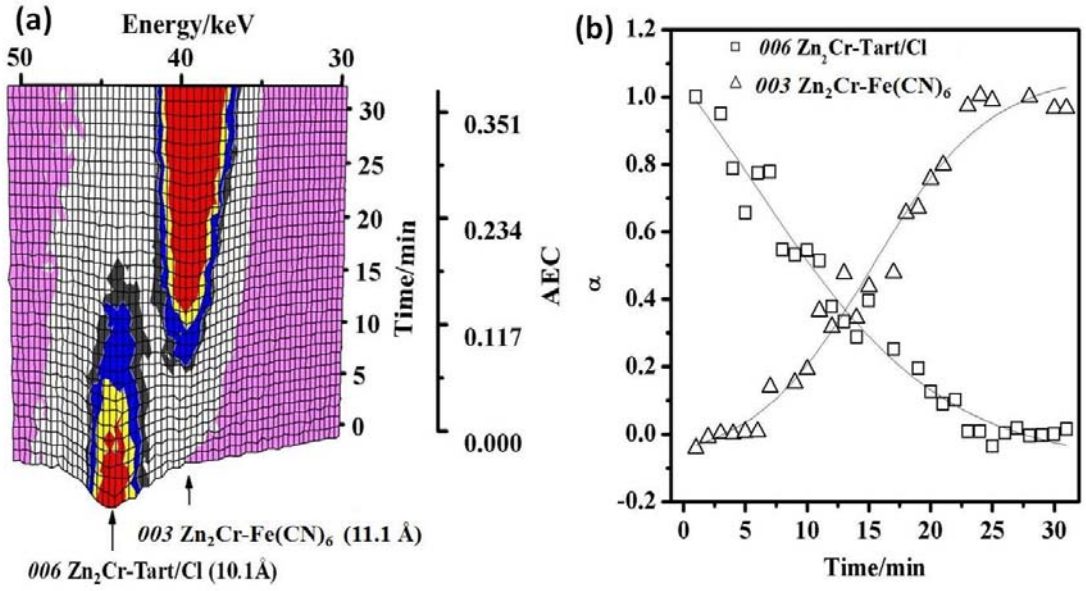

Figure 4-15: EDXRD data showing the the course of the exchange reaction of Zn_2Cr-Tart/Cl with ferricyanide anions at 55 ℃. (a) 3D stacked plot showing the evolution of Zn_2Cr-Tart/Cl host *006* and Zn_2Cr-$Fe(CN)_6$ product *003* Bragg reflections as a function of time, (b) 2D plots showing the same, (c) extent of reaction *vs.* time curves for host *006* and product *003* Bragg reflections. The guest ferricyanide anions solution (0.075 M) was added at a rate of 0.035 mL · min^{-1}.

Figure 4-15 shows the EDXRD data concerning the exchange reaction of Zn_2Cr-Tart/Cl with ferricyanide anions and only two reflections are observed: at 10.1 Å corresponding to the *006* reflection of Zn_2Cr-Tart/Cl and at 11.1 Å assigned to the *003* reflection of Zn_2Cr-$Fe(CN)_6$. The crossing point of the α(t) curves occurs close to α = 0.5 indicating the absence of the intermediate phase under the present conditions. Probably, no formation of staging phase is resulted from a fast exchange reaction due to the high negative charge of the ferricyanide anions.

4.12 Conclusions

The exchange reaction of VBS with Zn_2Cr-Cl, Zn_2Al-Cl first stage LDH and Zn_2Cr-Tart/Cl second-stage LDH, were investigated by means of EDXRD as well as the exchange reaction of CO_3^{2-} with Zn_2Al-VBS. The formation of Zn_2Cr-VBS/Cl and Zn_2Al-VBS/CO_3 second-stage intermediates was observed.

Zn_2Cr-VBS/Cl was obtained by reacting Zn_2Cr-Tart/Cl with VBS, while it is not formed during the anion-exchange reaction of Zn_2Cr-Cl with VBS. This may indicate that the present phase can only be prepared starting from a second-stage structure such as Zn_2Cr-Tart/Cl. On the other hand, a preliminary study allowed us to observe the in situ thermal polymerization of VBS in Zn_2Cr-VBS/Cl leading to Zn_2Cr-PSS/Cl.

The exchange reaction of ferricyanide anions with Zn_2Cr-Cl, Zn_2Cr-Tart and Zn_2Cr-Tart/Cl LDH materials were investigated by means of EDXRD. The formation of Zn_2Cr-Tart/$Fe(CN)_6$ second-stage intermediate was observed by reacting Zn_2Cr-Tart with ferricyanide anions.

4.13 References

1 K. Tokuoka, M. Senna and H. Kung, *J. Mater. Sci.*, **1986**, *21 (2)*, 493.
2 F. Leroux, *J. Nanosci. Nanotech.*, **2006**, *6(2)*, 303.
3 A. D. Pomogailo, *Russ. Chem. Rev.*, **2000**, *69 (1)*, 53.
4 K. H. Haas and K. Rose, *Rev. Adv. Mater. Sci.*, **2003**, *5*, 47.
5 K. G. Sharp, *Adv. Mater.*, **1998**, *10 (15)*, 1243.
6 A. M. Herring, *Poly. Rev.*, **2006**, *46 (3)*, 245.
7 C. Taviot-Gueho and F. Leroux, *Struct. Bond.*, **2006**, *119*, 121.
8 D. G. Evans and X. Duan, *Chem. Commun.*, **2006**, 485.
9 J. Q. Wang and W. K. Chow, *J. Appl. Poly. Sci.*, **2005**, *97 (1)*, 366.

10 F. Leroux and C. Taviot-Gueho, J. *Mater. Chem.*, **2005**, *15 (35-36)*, 3628.
11 F. Leroux and J. P. Besse, *Interface Sci. Technolog.*, **2004**, *1*, 459.
12 N. T. Whilton, P. J. Vickers and S. Mann, *J. Mater. Chem*., **1997**, *7*, 1623.
13 El M. Moujahid, M. Dubois, J. P. Besse and F. Leroux, *Chem. Mater.*, **2002**, *14*, 3799.
14 El M. Moujahid and J. P. Besse, *J. Mater. Chem.*, **2002**, *12*, 3324.
15 L. Vieille, El M. Moujahid, C. Taviot-Guého, J. Cellier, J. P. Besse and F. Leroux, *J. Phys. Chem. Solids*, **2004**, *65*, 385.
16 El M. Moujahid, F. Leroux, M. Dubois and J. P. Besse, *C. R. Chimie*, **2003**, *6*, 259.
17 R. L. Frost, A. W. Musumeci, J. Bouzaid, M. O. Adebajo, W. N. Marteus and J. T. Kloprogge, *J. Solid State Chem.*, **2005**, *178*, 1940.
18 J. W. Boclais, P. S. Braterman, B. D. Brister, Z. Wang and F. Yaibery, *J. Solid State Chem.*, **2001**, *161*, 249.
19 K. Yao, M. Taniguchi, M. Nakata, M. Takakaski and A. Yamagiski, *Langmuir*, **1998**, *14*, 2410.
20 H. Nijs, M. de Bock and E. F. Vansant, *Microporous Mesoporous Mater.*, **1999**, *30*, 243.
21 M. T. Hisvonen, A. P. Jauho, T. E. Katila and K. J. Riski, *Phys. Rev. B*, **1977**, *15 (3)*, 1445
22 A. S. Prakash, P. V. Kamath and M. S. Hegde, *Mater. Res. Bull*., **2000**, *35*, 2189.
23 W. Q. Meng, F. Li, D. G. Evans and X. Duan, *J. Mater. Sci*., **2004**, *39*, 4655.
24 J. M. Fernandez, M. A. Ulibarri, F. M. Labajoss and V. Rives, *J. Mater. Chem*., **1998**, *8*, 2507.

Conclusion

This thesis work has been devoted to the study of the anion exchange reaction mechanism for two LDH host compositions namely Zn_2Cr and Zn_2Al and for a series of inorganic namely Cl^-, F^-, CO_3^{2-}, SO_4^{2-} and $Fe(CN)_6^{3-}$ and organic anions (tartrate, succinate, adipate and styrene-4-sulfonate VBS anions). Monitoring the process in situ by means of energy dispersive X-ray diffraction reveals two reactions mechanisms: either anion exchange reaction occurs in a one-step direct transformation from the host to the fully-exchanged phase or the reaction proceeds *via* a second-stage intermediate with alternating interlayer occupied by two different anions and then conversion to the first stage.

The aim of this work was first to determine the factors influencing staging. One important remark concerns the high rate of these reactions, typically with a half-time of 1-2 minutes. Therefore, in order to study these reactions in details and detect the presence of intermediate phases, it was necessary to slow down the reaction by adding the guest anion solution in a dropwise manner.

A general trend is that inorganic-inorganic anion exchange reactions occur in a one-step process while inorganic-organic exchanges often proceed *via* a second-stage intermediate. This leads us to suggest that staging occurs partly as a result of organic-inorganic separation. Yet, one must keep in mind that staging is not observed for all organic anions (for instance, in the case of the exchange of chloride anions by VBS anions) indicating that other factors must be considered such as the anion size, the solvatation and the affinity for different anions. Concerning this last parameter, we believed in a correlation between the occurrence of a two-step process and the difficulty of exchange of the initial anion, as established by O'Hare *et al.* in the case

of $LiAl_2$ system.[1] Indeed, microcalorimetric measurements reported elsewhere[2, 3] clearly indicate that chloride anions are easier to replace by inorganic anions such as sulfate, carbonate or ferricyanide anions than by organic anions like tartrate or succinate anions. In these conditions, the exchange of chloride anions by inorganic anions occurs in one stage while staging is needed to overcome the energy barrier in the case of organic anions. On the other hand, the fact that the formation of second and first-stage products obeys either a consecutive process with the formation of second-stage intermediates and then conversion into fully exchanged phases or parallel processes with a route going through the intermediate as well as a direct transformation of the host, may be attributed also to differences in anion affinities. Indeed, a rapid and consecutive process is observed for anions relatively easy to replace while low and parallel processes take place for anions difficult to replace; this interpretation is supported by the enhancing effect of temperature on the formation of second-stage intermediates indicating higher activation energies in this latter case. However, another explanation given by O'Hare *et al.* might be that consecutive processes would arise from an ordered replacement of interlayer anions while a random replacement would lead to parallel processes. [1]

The kinetic of the exchange reaction of chloride anions in Zn_2Cr-Cl with tartrate anions was examined. A rate constant *k* of $1.2(4)*10^{-2}\ s^{-1}$ at 25 ℃ was obtained for a addition rate 1.0 $mL \cdot min^{-1}$ of the tartrate anion solution. This value is comparable with rate constants reported elsewhere for intercalation reactions in other layered

1 G. R. Williams and D. O'Hare, *Chem. Mater*., **2005**, *17*, 2632.

2 Y. Israeli, C. Taviot-Gu ho, J. P. Besse, J. P. Morel and N. Morel-Desrosiers, *J. Chem. Soc. Dalton Trans.*, **2000**, *5*, 791.

3 N. Morel-Desrosiers, J. Pisson, Y. Israeli, C. Taviot-Gueho, J.-P. Besse and J.-P. Morel, *J Mater. Chem*., **2003**, *13*, 2583.

materials.[4] The anion exchange reaction in LDH system is expected to be a 2D processes with deceleratory nucleation. The Avrami exponent value *n* obtained from Sharp-Hancock analysis i.e. 2-3 is in favor of a phase boundary controlled process i.e. the reaction rate is limited by the expansion of the interlayer space necessary to accommodate tartrate anions.

An important result of this study is the formation of intermediate phases of higher-order staging than 2 during the exchange reaction of CO_3^{2-} anions with Zn_2Cr-Tart, since only LDH second-stage intermediates have been reported so far. The gradual variation of the interlayer distance of the intermediate product clearly indicates a variation of the number of the interlayer spaces concerned with the exchange process. Of course this result must be further confirmed by means of HRTEM technique to better characterize the intermediate compositions. On the other hand, one may think that for the other anion-exchange reactions examined here, the high rate of these reactions is likely to prevent the observation of higher-staging than 2, if existing.

In a second step, we went further by examining the anion exchange properties of these second-stage intermediates. Selective anion-exchange reactions were observed that were a result of the segregation between organic and inorganic anions. Indeed, the reaction of Zn_2Cr-Succ/Cl and Zn_2Cr-Tart/Cl second-stage compounds with either fluoride or adipate anions initially occurs with preferential replacement of the hydrophilic Cl ion with F, or of the organic succinate or tartrate anions with adipate leading to the formation of new second-stage intermediates Zn_2Cr-Succ/F and

4 J. S. O. Evans, S. J. Price, H.-V. Wong and D. O'Hare, *J. Am. Chem. Soc.*, **1998**, *120*, 10837.

Zn_2Cr-Tart/F or Zn_2Cr-Adip/Cl. Because of this great selectivity, new heterostructures can be formed that may not be achieved starting from a first-stage product. Indeed, attempts to prepare Zn_2Cr-Tart/F second stage materials from respectively the exchange Zn_2Cr-Tart with fluoride anions failed, suggesting that the present phases can be obtained starting only from Zn_2Cr-Tart/Cl second-stage structure.

Such amphiphilic heterostructures should find applications in many fields as ion exchangers, adsorbent for environmental remediation, nanolayer reinforcements in hybrid organic-inorganic polymer composite. Compared to first-stage LDH, these LDH heterostructures may give access to multifunctional properties. Preliminary measurements have been reported showing the formation of VBS (styrene-4-sulfonate)/ Cl and tartrate/ferricyanide heterostructures. In the former case, the in situ thermal polymerization of VBS into PSS was evidenced by means of in situ high temperature powder X-ray diffraction. On the other hand, magnetic measurements on Zn_2M-Tart/$Fe(CN)_6$ (M: Al, Cr) sample are underway to characterize the effect of either the lamellar sequestration and/or the alternative location on the dimensionality of the properties.